Environmental Chemistry Letters (2021) 19:1229–1274
https://doi.org/10.1007/s10311-020-01134-2

REVIEW

# Synthesis of iron-based magnetic nanocomposites and applications in adsorption processes for water treatment: a review

Luciana Resende Marcelo[1,2] · Jefferson Santos de Gois[1,3] · Alexsandro Araujo da Silva[4] · Deborah Vargas Cesar[1,3]

Received: 29 May 2020 / Accepted: 30 October 2020 / Published online: 17 November 2020


## Abstract

Rising worldwide concern about the quantity and quality of water available to living beings calls for efficient technologies of water treatment. Nanomaterials are promising adsorbents to remove contamination from aqueous solution, and magnetic nanomaterials based on iron have attracted attention because magnetic materials are easy to separate. Here, we review iron magnetic nanomaterials applied for water and wastewater treatment, with focus on toxic elements, pharmaceuticals and pesticides. Major advances are: coprecipitation is the most used method for synthesis of iron magnetic nanoparticles, followed by solvothermal and hydrothermal methods. Magnetite is the most common magnetic nanoparticles applied as magnetic adsorbent. In general, magnetic nanocomposites are superparamagnetic, and the highest magnetization is sought for core–shell structures, reaching 65 emu/g. Most reports focus on removal of toxic metals. Adsorption is explained by the Langmuir isothermal model, kinetic patterns being correlated with pseudo-second-order equations. Overall, iron-based magnetic nanocomposites display promising performances for pollutant removal, yet few investigations report the toxic impacts of magnetic nanoparticles on the environment.

**Keywords** Adsorption · Magnetic nanoparticles · Nanocomposites · Toxic elements · Pharmaceutical-derived compounds · Pesticides

## Introduction

Industrial growth and urbanization have led to the release of pollutants in environment making; sometimes, the water is unfit for consumption (Mehta et al. 2015; Khan and Malik 2019). Several substances with harmful potential have been detected in aquatic systems (Petrie et al. 2014). Many contaminants are not eliminated during wastewater treatment and are not biodegraded in the environment. The commitment and scarcity of water resources and the limitations of available water treatments indicate that the search for new technologies to recover contaminated water is an urgent matter (Zhang et al. 2016). Therefore, nanotechnology has received attention as a proposal of advanced treatment complementary to the conventional (Zhang et al. 2016; Lu and Astruc 2018; Madhura et al. 2019).

Nanomaterials are defined as materials with physical dimensions in the range of 1 to 100 nm. The nanometer-sized results in unique properties are not typically found in the material on the micrometric scale, such as large surface area, high reactivity, rapid kinetics, and specific affinity (Lu and Astruc 2018). In water treatment, the nanomaterials can

✉ Luciana Resende Marcelo
luciana.marcelo@ifrj.edu.br

✉ Jefferson Santos de Gois
jefferson.gois@uerj.br

Alexsandro Araujo da Silva
alexsandro.silva@uerj.br

Deborah Vargas Cesar
dvargas@uerj.br

1 Graduate Program in Chemical Engineering, Rio de Janeiro State University, Rua São Francisco Xavier, 524, Maracanã, Rio de Janeiro 20550-013, Brazil

2 Institute of Education, Science and Technology - Rio de Janeiro, República do Paraguai Avenue, 120, Sarapuí, Duque de Caxias 25050-100, Brazil

3 Department of Analytical Chemistry, Chemical Institute, Rio de Janeiro State University, São Francisco Xavier, 524, Maracanã, Rio de Janeiro 20550-013, Brazil

4 Department of Organic Chemistry, Rio de Janeiro State University, Rua São Francisco Xavier, 524, Maracanã, Rio de Janeiro 20550-013, Brazil

be used in several processes, such as adsorption, catalytic oxidation, and disinfection (Zhang et al. 2016). Perhaps adsorption is the most studied given the simplicity for operation, flexibility, and high efficiency (Mehta et al. 2015; Singh et al. 2018). The use of nanomaterials as adsorbents has been described in different works (Khajeh et al. 2013) such as carbon nanotubes (Kumar et al. 2014; Dutra et al. 2018; Zhang et al. 2019a), graphene oxide (Gao et al. 2012; Nam et al. 2015; Baig et al. 2019; Sánchez-García et al. 2019), metal nanoparticles (Oliveira et al. 2018; Jin et al. 2019), among others. Iron-based magnetic nanoparticles have been suggested as a promising adsorbent in the removal of organic and inorganic pollutants, with the additional advantages of relatively low cost, environmentally friendly, and easy to separation and recover from the aqueous solution (Tang and Lo 2013; Wang et al. 2013; Chen et al. 2016a). Therefore, the methods for the synthesis and characterization of iron-based magnetic nanomaterials will be described and discussed so the reader can have a critical point of view of the challenges and state of the art. Moreover, a survey and discussion of the applications in adsorption processes including recovery and reuse, with particular focus on the removal of toxic elements, pharmaceutical-derived compounds, and pesticides in aqueous solutions will be made.

## Iron-based magnetic nanoparticles

Magnetic nanoparticle applications are diverse; in water treatment, the iron-based magnetic nanoparticles mainly used are the nanoscale zero-valent iron, $Fe_3O_4$ that is known as magnetite, and ɣ-$Fe_2O_3$ that is known as maghemite (Zhang et al. 2016; Mohammed et al. 2017). The nanoparticles exhibit superparamagnetic behavior; therefore, magnetic properties are present only under the action of an external magnetic field (Chen et al. 2016a). The magnetic properties enable the separation of the material after the water treatment, making the recovery and reuse afterward a possibility (Mehta et al. 2015). Besides, iron nanoparticles are naturally abundant and present a low cost, low toxicity to the environment when compared to nanoparticles of other metals, and great adsorption capacity, due to the possibility of functionalization or coating the surface with other materials, eg., polymers, graphene oxide, and silica (Xu et al. 2012b; Silva et al. 2014; Reddy and Yun 2016). The efficiency of iron nanoparticles has been proved in the adsorption of inorganic and organic substances from contaminated water.

The mechanism of contaminant removal by iron-based nanoparticles will depend on the oxidation states of iron, including adsorption, chemical reduction, and reductive precipitation, according to Fig. 1 (Tang and Lo 2013). $Fe^0$ and $Fe^{2+}$ solid materials remove contaminants from the water via chemical reduction. Adsorption and reductive precipitation

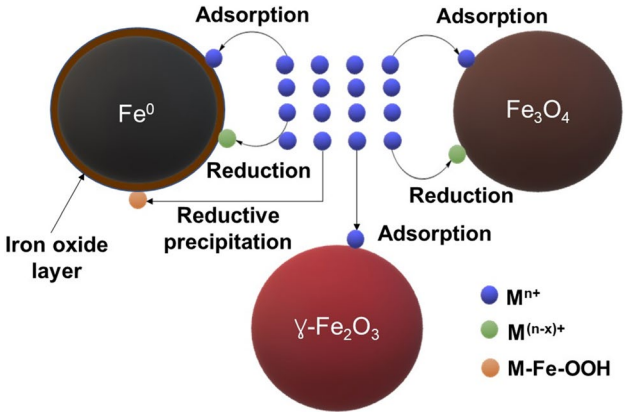


**Fig. 1** Mechanisms of toxic metal removal from aqueous solution by iron-based nanoparticles. For zero-valent iron, the toxic metal removal occurs via the adsorption, reduction, and reductive precipitation processes. For magnetite, the toxic metal removal occurs through the adsorption and reduction processes, while for maghemite, the removal mechanism occurs mainly by adsorption

also occur on the iron oxides or hydroxides surfaces (Zhang et al. 2016). The adsorption mechanism includes hydrogen bonding, π-π interactions, complexation, electrostatic interactions, chemisorption, and ion exchange. Surface hydroxyl groups and surface charge of iron oxides are responsible for the interactions (Singh et al. 2018). For $Fe_3O_4$ nanoparticles, both physical and chemical adsorptions were reported. While for ɣ-$Fe_2O_3$ nanoparticles, the main contaminant removal mechanism is the physical adsorption (Tang and Lo 2013).

Since 90s, the nanoscale zero-valent iron was first synthesized and used in pollutants removal from water and wastewater, including pilot projects (Mueller et al. 2012; Ma et al. 2013). The production of nanoscale zero-valent iron is commonly performed by chemical reduction employing iron salts and sodium borohydride (Crane and Scott 2012). Since zero-valent iron is a strong reducing agent, nanoscale zero-valent iron acts mainly on the degradation of a wide range of pollutants (Grieger et al. 2010; Tang and Lo 2013), such as chlorinated organic contaminants (Xiu et al. 2010) and heavy metals (Boparai et al. 2011; Tajuddin Sikder et al. 2014; Arancibia-Miranda et al. 2016). Nanoscale zero-valent iron in aqueous media usually presents as a core–shell structure with the inner layer of $Fe^0$ and the outer layer of iron oxides or hydroxides. The $Fe^0$ core can be oxidized to $Fe^{2+}$ and $Fe^{3+}$ and, subsequently, to iron oxide, causing the chemical reduction of the pollutants (Crane and Scott 2012; Zhang et al. 2016). Besides, surface sorption and reductive precipitation of contaminants may occur, mainly inorganic elements, through the outer layer of iron oxides or hydroxides (Tang and Lo 2013). On the other hand, the hydroxide or oxide layer formed on nanoscale zero-valent iron surface during the reaction considerably decreases the effective

use of nanoscale zero-valent iron and, to avoid it, a second metal is usually added, resulting in bimetallic nanoparticles, including Fe and Ag (Gallo et al. 2019), Fe and Cu (Hu et al. 2010) and Fe and Ni (Zhou et al. 2014c; Mansouriieh et al. 2016).

The iron oxides magnetite and maghemite exhibit a spinel crystal structure (Tombácz et al. 2015); however, the magnetite, $Fe_3O_4$, presents Fe cations in the divalent and trivalent state coordinated by $O^{2-}$ ions in the interstitial tetrahedral and octahedral sites, whereas maghemite, ɣ-$Fe_2O_3$, presents Fe cations only in the trivalent state (Shokrollahi 2017; Abdullah et al. 2019). Both are ferrimagnetic at room temperature as a result of super-exchange interactions between magnetic ions and $O^{2-}$. Bulk magnetite possesses high saturation magnetization among the different iron oxides of around 92–100 emu/g. Maghemite has a saturation magnetization lower values than that of magnetite, ranging from 60 to 80 emu/g (Ramimoghadam et al. 2014). In contrast, iron oxide nanoparticles that are smaller than 20 nm often display superparamagnetic behavior at room temperature and magnitude of saturation magnetization lower than that bulk magnetic materials, although magnetic properties depend strongly on the nanoparticles shape and the methods used in the synthesis (Teja and Koh 2009; Chen et al. 2016a). Larraza et al. (2012) used the solvothermal method for the synthesis of $Fe_3O_4$ nanoparticles and obtained cube-shaped structures with a saturation magnetization of 87.4 emu/g. Values of saturation magnetization around 60 emu/g have been reported for spherical-shaped $Fe_3O_4$ nanoparticles synthesized by the coprecipitation method (Davodi et al. 2017; Huong et al. 2018).

Another group of iron oxides that have recently attracted attention is the spinel ferrites, whose general composition is $MF_2O_4$, where M is Li, Ni, Mg, Zn, Cu, Co, Mn, among others (Chen et al. 2016a; Singh et al. 2018). Compared to magnetite, spinel ferrites nanoparticles have more strong magnetic proprieties (Reddy and Yun 2016; Nadar et al. 2018). Studies show that $Fe_3O_4$ magnetization can be improved by incorporating a metal element into the structure (Xu et al. 2013; Bakhshayesh and Dehghani 2014). Typically, saturation magnetization of nanometer-sized magnetite was reported as about 50 emu/g (Liu et al. 2012a). Besides, ferrites generally have high stability in an acid medium (Tu et al. 2012a, b).

Different methods can be used to synthesize iron oxide nanoparticles (Teja and Koh 2009), including coprecipitation (Sun et al. 2014), sol-gel (Stanicki et al. 2015), hydrothermal (Mao et al. 2016), and solvothermal (Chella et al. 2015). Coprecipitation is widely reported as a relatively simple and low-cost method (Xu et al. 2012b; Mohammed et al. 2017; Shokrollahi 2017). The formation of magnetite and maghemite occurs from aqueous precipitation of Fe(II) and Fe(III) salts with alkali at a suitable aging time (Chen et al. 2016a). Maghemite can also be formed from the oxidation of magnetite (Shokrollahi 2017). The chemical reactions expressed by Eqs. (1) and (2) present the formation of magnetite and maghemite from the oxidation of magnetite (Ramimoghadam et al. 2014).

$$Fe^{2+}_{(aq)} + 2Fe^{3+}_{(aq)} + 8OH^{-}_{(aq)} \rightarrow Fe_3O_{4_{(s)}} + 4H_2O_{(l)} \quad (1)$$

$$Fe_3O_{4_{(s)}} + 2H^{+}_{(aq)} \rightarrow \gamma - Fe_2O_{3_{(s)}} + Fe^{2+}_{(aq)} + H_2O_{(l)} \quad (2)$$

Generally, the irreversible aggregation of magnetic nanoparticles is inevitable due to van der Waals interactions and magnetic forces, which decreases the surface area and limits the sorption capacity (Arancibia-Miranda et al. 2016; Martínez-Fernández and Komárek 2016). Also, as iron tends to oxidize, the stability of the magnetic nanoparticles is compromised in an aqueous medium. Thus, a typical method is to use matrix materials to isolate, accommodate, and stabilize magnetic nanoparticles, forming a magnetic nanocomposite (Chen et al. 2016a; Zhang et al. 2016). Several matrices can be employed to form a magnetic nanocomposite and will be presented and discussed in the following section.

## Synthesis and characterization of magnetic nanocomposites

The magnetic nanocomposite is a multiphase material in which at least one of the constituent phases is a magnetic nanoparticle. In general, the magnetic nanocomposite is prepared by embedding magnetic nanoparticles into various materials, such as polymers, silica, and carbon (Behrens and Appel 2016), nominated as matrix. Nanocomposites can combine the advantages of two or more materials with distinct physicochemical properties and are promising to be applied in many processes, such as water and wastewater treatment (Abdullah et al. 2019; Khan and Malik 2019).

Magnetic nanoparticles can be incorporated into inorganic or organic matrices (Zhang et al. 2016; Wang et al. 2018), depending on the characteristics of the material used (Chen et al. 2016a). For example, the magnetic nanoparticles may be coated by a coating agent, eg., silica or dispersed in the pores of carbonaceous material, eg., activated carbon (Baghdadi et al. 2016). Figure 2 illustrates the structure of some typical magnetic nanocomposites. In some cases, to obtain higher stability, magnetic nanoparticles or magnetic nanoparticles matrix can be functionalized. In many works, functionalization is performed by the insertion of amino groups (Donia et al. 2012; Guo et al. 2014; Zhou et al. 2014a; Masoumi et al. 2016; Kheshti and Hassanajili 2017; Li et al. 2017b; Langeroudi and Binaeian 2018).

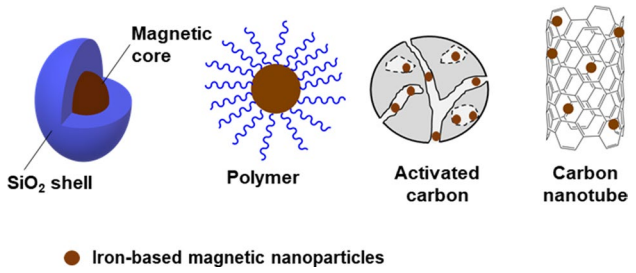


**Fig. 2** Typical iron-based magnetic nanocomposites that can be synthesized by embedding magnetic nanoparticles into various materials such as silica, polymer, activated carbon, and carbon nanotube

Different approaches to the preparation of magnetic nanocomposites are described in the literature. The core–shell structure nanocomposites are prepared from the encapsulation of the magnetic nanoparticles in a matrix, which acts coating the magnetic core (Lu and Astruc 2018; Nadar et al. 2018). Alternatively, core–shell type nanocomposites can be prepared coating layer by layer, in which the magnetic nanoparticles are functionalized and subsequently coated (Nadar et al. 2018). Core–shell structures are represented by X@Y, where X is the core and Y is the shell. For non-core–shell structure nanocomposites, the most used technique is the mixing of magnetic nanoparticles with the matrix under the influence of sonication to prevent aggregation. The magnetic nanoparticles can be synthesized separately and then mixed with the matrix or synthesized together with the matrix (Chen et al. 2016a; Li et al. 2018).

The determination of the physical and chemical properties of the material prepared is fundamental to evaluate the efficiency of the adopted synthesis and correlates to performance material as adsorbent (Mehta et al. 2015; Singh et al. 2018). Different analytical techniques are employed to characterize iron-based magnetic nanocomposites. X-ray diffraction, transmission electron microscopy, scanning electron microscopy, saturation magnetization, and nitrogen sorption are the most used techniques. Other analytical techniques are also used, such as Fourier transform infrared spectroscopy and photoelectron X-ray spectroscopy. If taken together, the analytical techniques are complementary and provide information on the morphology, structure, texture, and composition of the magnetic nanoparticles (Ramimoghadam et al. 2014; Dendisová et al. 2018).

Therefore, the synthesis and characterization techniques of magnetic nanocomposites of inorganics and organics matrices applied for water treatment by adsorption are discussed, with the emphasis on toxic elements, pesticides, and pharmaceutical-derived compounds. Table 1 summarizes the main data reported about the subject.

## Magnetic iron-inorganics nanosorbents

The majority widely used inorganic materials for the synthesis of magnetic nanocomposites for adsorptive purposes are activated carbon, carbon nanotubes, zeolites, clays, and minerals (Chen et al. 2016a; Zhang et al. 2016; Lu and Astruc 2018), where the clay minerals (Arancibia-Miranda et al. 2016; Javanbakht et al. 2016), zeolite (Liu et al. 2014a; Arancibia-Miranda et al. 2016), hydroxyapatite (Dong et al. 2010; Feng et al. 2010; Zhuang et al. 2015), and silica-based materials (Zhang et al. 2013; Kheshti and Hassanajili 2017; Peng et al. 2018) were the most studied.

Many materials are naturally occurring, relatively low cost, and environment-friendly (Zhang et al. 2016) and are applied in the removal of toxic elements in aqueous solution (Zhang et al. 2013; Zhuang et al. 2015; Javanbakht et al. 2016; Kheshti and Hassanajili 2017). However, inorganic materials can be easily functionalized, enabling the adsorption of organic pollutants (Chen et al. 2016a). Amino groups can be used, and the introduction onto the surface of magnetic nanoparticles usually occurs by grafting technique. Due to the good structure preservation of nanoparticles after post-modification, grafting technique has become the more common method in performing surface modification of nanocomposites, mainly toward silica bases materials (Wang et al. 2010; Egodawatte et al. 2015; Kheshti and Hassanajili 2017).

Nevertheless, grafting technique requires long reaction times and uses toxic organic solvents, eg., toluene. Aiming strategy to more environmentally friendly, the functionalization of magnetic nanoparticles surface can be performed by direct synthesis (Zhang et al. 2013). The preparation of molecules that have amino groups is introduced into the reaction medium at the end of the synthesis (Qu et al. 2011).

### Silica-based nanomaterials

Silica is one of the most used inorganic materials in the preparation of magnetic nanocomposites for the treatment of water by adsorption due to good chemical stability, large specific surface area and structure that allows functionalization (Tombácz et al. 2015; Morin-Crini et al. 2019). Silica can act as a coating of the magnetic nanoparticles that will be dispersed in a carbonaceous or polymeric matrix, for example, or act as a mesoporous matrix to disperse and stabilize the magnetic nanoparticles (Mallakpour and Naghdi 2018).

In the majority works reported in the literature, silica-based magnetic nanocomposites are prepared by employing magnetite as silica-coated magnetic nanoparticles. In general, Stöber's method is used for coating magnetite nanoparticles with a silica shell, where the sol-gel method is used through the tetraethoxysilane hydrolysis and subsequent

**Table 1** Methods of synthesis and features of magnetic iron oxide nanocomposites

| Magnetic nanosorbent | Synthesis of magnetic nanocomposite | | | | | Magnetic nanosorbent features | | | | References |
|---|---|---|---|---|---|---|---|---|---|---|
| | MNPs | Matrix | Functionalizing agent | Preparation method of MNPs | Synthesis conditions of MNPs | Size (nm) | $S_{BET}$ ($m^2$/g) | $M_s$ (emu/g) | $pH_{pzc}$ | |
| $Fe_3O_4$@$SiO_2$ | $Fe_3O_4$ | Silica | – | Coprecipitation | Precursor(s):$FeCl_2.4H_2O$ and $FeCl_3.6H_2O$ (molar ratio 1:2)<br>Base: $NH_4OH$ | 11 | – | 31.5 | – | Emadi et al. (2013) |
| $Fe_3O_4$@$SiO_2$–$NH_2$ | $Fe_3O_4$ | Silica | APTMS | Solvothermal | Precursor(s): $FeCl_3.6H_2O$<br>Solvent: ethyleneglycol<br>Heating at 200 °C for 12 h | 20 | 138 | 29.3 | 6.5 | Zhang et al. (2013) |
| $Fe_3O_4$@$SiO_2$–$NH_2$ | $Fe_3O_4$ | Silica | APTMS | Coprecipitation | Precursor(s): $FeCl_2.4H_2O$ and $FeCl_3.6H_2O$<br>Base: NaOH | 12 | 216 | 34 | | Wang et al. (2010) |
| $Fe_3O_4$–$SiO_2$–$NH_2$ | $Fe_3O_4$ | Silica | APTES | Coprecipitation | Precursor(s):$FeCl_2.4H_2O$ and $FeCl_3.6H_2O$ (molar ratio 1:1)<br>Base: $NH_4OH$ | 3.2 | 540 | 4.4 | 5.4 | Egodawatte et al. (2015) |
| $Fe_3O_4$@$SiO_2$@meso-$SiO_2$–$NH_2$ | $Fe_3O_4$ | Silica | APTES | Coprecipitation | Precursor(s):$FeCl_2.4H_2O$ and $FeCl_3.6H_2O$ (molar ratio 1:1)<br>Base: $NH_4OH$ | 15–20 | 617 | 32 | 6.3 | Kheshti and Hassanajili (2017) |
| γ-$Fe_2O_3$-SBA-15 | γ-$Fe_2O_3$ | SBA-15 | – | Acidic hydrolysis | Precursor(s): $FeSO_4.7H_2O$ | 10 | 1049 | 6.23 | – | Peng et al. (2018) |
| $Fe_3O_4$–zeolite | $Fe_3O_4$ | Zeolite | – | In situ coprecipitation | Precursor(s): $FeSO_4.7H_2O$ and $FeCl_3.6H_2O$<br>Base: NaOH | 10–20 | 126 | – | – | Salem Attia et al. (2014) |
| $Fe_3O_4$–zeolite | $Fe_3O_4$ | Zeolite | – | Coprecipitation | Precursor(s):$FeCl_2.4H_2O$ and $FeCl_3.6H_2O$ (molar ratio 1:1)<br>Base: $NH_4OH$ | 13 | 572 | 3.7 | – | Yuan et al. (2011) |
| Chitosan–clinoptilolite–$Fe_3O_4$ | $Fe_3O_4$ | Clinoptilolite (Zeolite) | Chitosan | In situ coprecipitation | Precursor(s): $FeCl_2.4H_2O$ and $FeCl_3.6H_2O$ (molar ratio 2:1)<br>Base: NaOH | – | 28 | 9.50 | – | Javanbakht et al. (2016) |
| Sepiolite–$Fe_3O_4$ | $Fe_3O_4$ | Sepiolite (Clay) | – | In situ coprecipitation | Precursor(s): $FeSO_4.7H_2O$ and $FeCl_3.6H_2O$<br>Base: $NH_4OH$ | – | 112 | 31.82 | 7.7 | Liu et al. (2014a) |
| $Fe_3O_4$–montmorillonite | $Fe_3O_4$ | Montmorillonite (Clay) | – | In situ coprecipitation | Precursor(s): $FeCl_2.4H_2O$ and $FeCl_3.6H_2O$ (molar ratio 2:1)<br>Base: NaOH | 8.3 | 211 | 2.9 | – | Kalantari et al. (2015) |
| $Fe_3O_4$–PEI–montmorillonite | $Fe_3O_4$ | Montmorillonite (Clay) | PEI | Solvothermal | Precursor(s): $Fe(acac)_3$<br>Solvent: benzyl ether<br>Heating at 290 °C for 1 h | 30–50 | – | 4.2 | 8.3 | Larraza et al. (2012) |
| $Fe_3O_4$–bentonite | $Fe_3O_4$ | Bentonite (Clay) | – | Solvothermal | Precursor(s): $FeCl_3.6H_2O$<br>Solvent: ethyleneglycol<br>Heating at 200 °C for 8 h | 10–50 | 111 | 22.7 | – | Yan et al. (2016) |

**Table 1** (continued)

| Magnetic nanosorbent | Synthesis of magnetic nanocomposite | | | | | Magnetic nanosorbent features | | | | References |
|---|---|---|---|---|---|---|---|---|---|---|
| | MNPs | Matrix | Functionalizing agent | Preparation method of MNPs | Synthesis conditions of MNPs | Size (nm) | $S_{BET}$ ($m^2$/g) | $M_s$ (emu/g) | $pH_{pzc}$ | |
| $Fe_3O_4$–bentonite | $Fe_3O_4$ | Bentonite (Clay) | – | In situ coprecipitation | Precursor(s):$FeCl_2.4H_2O$ and $FeCl_3.6H_2O$ (molar ratio 2:1)<br>Base: NaOH | 10 | 141 | – | – | Hashemian et al. (2015) |
| $MnFe_2O_4$–bentonite | $MnFe_2O_4$ | Bentonite (Clay) | – | Sol–gel | Precursor(s): $Fe(NO_3)_3$ and $Mg(NO_3)_2$<br>Base: $NH_4OH$<br>Citric acid<br>Calcination at 300 °C for 3 h | 50–55 | 75 | 5.69 | – | Kaur et al. (2015) |
| Hydroxyapatite–$Fe_3O_4$ | $Fe_3O_4$ | Hydroxyapatite | – | In situ coprecipitation | Precursor(s): $FeCl_2.4H_2O$ and $FeCl_3.6H_2O$<br>Base: $NH_4OH$ | 30 | 59.4 | 26.7 | – | Zhuang et al. (2015) |
| Hydroxyapatite–$Fe_3O_4$ | $Fe_3O_4$ | Hydroxyapatite | – | In situ coprecipitation | Precursor(s):Fe(II) and Fe(III) (molar ratio 1:2)<br>Base: $NH_4OH$ | 9.38 | 109 | – | 6.95 | Dong et al. (2010) |
| Hydroxyapatite–$Fe_3O_4$ | $Fe_3O_4$ | Hydroxyapatite | – | In situ coprecipitation | Precursor(s): $FeCl_2.4H_2O$ and $FeCl_3.6H_2O$<br>Base: $NH_4OH$ | – | 143 | 59.4 | – | Feng et al. (2010) |
| $Fe_3O_4$@hydroxyapatite | $Fe_3O_4$ | Hydroxyapatite | L-aspartic acid | Solvothermal | Precursor(s): $FeCl_3.6H_2O$<br>Solvent: ethyleneglycol<br>Heating at 200 °C for 10 h | 10–20 | – | 43.9 | | Yang et al. (2014a) |
| $Fe_3O_4$–cellulose–$NH_2$ | $Fe_3O_4$ | Cellulose | TEP | In situ coprecipitation | Precursor(s):$FeSO_4.7H_2O$ and $FeCl_3.6H_2O$ (molar ratio 1:2)<br>Base: NaOH | 0.7–1.2 | 138 | – | | Donia et al. (2012) |
| $Fe_3O_4$@$SiO_2$@cellulose@$NH_2$ | $Fe_3O_4$ | Cellulose | EDA | Coprecipitation | Precursor(s):$FeSO_4.7H_2O$ and $FeCl_3.6H_2O$ (molar ratio 1:1)<br>Base: NaOH | 10.6 | – | 10.1 | 7.92 | Sun et al. (2014) |
| $Fe_3O_4$–bacterial cellulose | $Fe_3O_4$ | Bacterial cellulose | – | Coprecipitation | Precursor(s):$FeCl_2.4H_2O$ and $FeCl_3.6H_2O$ (molar ratio 1:1)<br>Base: NaOH | 15 | – | 41 | – | Zhu et al. (2011) |
| $Fe_3O_4$–chitosan–cyanoguanidine | $Fe_3O_4$ | Chitosan | Cyanoguanidine | Coprecipitation | Precursor(s): $FeCl_2.4H_2O$ and $FeCl_3.6H_2O$<br>Base: $NH_4OH$ | 20 | – | 21.6 | – | Wang et al. (2013) |
| $Fe_3O_4$–chitosan–PIB | $Fe_3O_4$ | Chitosan | PIB | Coprecipitation | Precursor(s): $FeCl_2.4H_2O$ and $FeCl_3.6H_2O$<br>Base: $NH_4OH$ | 100 | – | 29.6 | – | Gutha and Munagapati(2016) |
| $Fe_3O_4$–$SiO_2$–chitosan–EDTA | $Fe_3O_4$ | Chitosan | EDTA | Solvothermal | Precursor(s): $FeCl_3.6H_2O$<br>Solvent: ethyleneglycol<br>Heating at 200 °C for 10 h | – | 1.0 | 18.2 | – | Ren et al. (2013) |
| $Fe_3O_4$@$SiO_2$–quaternary chitosan | $Fe_3O_4$ | Quaternary chitosan | TEOS | Coprecipitation | Precursor(s): $FeSO_4.7H_2O$<br>Base: $NH_4OH$ | 90 | 5 | – | 7.5 | Soares et al. (2019) |

**Table 1** (continued)

| Magnetic nanosorbent | Synthesis of magnetic nanocomposite | | | | | Magnetic nanosorbent features | | | | References |
|---|---|---|---|---|---|---|---|---|---|---|
| | MNPs | Matrix | Functionalizing agent | Preparation method of MNPs | Synthesis conditions of MNPs | Size (nm) | $S_{BET}$ ($m^2$/g) | $M_s$ (emu/g) | $pH_{pzc}$ | |
| $CoFe_2O_4$–alginate | $CoFe_2O_4$ | Alginate | – | Coprecipitation | Precursor(s):$Fe(NO_3)_3{\cdot}9H_2O$ and $Co(NO_3)_2{\cdot}6H_2O$<br>Base: NaOH | 27 | – | 24.64 | 5.5 | Esmat et al. (2017) |
| $NiFe_2O_4$–alginate | $NiFe_2O_4$ | Alginate | – | Coprecipitation | Precursor(s):$FeCl_3.6H_2O$, $NiCl_2.6H_2O$and$FeSO_4.7H_2O$<br>Base: NaOH | 9 | – | 15.04 | 6 | Bakr et al. (2015) |
| ɣ-$Fe_2O_3$–alginate | ɣ-$Fe_2O_3$ | Alginate | – | Coprecipitation | Precursor(s): $FeCl_2.4H_2O$ and $FeCl_3.6H_2O$<br>Base: $NH_4OH$ | 9 | | 35 | | Idris et al. (2012) |
| ɣ-$Fe_2O_3$–alginate | ɣ-$Fe_2O_3$ | Alginate | – | Coprecipitation | Precursor(s): $FeCl_2.4H_2O$ and $FeCl_3.6H_2O$<br>Base: $NH_4OH$ | 2 | – | 32.2 | – | Bée et al. (2011) |
| $Fe_3O_4$–alginate | $Fe_3O_4$ | Alginate | – | In situ coprecipitation | Precursor(s): $FeCl_2.4H_2O$ and $FeCl_3.6H_2O$<br>Base: $NH_4OH$ | 22 | – | 45.6 | – | Lakouraj et al. (2014) |
| $Fe_3O_4$@polyaniline | $Fe_3O_4$ | Polydopamine | – | Coprecipitation | Precursor(s): $FeCl_2.4H_2O$ and $FeCl_3.6H_2O$<br>Base: $NH_4OH$ | 15 | 124 | 44.7 | 3.04 | Davodi et al. (2017) |
| $Fe_3O_4$@$NH_2$–polydopamine | $Fe_3O_4$ | Polydopamine | APTMS | Coprecipitation | Precursor(s): $FeCl_2.4H_2O$ and $FeCl_3.6H_2O$<br>Base: $NH_4OH$ | – | 26.5 | 10.66 | 4.0 | Li et al. (2017b) |
| $Fe_3O_4$@polyaniline | $Fe_3O_4$ | Polyaniline | – | Solvothermal | Precursor(s): $FeCl_3.6H_2O$<br>Solvent: glycol<br>Heating at 200 °C for 12 h | 30–50 | – | 58.1 | – | Han et al. (2013) |
| Polyaniline–ɣ-$Fe_2O_3$ | ɣ-$Fe_2O_3$ | Polyaniline | – | Coprecipitation | Precursor(s):$FeCl_2.4H_2O$ and $FeCl_3.6H_2O$ (molar ratio 2:1)<br>Base: $NH_4OH$ | 51–148 | 60 | 30 | – | Chávez-Guajardo et al. (2015) |
| $Fe_3O_4$–$NH_2$–molecularly imprinted polymer | $Fe_3O_4$ | Molecularly imprinted polymer | TETA | Solvothermal | Precursor(s): $FeCl_3.6H_2O$<br>Solvent: ethyleneglycol<br>Heating at 200 °C for 10 h | 27.9 | – | 35 | – | Masoumi et al. (2016) |
| $Fe_3O_4$@C | $Fe_3O_4$ | Carbon | – | Hydrothermal | Precursor(s): $Fe(NO_3)_3{\cdot}9H_2O$ and $FeCl_3.6H_2O$<br>Heating at 180 °C for 14 h | 20–50 | 79 | 9.91 | 7.3 | Mao et al. (2016) |
| $Fe_3O_4$@C | $Fe_3O_4$ | Carbon | – | Coprecipitation | Precursor(s):$FeCl_2.4H_2O$ and $FeCl_3.6H_2O$ (molar ratio 2:1)<br>Base: NaOH | 20 | – | 12.2 | | Huong et al. (2018) |
| $Fe_3O_4$@C | $Fe_3O_4$ | Carbon | | Hydrothermal | Precursor(s): $FeCl_3.6H_2O$<br>Heating at 200 °C for 10 h | 100 | 75 | 63.5 | – | Chen et al. (2016b) |
| Hydroxyapatite@C–$Fe_3O_4$ | $Fe_3O_4$ | Carbon | Hydroxyapatite | Coprecipitation | Precursor(s): $FeCl_2.4H_2O$<br>Base: $NH_4OH$ | 4–10 | 355 | 14 | – | Yang et al. (2015) |
| $Fe_3O_4$–activated carbon | $Fe_3O_4$ | Activated carbon | – | Coprecipitation | Precursor(s): $FeCl_2.4H_2O$ and $FeCl_3.6H_2O$<br>Base: $NH_4OH$ | 50 | 1241 | 5.06 | – | Baghdadi et al. (2016) |

**Table 1** (continued)

| Magnetic nanosorbent | Synthesis of magnetic nanocomposite | | | | | Magnetic nanosorbent features | | | | References |
|---|---|---|---|---|---|---|---|---|---|---|
| | MNPs | Matrix | Functionalizing agent | Preparation method of MNPs | Synthesis conditions of MNPs | Size (nm) | $S_{BET}$ ($m^2$/g) | $M_s$ (emu/g) | $pH_{pzc}$ | |
| $Fe_3O_4$–activated carbon | $Fe_3O_4$ | Activated carbon | – | Coprecipitation | Precursor(s): $FeCl_2.4H_2O$ and $FeCl_3.6H_2O$<br>Base: $NH_4OH$ | 44 | 1257 | 5.06 | – | Kang et al. (2016) |
| $Fe_3O_4$–activated carbon–chitosan | $Fe_3O_4$ | Activated carbon | Chitosan | Coprecipitation | Precursor(s): $Fe(NO_3)_3{\cdot}9H_2O$ and $FeSO_4.7H_2O$ (molar ratio 2:1)<br>Base: $NH_4OH$ | – | 204 | 5.78 | – | Danalıoğlu et al. (2017) |
| Multiwalled carbon nanotubes–N–$CoFe_2O_4$ | $CoFe_2O_4$ | Multiwalled carbon nanotubes | – | Hydrothermal | Precursor(s): $Fe(NO_3)_3{\cdot}9H_2O$ and $Co(NO_3)_3{\cdot}6H_2O$ (molar ratio 1:2)<br>Heating at 220 °C for 12 h | 25 | 134 | 43.6 | 3.0 | Wang et al. (2015a) |
| Multiwalled carbon nanotubes–$CoFe_2O_4$–$NH_2$–chitosan | $CoFe_2O_4$ | Multiwalled carbon nanotubes | Chitosan | Solvothermal | Precursor(s): $Fe(acac)_3$ and $CoCl_2.6H_2O$<br>Solvent: ethylene glycol<br>Heating at 200 °C for 8 h | 37.2 | 158 | 4.68 | – | Zhou et al. (2014a) |
| $Fe_3O_4$–multiwalled carbon nanotubes | $Fe_3O_4$ | Multiwalled carbon nanotubes | – | Coprecipitation | Precursor(s): $(NH_4)_2Fe(SO_4)_2.6H_2O$ and $NH_4Fe(SO_4)_2.12H_2O$<br>Base: $NH_4OH$ | 10–20 | – | 50.10 | 2.0 | Jiang et al. (2016) |
| $Fe_3O_4$–multiwalled carbon nanotubes | $Fe_3O_4$ | Multiwalled carbon nanotubes | – | Coprecipitation | Precursor(s): $FeCl_2.4H_2O$ and $FeCl_3.6H_2O$ (molar ratio 2:1)<br>Base: $NH_4OH$ | 18 | 92 | 5.06 | 2.0 | Gupta et al. (2011) |
| $Fe_3O_4$–multiwalled carbon nanotubes | $Fe_3O_4$ | Multiwalled carbon nanotubes | – | Coprecipitation | Precursor(s): $FeSO_4.7H_2O$<br>Base: NaOH | 40–100 | 21 | – | – | Hu et al. (2011) |
| $Fe_3O_4$@$SiO_2$–multiwalled carbon nanotubes | $Fe_3O_4$ | Multiwalled carbon nanotubes | TEOS | Solvothermal | Precursor(s): $Fe(acac)_3$ and $CoCl_2.6H_2O$<br>Solvent: ethylene glycol<br>Heating at 200 °C for 6 h | – | – | 47.7 | 4.1 | Zhou et al. (2014b) |
| Thiol-carbon nanotubes–$Fe_3O_4$ | $Fe_3O_4$ | Carbon nanotubes | MTPS | Solvothermal | Precursor(s): $Fe(acac)_3$ and $CoCl_2.6H_2O$<br>Solvent: triethylene glycol<br>Heating at 286 °C for 30 min | 6 | 97 | 22.85 | 2.0 | Zhang et al. (2012) |
| Graphene oxide–$Fe_3O_4$ | $Fe_3O_4$ | Graphene oxide | – | In situ coprecipitation | Precursor(s): $Fe(SO_4)_3$ and $FeSO_4.12H_2O$ (molar ratio 1:1)<br>Base: $NH_4OH$ | 10–20 | 341 | – | 5.9 | Su et al. (2017) |
| Graphene oxide–$Fe_3O_4$ | $Fe_3O_4$ | Graphene oxide | – | Solvothermal | Precursor(s): $Fe(acac)_3$<br>Solvent: triethylene glycol<br>Heating at 180 °C for 16 h | 50 | – | 37.28 | 4 | Nethaji and Sivasamy (2017) |
| Graphene oxide–$Fe_3O_4$ | $Fe_3O_4$ | Graphene oxide | – | In situ coprecipitation | Precursor(s): $FeCl_2.4H_2O$ and $FeCl_3.6H_2O$ (molar ratio 2:1) | 9.5 | 90 | 65 | – | Gupta et al. (2017) |

**Table 1** (continued)

| Magnetic nanosorbent | Synthesis of magnetic nanocomposite | | | | | Magnetic nanosorbent features | | | | References |
|---|---|---|---|---|---|---|---|---|---|---|
| | MNPs | Matrix | Functionalizing agent | Preparation method of MNPs | Synthesis conditions of MNPs | Size (nm) | $S_{BET}$ ($m^2$/g) | $M_s$ (emu/g) | $pH_{pzc}$ | |
| Graphene oxide–$Fe_3O_4$ | $Fe_3O_4$ | Graphene oxide | – | In situ coprecipitation | Precursor(s): $FeCl_3.6H_2O$ and $FeSO_4.7H_2O$<br>Base: $NH_4OH$ | 20 | 142 | 31 | 4.3 | Yang et al. (2012) |
| $Fe_3O_4$@graphene oxide | $Fe_3O_4$ | Graphene oxide | – | In situ coprecipitation | Precursor(s): $FeCl_3.6H_2O$ and $FeSO_4.7H_2O$ (molar ratio 2:1)<br>Base: $NH_4OH$ | 50 | 88 | 33.64 | – | Yang et al. (2018) |
| $Fe_3O_4$@$SiO_2$@graphene oxide–PEA | $Fe_3O_4$ | Graphene oxide | PEA | Coprecipitation | Precursor(s): $FeCl_2.4H_2O$ and $FeCl_3.6H_2O$ (molar ratio 2:1)<br>Base: $NH_4OH$ and hydrazine | 12.3 | 133 | 33 | 6.6 | Wanjeri et al. (2018) |
| EDTA–$Fe_3O_4$–graphene oxide | $Fe_3O_4$ | Graphene oxide | EDTA | Hydrothermal | Precursor(s): $FeCl_3.6H_2O$<br>Solvent: ethyleneglycol<br>Heating at 200 °C for 8 h | 42 | 50 | 28.9 | 4.1 | Cui et al. (2015) |
| Chitosan–$Fe_3O_4$–graphene oxide | $Fe_3O_4$ | Graphene oxide | Chitosan | In situ coprecipitation | Precursor(s): $FeCl_2.4H_2O$ and $FeCl_3.6H_2O$ (molar ratio 2:1)<br>Base: $NH_4OH$ | – | 152 | 49.30 | 6.8 | Sherlala et al. (2019) |
| Chitosan–$Fe_3O_4$–graphene oxide | $Fe_3O_4$ | Graphene oxide | Chitosan | In situ coprecipitation | Precursor(s): $FeCl_2.4H_2O$ and $FeCl_3.6H_2O$ (molar ratio 2:1)<br>Base: $NH_4OH$ | 15 | 133 | 3.82 | – | Hosseinzadeh and Ramin (2018) |
| $Fe_3O_4$–graphene oxide–$NH_2$ | $Fe_3O_4$ | Graphene oxide | Diethylenetriamine | Hydrothermal | Precursor(s): $FeCl_3.6H_2O$<br>Solvent: ethyleneglycol<br>Heating at 200 °C for 6 h | 17 | 58 | 30.2 | 3.4 | Zhao et al. (2016) |
| $MnFe_2O_4$–reduced graphene oxide | $MnFe_2O_4$ | Reduced graphene oxide | – | Solvothermal | Precursor(s): $FeCl_3{\cdot}6H_2O$ and $MnCl_2{\cdot}4H_2O$<br>Solvent: ethylene glycol<br>Heating at 200 °C for 10 h | 12–15 | 79 | 41.39 | – | Chella et al. (2015) |
| $Fe_3O_4$–reduced graphene oxide–thiourea dioxide | $Fe_3O_4$ | Reduced graphene oxide | Thiourea dioxide | In situ coprecipitation | Precursor(s): $FeCl_3.6H_2O$ and $FeSO_4.7H_2O$<br>Base: $NH_4OH$ | – | – | 4.38 | – | Yang et al. (2017) |
| $Fe_3O_4$–reduced graphene oxide | $Fe_3O_4$ | Reduced graphene oxide | – | In situ coprecipitation | Precursor(s): $FeCl_3.6H_2O$ and $FeSO_4.7H_2O$<br>Base: $NH_4OH$ | 20 | 273 | 31 | 4.8 | Yang et al. (2012) |
| $Fe_3O_4$–reduced graphene oxide–$NH_2$ | $Fe_3O_4$ | Reduced graphene oxide | Diethylenetriamine | Hydrothermal | Precursor(s): $FeCl_3.6H_2O$<br>Solvent: ethyleneglycol<br>Heating at 200 °C for 8 h | 38.5 | 62 | – | 3.5 | Guo et al. (2014) |

*MNPs* magnetic nanoparticles; $S_{BET}$ BET surface area; $M_s$ saturation magnetization; $pH_{pzc}$ pH of point of zero charge; *APTES* 3-aminopropyl triethoxysilane; *APTMS* 3-aminopropyl trimethoxysilane; *EDA* ethylenediamine; *EDTA* ethylenediaminetetraacetic acid; *MTPS* 3-mercaptopropyltriethoxysilane; *PEA* 2-phenylethylamine; *PEI* polyethyleneimine; *PIB* 4-((pyridin-2-ylimino) methyl) benzaldehyde; *SBA-15* mesoporous silica santa barbara amorphous-15; *TEOS* tetraethoxysilane; *TEP* tetraethylenepentamine; *TETA* triethylenetetramine

condensation of silicic acid in alcoholic solution (Stöber et al. 1968). Generally, the obtained nanomaterial exhibits uniform core–shell structure, $Fe_3O_4$@$SiO_2$, being applied for the adsorption of inorganic elements in aqueous systems.

In the studies reported by Emadi et al. (2013), $Fe_3O_4$@$SiO_2$ nanomaterial was synthesized by combining coprecipitation and sol-gel methods and applied to the removal of Zn(II) in aqueous solutions. The X-ray diffraction spectra revealed the formation of $Fe_3O_4$ crystalline phase with characteristic 2θ peaks at 30.4°, 35.6°, 43.3°, 57.3°, and 62.8°. The Fourier transform infrared spectrum exhibited adsorption bands around 580–610 $cm^{-1}$ corresponding to Fe–O bonds and are attributed to the formation of the $Fe_3O_4$ phase, while silica coating was confirmed by the bands at 970 and 1088 $cm^{-1}$ corresponding to symmetric stretching of Si–O and Si–O–Si, respectively. The transmission electron microscopy results of the $Fe_3O_4$@$SiO_2$ revealed the formation of nanospheres with an average diameter of 30 nm, while the saturation magnetization for $Fe_3O_4$ and $Fe_3O_4$@$SiO_2$ was 65.5 and 31.5 emu/g, respectively. The decrease in $Fe_3O_4$@$SiO_2$ saturation magnetization was explained by considering the diamagnetic contribution of the silica shells surrounding the $Fe_3O_4$ nanoparticles.

Similar materials were obtained by Wang et al. (2010) and Zhang et al. (2013) and applied to the removal of metal ions, but the nanospheres were functionalized with amino groups using 3-aminopropyl trimethoxysilane by grafting technique. The Fourier transform infrared spectrum exhibited adsorption bands at 1563 $cm^{-1}$ due to vibrational modes of N–H bonds that are attributed to amino groups, indicating that $–NH_2$ groups were introduced onto the surface of $Fe_3O_4$@$SiO_2$ particles. The insertion of amino groups was also be proved by pH of point of zero charge, whose value increased from 1.4 to 6.0 for $Fe_3O_4$@$SiO_2$ and $Fe_3O_4$@$SiO_2$–$NH_2$, respectively (Wang et al. 2010). In the works of Wang et al. (2010), saturation magnetization values toward $Fe_3O_4$ and $Fe_3O_4$@$SiO_2$–$NH_2$ were 68.0 and 34.0 emu/g, respectively. The materials synthesized by Zhang et al. (2013) had saturation magnetization of 63.9 emu/g for $Fe_3O_4$ and 29.3 emu/g for $Fe_3O_4$@$SiO_2$–$NH_2$. Therefore, the results suggest that the loading of $–NH_2$ on $Fe_3O_4$@$SiO_2$ had little influences on the magnetic properties of core–shell structure materials, as the saturation magnetization values for $Fe_3O_4$@$SiO_2$ and $Fe_3O_4$@$SiO_2$–$NH_2$ nanocomposites were approximate.

Another strategy to synthesize amino-functionalized $Fe_3O_4$@$SiO_2$ nanospheres was adopted by Kheshti and Hassanajili (2017) for aqueous Zn(II) removal. The magnetic nanoparticles were prepared by the coprecipitation method and coated of silica through a two-step, forming mesoporous magnetic nanocomposite. In the first step, the magnetic core $Fe_3O_4$ was coated by silica following the Stöber method. In the second step, $Fe_3O_4$@$SiO_2$ nanospheres were coated whit one more silica layer, forming the $Fe_3O_4$@$SiO_2$@meso–$SiO_2$ microspheres. The microspheres were functionalized with groups amino by grafting technique using 3-aminopropyl trimethoxysilane. The average pore size value of the $Fe_3O_4$@$SiO_2$@meso–$SiO_2$ was 2.85 nm, proving the formation of a mesoporous material. Saturation magnetization was 32 emu/g, which is in agreement with the values found for $Fe_3O_4$@$SiO_2$ nanospheres.

On the other hand, the specific surface area was larger than the area found for $Fe_3O_4$@$SiO_2$–$NH_2$ materials synthesized by Zhang et al. (2013) and Wang et al. (2010) due to the formation of a mesoporous silica shell, suggesting that a high specific surface area is desirable for materials that are employed in adsorption processes. Besides, a higher surface area can facilitate surface loading with amino groups, increasing the adsorption sites in the material.

Although the silica-based magnetic nanomaterials commonly have a spherical morphology, other particle shapes are observed. The method of synthesis and the conditions employed, eg., temperature, reagent ratio, and agitation form, may influence material morphology (Mallakpour and Naghdi 2018). Egodawatte et al. (2015) prepared a mesoporous $Fe_3O_4$–$SiO_2$–$NH_2$ material following a synthesis route similar to Kheshti and Hassanajili (2017), but with a single silica coating. Unlike the material obtained by Kheshti and Hassanajili (2017), the nanocomposite did not have a core–shell structure. Transmission electron microscopy images showed that iron oxide nanoparticles were embedded into the mesoporous silica. The surface area of the material was 540 $m^2$/g, which is a greaterthan other silica-based magnetic nanocomposites. Nevertheless, the saturation magnetization was lower than that reported values, being equal to 4.4 emu/g (Egodawatte et al. 2015). A possible reason is that the low-value saturation magnetization for nanocomposite may be related to the small saturation magnetization value of nanoparticles used. The saturation magnetization of $Fe_3O_4$ nanoparticles was 29 emu/g.

The use of maghemite as magnetic nanoparticles in silica-based materials is less common. In the studies of Peng et al. (2018), maghemite was incorporated into the matrix of a mesoporous silica called santa barbara amorphous-15. The typical synthesis of santa barbara amorphous occurs in acidic medium using the triblock copolymer called Pluronic P123 as an organic driver and tetraethoxysilane as a silica source (Li et al. 2010). The authors proposed a one-step method for the synthesis of ɣ-$Fe_2O_3$–santa barbara amorphous-15 nanocomposite without the addition of mineral acid. The ferrous sulfate solution was used as the precursor of iron oxide and acid source. The acidity generated by the $FeSO_4$ solution catalyzed the hydrolysis of tetraethoxysilane. Transmission electron microscopy images showed that ɣ-$Fe_2O_3$–santa barbara amorphous-15 exhibits highly ordered hexagonal matrix incorporates with magnetic nanoparticles of size about 10 nm estimated by X-ray

diffraction. The material presented the average pore size of 5.8 nm, confirming as a mesoporous material. The surface area was 1043 $m^2$/g higher than that reported in other studies that used acid for the mesoporous silica called santa barbara amorphous-15 synthesis (Dai et al. 2012; Liang et al. 2013). However, saturation magnetization had a low value of 6.53 emu/g compared to other silica-based magnetic nanocomposites reported.

The data in Table 1 show that the specific surface area and saturation magnetization were the properties that had the most variable values varied for silica-based magnetic nanocomposites. In general, the mesoporous materials have a high specific surface area, and functionalization with amino groups led to a reduction in surface area and pore volume, as compared to non-functionalized material due to the presence of $–NH_2$ groups on the silica surface. For example, in the works of Egodawatte et al. (2015), the surface area and pore volume of $Fe_3O_4$–$SiO_2$ were 970 $m^2$/g and 0.7 $cm^3$/g, respectively, and for the $Fe_3O_4$–$SiO_2$–$NH_2$ the values were 540 $m^2$/g and 0.38 $cm^3$/g. However, the presence of $–NH_2$ groups is desirable because of metal ion adsorption, and the groups can act as complexation sites (Wang et al. 2010).

Based on the presented above, materials with core–shell structures showed the highest saturation magnetization values. In core–shell structure, the magnetic nanoparticle coating with silica acts as a protective layer, stabilizing the magnetic nanoparticles. Although the studies suggest the formation of magnetite, there is also the formation of maghemite from the oxidation of $Fe_3O_4$. Since maghemite has a saturation magnetization value lower than magnetite, the magnetic properties of the nanocomposite will depend on the stability of the magnetic nanoparticles. Despite the difference in saturation magnetization values for the materials presented in Table 1, all exhibited superparamagnetic behavior and were of easy separation of the aqueous solution by the external magnetic field. In Table 1, it is possible to observe that coprecipitation is widely employed for the synthesis of magnetic iron oxide; however, the major drawback of the coprecipitation method is difficult to control the particle size and shape (Qu et al. 2011).

On the other hand, in the solvothermal method, controlling the particle size and shape is simpler, once the temperature and pressure of synthesis are controlled (Abdullah et al. 2019). Nonetheless, the magnetic nanoparticles obtained by the solvothermal method in the work conducted by Zhang et al. (2013) had mean particle size values of 7 nm, and saturation magnetization values of 63.9 emu/g, which were similar to the values found for $Fe_3O_4$ obtained by the coprecipitation method, with size range 11–12 nm and saturation magnetization 68–65.5 emu/g (Wang et al. 2010; Emadi et al. 2013). Due to the cost-effectiveness and green approach, the coprecipitation method is more viable for the preparation of nanocomposites.

### Clay-mineral and zeolites-based nanomaterials

Among the different materials used for the synthesis of magnetic nanocomposites, clay minerals and zeolites possess unique properties, since the interlayer spaces and edges provide sites to host and stabilize magnetic nanoparticles. Moreover, the surface can be modified by acids, alkalis, surfactants, or other organic matters, enabling the possibility of generating material with hydrophilic or hydrophobic characteristics. Also, the clay minerals and zeolites have the advantages of low cost and being environmentally friendly (Crane and Scott 2012). Some of the studies that used magnetic nanocomposites based on clay minerals and zeolites are reported in Table 1.

Zeolite is a hydrated aluminosilicate highly crystalline with a cage-like structure, containing exchangeable cations in the structure (Ji et al. 2012; Salem Attia et al. 2014). Due to the adsorbing properties, natural or synthetic zeolites have been combined with magnetic nanoparticles. Clay minerals also can be used as a matrix to obtain magnetic nanocomposites, and the most commonly reported clay for used is bentonite. Bentonite is part of the smectite group, in which the significant portion is montmorillonite (Kaur et al. 2015). Montmorillonite is a type 2:1 clay, characterized by laminar organization, consisting of two tetrahedral layers of silica and a central octahedral layer of aluminum oxide (Chen et al. 2015). Both zeolite and montmorillonite possess a negative charge due to the isomorphous substitution process, providing a high cation-exchange capacity of ions (Arancibia-Miranda et al. 2016).

In summary, in clay or zeolite nanocomposites, magnetic nanoparticles are dispersed on the matrix surface, where the morphologies should influence the performance. In zeolites, magnetic nanoparticles occupy the surface of zeolite forming clusters (Yamaura and Fungaro 2013). In clays, the nanocomposite morphology will depend on the type of the clay mineral used. For example, in sepiolite, a type 2:1 magnesium hydrosilicate, the magnetic nanoparticles are loaded onto the sepiolite fibrous structure (Liu et al. 2014a), while for the montmorillonite matrix, the magnetic nanoparticles cover the flaky structure of montmorillonite (Ai et al. 2011).

The most common procedure for the synthesis of zeolite-based magnetic nanocomposite consists of mixing magnetic nanoparticles with the zeolite matrix. Salem Attia et al. (2014) reported a one-step synthesis of maghemite-zeolite nanocomposite and evaluated the adsorptive capacity for arsenic in aqueous solution. Iron oxide was produced by coprecipitation in the presence of the matrix. The $Fe_3O_4$–zeolite was then oxidized in air at 300 °C for 3 h to obtain ɣ-$Fe_2O_3$–zeolite. The X-ray diffraction pattern of the ɣ-$Fe_2O_3$–zeolite showed characteristic peaks of the ɣ-$Fe_2O_3$ phase. Typical absorption bands of Fe–O bonds in ɣ-$Fe_2O_3$ structure around 628, 580, and 447 $cm^{-1}$ in the

infrared spectrum confirmed the formation of the maghemite phase. The magnetic nanoparticles addition to the zeolite increased the surface area value from 65 to 126 $m^2$/g for zeolite and ɣ-$Fe_2O_3$–zeolite, respectively. Javanbakht et al. (2016) also performed a one-step synthesis using chitosan-coated clinoptilolite for Pb(II) removal. In the dispersive energy spectroscopy spectrum, the peaks related to the binding energies of O, Na, Al, Si, K, Ca, $Fe_3O_4$, C, and N were observed, proving the formation of material chitosan–clinoptilolite–$Fe_3O_4$. The surface area for clinoptilolite–$Fe_3O_4$ was higher, 47 $m^2$/g, than that found for chitosan–clinoptilolite–$Fe_3O_4$, 28 $m^2$/g. However, the adsorption capacity was lower than that of chitosan–clinoptilolite–$Fe_3O_4$, which will be discussed further in "Application in adsorption processes" section, showing the importance of chitosan in the adsorption process of the evaluated metal. Saturation magnetization was also reduced from 39.21 emu/g to 9.50 emu/g for clinoptilolite–$Fe_3O_4$ and chitosan–clinoptilolite–$Fe_3O_4$, respectively. The decrease in saturation magnetization values was attributed to the chitosan coating layer. However, in practice, the nanocomposite was easily separated from the aqueous solution by a permanent magnet.

Some authors report that synthesis under the hydrothermal conditions improves nanoparticle dispersion on the zeolite surface. A better dispersion was verified in the work of Yuan et al. (2011), whose synthesis of $Fe_3O_4$–zeolite was conducted at 100 °C under hydrothermal conditions for 16 h. Transmission electron microscopy images revealed that the magnetic nanoparticles were well dispersed on the zeolite surface. Besides, $Fe_3O_4$–zeolite nanocomposite had a high surface area, 571 $m^2$/g, compared to other magnetic zeolites. On the other hand, saturation magnetization was low, 3.7 emu/g. The low saturation magnetization was attributed to the low $Fe_3O_4$ content in $Fe_3O_4$–zeolite nanocomposite, whose value was 5 wt%.

Due to excellent surface properties, montmorillonite is one of the most common clay minerals used in the manufacture of magnetic nanocomposites (Larraza et al. 2012). Several strategies have been followed to incorporate magnetic nanoparticles in the silicate clay structures, including coprecipitation of iron salts in a solution containing a clay suspension described in the work of Kalantari et al. (2015). $Fe_3O_4$–montmorillonite was prepared in one-step by coprecipitation of $Fe^{3+}$ and $Fe^{2+}$ salts with the 1:2 molar ratio in the presence of montmorillonite. Transmission electron microscopy images showed that $Fe_3O_4$–montmorillonite nanoparticles had a diameter of about 8.24 nm. The saturation magnetization for the nanocomposite was 2.9 emu/g. $Fe_3O_4$–montmorillonite exhibited superparamagnetic behavior; normally $Fe_3O_4$ nanoparticles less than 20 nm diameter show superparamagnetism (Teja and Koh 2009). The surface area of montmorillonite was 121 $m^2$/g, and the value increased with the addition of magnetic nanoparticles to 211 $m^2$/g (Kalantari et al. 2015). The enhancement in the surface area of montmorillonite after the functionalization with magnetic nanoparticles is commonly observed. The increase in surface area is attributed to an enhanced basal space of montmorillonite by the intercalation of Fe, a phenomenon reported for expandable clays (Arancibia-Miranda et al. 2016; Uddin 2017).

Another strategy was adopted by Larraza et al. (2012), in which the magnetic nanoparticles synthesized by the solvothermal method were coated with polyethyleneimine polymer. A cationic exchange achieved the intercalation of the magnetite nanoparticles coated with polyethyleneimine polymer among montmorillonite platelets. Transmission electron microscopy images indicated that the material showed a high degree of exfoliation of the montmorillonite sheets and good dispersion of $Fe_3O_4$ nanoparticles on both the surface and among the layers of the nanocomposite. X-ray diffraction patterns of montmorillonite and $Fe_3O_4$-polyethyleneimine-montmorillonite presented characteristic peaks at 2θ equal to 8.92° and 6.2°, corresponding to an interlayer distance of 0.99 and 1.42 nm, respectively. The increase in interlayer distance value was confirming the insert of polymer-coated nanoparticles between the layers of the clay. The increase is justified by the fact that montmorillonite is one of the most expandable minerals. The saturation magnetization value of $Fe_3O_4$ nanoparticles was 87.4 emu/g very close to the bulk values. However, a saturation magnetization for nanocomposite decreased, 4.2 emu/g. The authors attributed the reduction in saturation magnetization value to the lower content of magnetic nanoparticles in the nanocomposite.

In addition to the synthesis method, the magnetic nanoparticles/matrix ratio may influence the physicochemical and magnetic properties of the nanocomposite. Yan et al. (2016) synthesized the bentonite magnetic nanocomposites by the one-step solvothermal method using different mass ratio bentonite–Fe: bentonite–$Fe_3O_4$-0.5, bentonite–$Fe_3O_4$-1.0, bentonite–$Fe_3O_4$-2.0, and bentonite–$Fe_3O_4$-5.0. The nanocomposites exhibited sizes of about 10–50 nm and spherical shape, and showed characteristic X-ray diffractiondiffraction peaks and Fourier transform infrared spectroscopy absorption bands from the bentonite and $Fe_3O_4$ phases, indicating that the lamellar structure of bentonite was not collapsed at high temperature and pressure during the solvothermal reaction. Furthermore, all nanocomposites showed superparamagnetic behavior with saturation magnetization values for bentonite–$Fe_3O_4$-0.5, bentonite–$Fe_3O_4$-1.0, bentonite–$Fe_3O_4$-2.0, and bentonite–$Fe_3O_4$-5.0 of 37.4, 34.1, 22.7, and 15.1 emu/g, respectively, were lower than 46.6 emu/g of $Fe_3O_4$. On the other hand, the surface area of the nanocomposites was larger than the area values for pure bentonite and $Fe_3O_4$, whose values were 89, 104, 111, and 124 $m^2$/g for bentonite–$Fe_3O_4$-0.5, bentonite–$Fe_3O_4$-1.0,

bentonite–$Fe_3O_4$-2.0, and bentonite–$Fe_3O_4$-5.0, respectively. In the adsorption studies, the authors selected bentonite–$Fe_3O_4$-2.0 nanocomposite to evaluate removal metal ions due to the considerable surface area and magnetization of material. The coprecipitation synthesis also provided a $Fe_3O_4$–bentonite material similar to that obtained by the solvothermal method, with spherical particles of diameter around 10 nm and a surface area of 141 $m^2$/g (Hashemian et al. 2015).

Other methods such as sol-gel may also be used for the synthesis of clay mineral nanocomposites, although few studies are reported. Sol-gel method can lead to material contamination by side-products of the reactions, which result in a post-treatment of the products. Thus, synthesis can become difficult and time-consuming (Teja and Koh 2009). Kaur et al. (2015) synthesized a magnetic bentonite nanocomposite by the sol-gel method using $MgFe_2O_4$ ferrite as magnetic nanoparticles. Stoichiometric amounts of ferric nitrate and magnesium nitrate were added in 5 wt% bentonite solutioncontaining citric acid. Ammonium hydroxide solution was added dropwise, and the mixture was stirred for 10 h at 100 °C until a gel formed. The gel was dried and calcined at 300 °C for 3 h. X-ray diffraction analysis showed that the phase purity of $MgFe_2O_4$ was maintained during the synthesis process, but the presence of broad peaks of the nanocomposite suggests a lower ordering degree in $MgFe_2O_4$–bentonite. Saturation magnetization value for $MgFe_2O_4$ was 13.22 emu/g, and for $MgFe_2O_4$–bentonite was 5.69 emu/g. The lower saturation magnetization of $MgFe_2O_4$–bentonite was attributed to the addition of non-magnetic clay to magnetic nanoparticles. The specific surface area was 61 and 75 $m^2$/g for $MgFe_2O_4$ and $MgFe_2O_4$–bentonite, respectively. The small increase in the surface area may be related to the amount of bentonite used in nanocomposite synthesis (Kaur et al. 2015).

Although clay minerals have a more extensive application for metals removal, polar organic molecules can also interact with adsorption sites of the magnetic nanocomposites (Uddin 2017). Sepiolite was used as an adsorbent to remove the atrazine herbicide from aqueous solution (Liu et al. 2014a). The sepiolite–$Fe_3O_4$ nanocomposite was prepared by the coprecipitation method. The results showed that the specific surface area increased from 71 $m^2$/g for the natural sepiolite to 112 $m^2$/g in sepiolite–$Fe_3O_4$. The increase in the specific surface area is due to the expansion capacity of 2:1 clays, corroborating with the results presented by Kalantari et al. (2015) for montmorillonite.

As can be observed, the embedded of magnetic nanoparticles changes some properties of clays, such as surface area. Another property that can be modified is the adsorbent surface charges. The magnetite has a point of zero charge of pH 8.3 (Larraza et al. 2012), and $Fe_3O_4$ addition can shift the isoelectric point of magnetic nanocomposite to higher pH values. Moreover, the higher the iron ions concentration, the larger is the shift of isoelectric point toward higher pH. The phenomenon was observed by Liu et al. (2014a), whose non-magnetic sepiolite clay isoelectronic point changed from 6.9 to 7.7 for the magnetic sepiolite clay. Hence, controlling the content of nanoparticles in the nanocomposite during synthesis enables the possibility to obtain materials with an adequate point of zero charge for desired contaminant removal.

### Hydroxyapatite-based nanomaterials

It is considered the most important inorganic biomaterial and can be applied in different areas (Dong et al. 2016). In the case of water treatment, hydroxyapatite exhibits excellent potential in adsorb metals in naturals water and wastewater (Feng et al. 2010; Zhuang et al. 2015). To facilitate the separation from the water, hydroxyapatite has been combined with magnetic nanoparticles. In situ precipitation is the most common strategy of combining hydroxyapatite with magnetic nanoparticles. In brief, magnetic nanoparticles are added to the mixture solution of calcium salts, for example, $Ca(NO_3)_2$ and $CaCl_2$, and phosphate ion. Additionally, modifications in the synthesis route may result in materials with distinct morphologies and textural properties.

Dong et al. (2010) prepared a hydroxyapatite–$Fe_3O_4$ adsorbent for the removal of Pb(II) in aqueous solution. $Fe_3O_4$ nanoparticles were synthesized by coprecipitation, and hydroxyapatite was combined with $Fe_3O_4$ by in situ precipitation. The scanning electron microscopy micrographs showed that a nano-flake-like irregularly shaped particle composed the hydroxyapatite–$Fe_3O_4$ material. The specific surface area was 109 $m^2$/g. Feng et al. (2010) synthesized a hydroxyapatite magnetic nanocomposite to the adsorption of Cd(II) and Zn(II) by a similar route, but the mixture was aged at room temperature for 12–24 h without stirring. Scanning electron microscopy analysis revealed that hydroxyapatite–$Fe_3O_4$ had aspherical shape and formed aggregates, which resulted in a rough surface and porous structure. The specific surface area, 143 $m^2$/g, was one of the largest reported for magnetic hydroxyapatite, thus suggesting that the aging process should contribute to the increase in the porosity of the material. The saturation magnetization value was 59.4 emu/g, greater than the commonly reported value for pure magnetite nanoparticles. Therefore, the saturation magnetization value found for hydroxyapatite–$Fe_3O_4$ nanocomposite indicates the presence of another magnetic constituent besides magnetite. Maghemite presence was confirmed by X-ray diffraction analysis (Feng et al. 2010).

In situ precipitation was also the synthesis method employed by Zhuang et al. (2015), but $Ca^{2+}$ and $PO_4^{2-}$ ions were not simultaneously precipitated. Initially, $CaCO_3$–$Fe_3O_4$ was formed and following the

hydroxyapatite–$Fe_3O_4$. Also, sodium dodecyl sulfate was added as a surfactant, which acts as dispersing agents and stabilizing the nanoparticles. Scanning electron microscopy images showed that uniform nanoparticles constructed the hydroxyapatite–$Fe_3O_4$ microspheres obtained. Thus, sodium dodecyl sulfate may have played a significant role in achieving a monodisperse structure (Teja and Koh 2009; Tombácz et al. 2015), resulting in the surface area reduction with a value of 59 $m^2$/g, which is lower than the area for the materials obtained without the surfactant addition.

Core–shell structures can also be obtained for hydroxyapatite magnetic nanocomposites by surface-controlled precipitation. The synthesis of $Fe_3O_4$@hydroxyapatite nanocomposite was the focus of the work of Yang et al. (2014a). The researchers opted for the solvothermal method for the synthesis of magnetic nanoparticles to control the size and shape of nanoparticles. Also, $Fe_3O_4$ was functionalized with L-aspartic acid to facilitate the coating of magnetic nanoparticles with hydroxyapatite. From the scanning electron microscopy and transmission electron microscopy images obtained for the material present the formation of the core–shell structure. The magnetic properties of pure magnetite and $Fe_3O_4$@hydroxyapatite nanocomposite were evaluated, and both showed superparamagnetic behavior. Therefore, hydroxyapatite did not affect the magnetic behavior of magnetite in the nanocomposite. $Fe_3O_4$@hydroxyapatite had a saturation magnetization of 43.9 emu/g, which was ca. 49% of that of pure magnetite, in agreement with the composition of nanocomposite, with a $Fe_3O_4$/hydroxyapatite weight ratio of 1:1.

Elemental analysis techniques were used to indicate the experimental Ca/P molar ratio in the hydroxyapatite magnetic nanocomposite. In hydroxyapatite–$Fe_3O_4$ nanocomposite synthesized by Feng et al. (2010), the molar ratio Ca/P was determined by X-ray dispersive energy spectroscopy, and the value was 1.65. A similar value was found for $Fe_3O_4$@hydroxyapatite by inorganic analysis, which molar ratio Ca/P was 1.63 (Yang et al. 2014a). The experimental values are close to the stoichiometric ratio of the hydroxyapatite of 1.67, demonstrating that the synthesis strategy used was capable of fabricating magnetic adsorbent of hydroxyapatite (Feng et al. 2010).

## Magnetic iron-biopolymer nanosorbents

Magnetic nanoparticles can be incorporated into a polymer matrix through the porous structure of polymers. Concerning water treatment, biopolymers have some advantages compared to synthetic polymers such as non-toxicity, biocompatibility, biodegradability, and low cost (Donia et al. 2012). Therefore, biopolymers have been widely employed in water purification. Moreover, biopolymers exhibit characteristics such as hydrophilicity that allows a greater interaction of the adsorbent with the water molecules in comparison with synthetic polymer (Liu et al. 2012b). Chitosan, cellulose, and alginate are the most reported materials in literature as a polymeric matrix for magnetic nanoparticles (Lofrano et al. 2016; Brião et al. 2020). Researches on the use of magnetic biodegradable nanocomposites focus on biomedical applications, eg., magnetic resonance tomography, hypothermic-therapy, drug delivery (Spiridonov et al. 2017), although some studies have evaluated the potential as an adsorbent for water treatment according to Table 1.

Polymeric nanocomposites can be obtained by adopting three main strategies: (i) simple mixing of the components—the magnetic nanoparticles are directly introduced and grafted into the polymer; (ii) in situ synthesis of the nanoparticles—metal ions are preloaded into the polymer matrix and the target nanoparticles synthesized; (iii) in situ matrix polymerization—the magnetic nanoparticles are added during the polymerization of the monomers (Lofrano et al. 2016; Mallakpour and Naghdi 2018).

### Cellulose-basednanomaterials

Cellulose is the most abundant renewable biopolymer and very promising raw material available at low cost for the preparation of various functional polymers (Donia et al. 2012). Some studies report the use of cellulose as a sorbent, mainly in the removal of metallic ions (Hokkanen et al. 2013; Anirudhan et al. 2016). However, cellulose could not be satisfactorily applied in adsorbing pollutants (Hokkanen et al. 2013). Hence, studies on the application of materials based on magnetic cellulose have been carried out.

The application of cellulose is limited due to low adsorption capacity as well as low physical stability (Anirudhan et al. 2009; Luo et al. 2016). Therefore, in the preparation of cellulose-based magnetic nanocomposites, there is a need for chemical modification of the cellulose matrix. Some attempts have been made, including modification with amino groups (Donia et al. 2012). Graft copolymerization is one of the most promising methods for modification of the polymeric substances, for instance, lignocellulosic (Anirudhan et al. 2009). Amino-cellulose synthesis involves (1) grafting of glycidyl methacrylate using cerium initiated polymerization and (2) ring-opening reaction of epoxy groups with amine, such as ethylenediamine and tetraethylenepentamine (Sun et al. 2014). Donia et al. (2012) obtained a microporous material $Fe_3O_4$–cellulose–$NH_2$ with a pore diameter lower than 2 nm and surface area of 138 $m^2$/g employing copolymerization. The amino group content was determined volumetrically and found to be 6 mmol/g, confirming the functionalization of cellulose.

Sun et al. (2014) also opted for the cellulose modification with amino groups through glycidyl methacrylate grafting followed by reaction with ethylenediamine. In the study,

the magnetic nanoparticles were coated with silica because the nanocomposite was applied under acidic conditions. As discussed earlier, iron oxides materials tend to oxidize or dissolved under acidic conditions. $SiO_2$ has been reported to be a suitable supporting matrix to immobilize $Fe_3O_4$ due to stability in the acid environment. The saturated magnetization and isoelectric point values of $Fe_3O_4$@$SiO_2$@cellulose and $Fe_3O_4$@$SiO_2$@cellulose@$NH_2$ were measured to be 12.3 and 10.1 emu/g and 2.81 e 7.92, respectively. The decrease in saturation magnetization value was expected since $Fe_3O_4$@$SiO_2$@cellulose@$NH_2$ had a lower $Fe_3O_4$ content, 14.8%, compared to $Fe_3O_4$@$SiO_2$@cellulose, 19.1%. The increase in the isoelectric point after functionalization was attributed to the protonation of the amino groups present in $Fe_3O_4$@$SiO_2$@cellulose@$NH_2$, indicating that the nanocomposite was positively charged at pH below 7.92. The result was desirable for the removal of the studied contaminant, Cr(VI), as will be detailed below.

Another possibility of increasing the adsorption capacity of cellulose nanocomposites is to combine cellulose with materials with high surface area and surface modifiability. Clay is a good option due to biocompatibility and low toxicity. $Fe_3O_4$–bentonite–cellulose nanocomposite showed a high saturation magnetization, whose value was 78 emu/g (Luo et al. 2016). In contrast, the adsorption capacity was not improved as expected. The $Fe_3O_4$–bentonite-cellulose adsorption capacity for Pb(II) was 2.8 mg/g. For $Fe_3O_4$–bentonite, adsorption capacity was 81.5 mg/g for Pb(II) (Yan et al. 2016).

Cellulose-based magnetic nanocomposites can also be obtained by the biosynthetic route as a proposal for the green synthesis. Zhu et al. (2011) proposed the synthesis of a magnetic nanocomposite of bacterial cellulose via fermentation of *Gluconacetobacter xylinum*. Magnetic nanoparticles were synthesized by coprecipitation and embedding into bacterial cellulose with pH controlling. Nanocomposites with different $Fe_3O_4$ amounts were produced, obtaining a nanocomposite with a Fe content of 14% and another containing 33%. Increasing the Fe content in $Fe_3O_4$–bacterial cellulose nanocomposites from 14 to 33%, the corresponding saturated magnetization increased from 12 to 41 emu/g. The authors chose to use $Fe_3O_4$–bacterial cellulose 33% Fe in the adsorption tests. However, Cr(VI) adsorption capacity was 65 mg/g, lower than the value found for the amino-cellulose magnetic nanocomposite, 171.5 mg/g. Thus, functionalization with amino groups has been shown to improve cellulose performance for Cr(VI).

### Chitosan-based nanomaterials

Chitosan is the second most naturally abundant polysaccharide with singular characteristics such as high reactivity, excellent chelation behavior, and chemical stability, making chitosan one of the most studied adsorbents in the removal of several classes of pollutants (Ren et al. 2013; Shukla et al. 2015; He et al. 2016). The amino and hydroxyl groups of chitosan can act in reactive sites for chemical modification (Wang et al. 2017). Therefore, chemical modification of chitosan is of interest in the last years, either chitosan used as a polymer matrix for magnetic nanoparticles or as a functionalizing agent (Gutha and Munagapati 2016; Brião et al. 2020).

Chitosan can be prepared in various ways, depending on the application. In several studies, chitosan has been used in the form of flakes, powder, gel, and beads, as adsorbent. Although the flakes, or powder form, are the most used, in the adsorption processes the flakes morphology is a disadvantage due to the low porosity (Liu et al. 2012b); thus, chitosan beads have been employed in the synthesis of chitosan-based adsorbents. Chemical cross-linking of chitosan with glutaraldehyde is usually employed to improve the mechanical properties of biopolymer spheres (He et al. 2016).

Many approaches have been used to synthesize iron oxide chitosan nanocomposites, and the most used are (i) simple mixing of components and (ii) synthesis of magnetic nanoparticles in situ. The chitosan functionalization was also evaluated by chemical modification with cyanoguanidine (Wang et al. 2013), ethylenediaminetetraacetic acid (Ren et al. 2013), polyethyleneimine (Wang et al. 2017), Shiff's base as 4-((pyridine-2-illimino) methyl) benzaldehyde (Gutha and Munagapati 2016), among others. Fourier transform infrared spectroscopy was the main technique used to confirm the chemical modification of chitosan. In the spectrum of chitosan, the characteristic absorption bands appear around 3424 and 1376 $cm^{-1}$, due to the stretching vibrations of N–H and C–N bonds of amino groups, respectively (Ren et al. 2013). Chemical modifications of chitosan occur in the amino groups, where the bands tend to disappear, and new bands are formed, such as bands at 1637 and 1662 $cm^{-1}$ for amide and imine, respectively (Gutha and Munagapati 2016).

The specific surface area of magnetic chitosan nanocomposites reported in the studies was less than 10 $m^2/g$. For example, the specific surface area of unmodified magnetic chitosan nanocomposite and modified magnetic chitosan nanocomposite was 0.5 $m^2/g$ and 5.2 $mg^2/g$, respectively (Zhang et al. 2014; Soares et al. 2019). However, some studies pointed out that biopolymers such as chitosan are good sorbents of gases, which may decrease the accuracy of specific surface area measurement by the Brunauer–Emmett–Teller method. Thus, magnetic chitosan nanocomposites may have been underestimated for the specific surface area value (Zhang et al. 2014).

The magnetic properties of chitosan nanocomposites depend on the synthesis route employed. For the magnetic nanocomposite whose chitosan was not subjected to the

modification process, the saturation magnetization value was higher than the modified chitosan nanocomposites. In work conducted by Tran et al. (2010), the chitosan–$Fe_3O_4$ nanocomposite and the uncoated $Fe_3O_4$ nanoparticles showed saturation magnetization of 54 and 55 emu/g, respectively. Similar magnetization values were attributed to the thin chitosan coating that not affecting the magnetic properties of the beads. On the other hand, functionalization generally decreases the saturation magnetization of the magnetic nanocomposite. Gutha and Munagapati (2016) prepared $Fe_3O_4$ nanoparticles with the magnetization of 67.6 emu/g, but the value was reduced to 29.6 emu/g for 4-((pyridin-2-ylimino) methyl) benzaldehyde modified chitosan nanocomposite.

Also, the magnetization decrease for $Fe_3O_4$–chitosan-(4-((pyridine-2-illimino) methyl)) benzaldehyde may be due to the cross-linking of chitosan-(4-((pyridine-2-illimino) methyl)), which reduced the relative percentage of iron oxide in the nanocomposite. The decrease in saturation magnetization value was also observed for cyanoguanidine, and ethylenediaminetetraacetic acid modified chitosan nanocomposites, whose saturation magnetization values were 21.6 and 18.2 emu/g, respectively (Ren et al. 2013; Wang et al. 2013).

The presence of amino groups in the polymeric matrix provides excellent properties for chitosan in the adsorption of metal ions. Thus, most studies with magnetic chitosan nanocomposites aim at the removal of toxic metals in water. Despite the high magnetization value of non-functionalized chitosan magnetic nanocomposite, chitosan functionalization aims to increase the adsorption capacity. Chitosan has been widely used as a biosorbent to remove metal ions from aqueous solutions; however, few studies are on the removal of pharmaceutical-derived compounds and pesticides in water using chitosan.

To improve the adsorption capacity of chitosan nanocomposite for diclofenac antibiotic removal, Soares et al. (2019) proposed chemical modification of the chitosan surface with *N*-(2-hydroxypropyl)-3-trimethylammonium chloride to obtain quaternary chitosan. Quaternary chitosan was coupled with a silane group and then combined with silica-coated magnetic nanoparticles to form $Fe_3O_4$@$SiO_2$–Si-quaternary chitosan nanocomposite. The magnetic quaternary chitosan exhibited an adsorption capacity for diclofenac of 240.4 mg/g, which is four times greater the value observed for magnetic chitosan (Zhang et al. 2014).

### Alginate-based nanomaterials

Alginate is a non-toxic, biocompatible, and biodegradable biopolymer extracted from seaweed (Esmat et al. 2017). Alginate is composed of mannuronate and guluronate units, each containing one carboxylate group (Bée et al. 2011). The use of alginate-based materials as adsorbents is related mainly to the presence of carboxylic groups in the alginate structure, which enable alginate-based materials to form complexes with metal ions in aqueous solutions (Idris et al. 2012). The use of magnetic nanoparticles in alginate beads improves the adsorption capacity because of the increase in specific surface area (Bée et al. 2011). Citric acid is commonly used as a coating of magnetic nanoparticles (Bakr et al. 2015).

The most adopted strategy for the synthesis of alginate-based magnetic nanocomposites was the simple mixing of the components. Magnetic nanoparticles were prepared by coprecipitation and, in some cases, coated with citrate (Bée et al. 2011; Idris et al. 2012; Bakr et al. 2015). Gel alginate was the most commonly used material due to the easy handling compared to powder materials. In the presence of divalent cations, especially $Ca^{2+}$ ions, the alginate can easily form cross-linked gel matrices (Esmat et al. 2017; Bakr et al. 2015). In the synthesis of magnetic alginate nanocomposite, the magnetic nanoparticles are added in an alginate solution and mixed understirring in the presence of calcium chloride.

Based on the findings in the literature, maghemite and ferrite were the nanoparticles chosen for the preparation of magnetic alginate nanocomposites. ɣ-$Fe_2O_3$-alginate nanocomposites prepared by Bée et al. (2011)and Idris et al. (2012) exhibited similar magnetic properties with saturation magnetization values of 32.2 and 35.0 emu/g, respectively. In both works, a similar synthesis route was employed. Magnetite nanoparticles were prepared by coprecipitation and then oxidized to maghemite using ferric nitrate at 90 °C. The obtained maghemite was coated with citric acid and dispersed in water as citrate ferrofluids, while ɣ-$Fe_2O_3$–alginate was synthesized by adding citrate ferrofluid in an alginate solution. The suspension was then added dropwise into a $CaCl_2$ bath for the formation of the magnetic beads. Transmission electron microscopy images showed that the average size of the nanoparticles decreased from 15 to 9 nm when maghemite was coated with citrate. The scanning electron microscopy images showed that the pure alginate surface exhibited the smooth texture while the surface of the ɣ-$Fe_2O_3$–alginate was rough, indicating that the maghemite nanoparticles were entrapped in the polymer (Idris et al. 2012). Citrate ions have a significant role in the preparation of maghemite nanoparticles as citrate ions can enhance the dispersion of the nanoparticles in the polymer matrix, reducing aggregation of the magnetic nanoparticles. Citrate ions increases the stability of magnetic nanoparticles by providing the nanocomposite with high saturation magnetization compared to other biopolymer-based nanocomposites.

Alginate nanocomposites with ferrite were prepared similarly to maghemite nanocomposites. In the study by Esmat et al. (2017), cobalt ferrite was used uncoated with citrate ions. The saturation magnetization of $CoFe_2O_4$ was 48.5 emu/g, and for $CoFe_2O_4$–alginate there was a reduction of about 50%. Besides, both pure ferrite and nanocomposite did not exhibit superparamagnetic behavior. The hysteresis

loop indicated that the materials were ferrimagnetic, i.e., the materials remained magnetized in the absence of the external magnetic field.

Bakr et al. (2015) also synthesized alginate nanocomposite with nickel ferrite in a citrate medium. $NiFe_2O_4$ and $NiFe_2O_4$–alginate exhibited superparamagnetic behavior and saturation magnetization values, 21.8 and 15.4 emu/g, respectively, which corresponds to a decrease of approximately 30%. Compared to the Esmat et al. (2017) study, the citrate ions addition resulted in a stabilization of alginate nanocomposites' magnetic nanoparticles. Besides that, citrate might improve the material's adsorption capacity due to the presence of surface binding groups (Lofrano et al. 2016).

In situ coprecipitation synthesis has been reported for the preparation of alginate magnetic nanocomposites. Nanogel alginate was prepared by adding thiacalix[4]arenetetrasulfonate for greater material stability. Thiacalix[4]arenes are macrocyclic oligomers that can exist in a relatively rigid and stable cone structure. The nanogel was mixed with the iron salt solution for in situ coprecipitation of magnetic nanoparticles, resulting in a high saturation magnetization value of 45.6 emu/g. Scanning electron microscopy and transmission electron microscopy images showed that the magnetic nanogel had a rod-like morphology. X-ray diffraction analysis indicated that the nanocomposite had a crystalline structure, which justifies a high saturation magnetization value. Noteworthy that, the crystalline nature of the material can have contributed to a low adsorption capacity, between 13.5 and 20.0 mg/g, for the evaluated metal ions (Lakouraj et al. 2014).

## Magnetic iron-polymer nanosorbents

Adsorbents composed of magnetic cores and polymeric shells have received great concern recently in water treatment. The advantages of polymer-based magnetic nanocomposites are not only the easy and rapid separation of the aqueous solution in the presence of a magnetic field, but also the selectivity of magnetic polymer toward target pollutants. Also, the functional modification is possible by the specific ligand on the surface of polymeric matrixes to improve the adsorption capacity and selectivity (Zhao et al. 2014; Chávez-Guajardo et al. 2015).

The embedded magnetic nanoparticles in the polymeric matrix can be carried out either during the synthesis in an insitu or exsitu process (Lofrano et al. 2016). While the in situ method refers to the fabrication of nanoparticles from precursors with the presence of another phase material, the ex situ or post-synthesis method coats polymer pre-synthesized nanoparticles using specific processing, usually in situ polymerization (Davodi et al. 2017). The ex situ process is the most reported and, in most cases, yields core–shell nanoparticles. However, the synthesis of well-defined core–shell structured magnetic composites requires the surfactant-directing polymerization approach to modify and stabilize the magnetic cores (Han et al. 2013).

Conducting polymers appear as a promising material for the functionalization of magnetic nanoparticles; polyaniline deserves special attention because of the excellent environmental stability and the presence of electron-donating groups on the polymer chains (Han et al. 2013; Kumar and Jain 2014). Another polymer that has been reported as a matrix for magnetic nanoparticles is polydopamine due to the numerous surface-active functional groups, such as amino and hydroxyl groups (Li et al. 2017b).

Chávez-Guajardo et al. (2015) synthesized the polyaniline magnetic nanocomposite employing maghemite as a magnetic nanoparticle. Magnetic nanoparticles were prepared by the coprecipitation method, in which the formation of the maghemite phase was confirmed by Fourier transform infrared spectroscopy analysis. The spectrum exhibited characteristic peaks of Fe–O vibrational mode in 577 $cm^{-1}$ and 637 $cm^{-1}$, corresponding to the phase ɣ-$Fe_2O_3$. Polyaniline-ɣ-$Fe_2O_3$ nanocomposite was obtained by in situ polymerization using aniline as a precursor. Although sodium dodecyl sulfate surfactant was used in the synthesis, the material exhibited an irregular morphology. The surfactant-free synthesis via in situ polymerization has also been reported. Han et al. (2013) used by the solvothermal method for the synthesis of $Fe_3O_4$ nanoparticles, which led to the formation of the $Fe_3O_4$@polyaniline nanocomposite with well-defined core–shell structure. Both syntheses with surfactant and surfactant-free synthesis provided nanocomposites with similar adsorption capabilities of ca. 200 mg/g toward Cr(VI).

On the other hand, the $Fe_3O_4$@polyaniline nanocomposite obtained by the surfactant-free route presented a higher saturation magnetization than polyaniline-ɣ-$Fe_2O_3$ nanocomposite using surfactant. The saturation magnetization for $Fe_3O_4$@polyaniline was 58.1 emu/g, while for polyaniline-ɣ-$Fe_2O_3$, the saturation magnetization was 30 emu/g. The solvothermal method makes easy to control the size and shape and, consequently, the magnetic properties. Thus, contributing to the high saturation magnetization value in surfactant-free synthesis, maghemite has a saturation magnetization lower than magnetite.

Another way of synthesizing a magnetic polymer is to use the molecular imprinting technique, where template-shaped cavities are created in the polymer to form specific sites to generate a molecular recognition based on the enzyme–substrate recognition. According to Ekberg and Mosbach, "host–guest" or "template" polymerization terms are also used to refer to selective polymers (Ekberg and Mosbach 1989). The synthesis process is divided into the following three steps: (1) copolymer formation; (2) cross-linking of the copolymer in the presence of magnetic nanoparticles and the template molecules to form model molecules; and (3)

solvent washing for the removal of the template molecules from the polymeric matrix (Zheng et al. 2014).

The material prepared by the molecular imprinting technique has cavities capable of selectively retaining the template molecule. Thus, the molecular imprinting technique becomes useful for the preparation of materials that can adsorb molecules such as pesticides and pharmaceutical-derived compounds that are difficult to remove (Xu et al. 2012a). Besides, studies have shown that magnetic molecularly imprinted polymers have saturation magnetization value of 35.0 emu/g, which is greater than 22.0 emu/g of the corresponding magnetic non-imprinted polymer (Masoumi et al. 2016).

As with magnetic inorganics nanosorbents, the chemical and magnetic properties of polymeric magnetic nanocomposites will depend on the architecture (Kumar and Jain 2014). Studies have shown that magnetic nanocomposites having the same type of structure, i.e., core–shell, exhibited different saturation magnetization values. Davodi et al. (2017) synthesized $Fe_3O_4$ e $Fe_3O_4$@polydopamine with saturation magnetization values of 57.9 and 44.7 emu/g, respectively. Transmission electron microscopy images showed that the magnetic core was covered by a thin layer of thickness 0.86 nm, which may have contributed to a nanocomposite with considerable saturation magnetization value. In work reported by (Li et al. 2017b), $Fe_3O_4$@$NH_2$-polydopamine saturation magnetization value was 10.7 emu/g. According to the authors, the lower saturation magnetization value can be attributed to the presence of amino groups in the nanocomposite, giving the material a rough surface. The insertion of amino groups became the $Fe_3O_4$ content low in the nanocomposite, which the value was 16.2wt%. Though the point of zero charges of $Fe_3O_4$@$NH_2$-polydopamine was higher, pH of point of zero charge 4.0, than the value of $Fe_3O_4$@polydopamine, pH of point of zero charge 3.0 (Davodi et al. 2017). Implying that $Fe_3O_4$@$NH_2$-polydopamine will be positively charged in a greater pH range, favoring the adsorption of Cr(VI), which is negatively charged in acidic conditions (Li et al. 2017b).

Most reports focus on the functionalization effect on the chemical and magnetic properties and performance of the polymeric nanocomposites. However, magnetic core content seems to play a crucial role in the properties and adsorption capacity of magnetic nanocomposites. Pan et al. (2012) verified that the removal of Hg(II) by polymeric magnetic nanocomposite was dependent on the amount of $Fe_3O_4$ in the material. As expected, the higher the $Fe_3O_4$ content in the nanocomposite, the greater the saturation magnetization value. Otherwise, nanocomposite with higher $Fe_3O_4$ content did not present the highest adsorption capacity. Although the addition of $Fe_3O_4$ provided a higher adsorption capacity for some nanocomposites, the authors concluded that the material performance might be an integrated result of both the number of functional groups onto the polymeric matrix and $Fe_3O_4$ content also, that the ratio between the magnetic nanoparticles and matrix is an important parameter to be evaluated in the synthesis.

## Magnetic iron-carbon nanosorbents

Activated carbon is reported to be one of the best adsorbents for water and wastewater treatment due to high porosity and large surface area (Gupta et al. 2013). However, with the discovery of fullerene $C_{60}$ in 1985, the use of carbonaceous nanomaterials as adsorbents became the focus of researches. Numerous types of nanostructured carbonaceous materials and functionalized forms have been evaluated as adsorbents (Azzouz et al. 2018). The application of carbon nanomaterials as nanoabsorbers is mainly focused on carbon nanotubes, graphene, and graphene oxide. However, the high cost and low regeneration restrict the use of the materials (Ahmadi et al. 2017). Therefore, the search for the development of carbon-based magnetic materials is underway. Table 1 shows a summary of reported magnetic iron oxide nanocomposite using nanostructured carbonaceous as matrices. The following are some synthesis approaches as well as the chemical, structural, and magnetic properties of carbon-based magnetic nanocomposites.

### Carbon-coated nanomaterials

Activated carbon is the main carbonaceous material used as a matrix for the synthesis of magnetic carbon nanocomposites (Siddiqui et al. 2018). The great specific surface area of ca. 1400 $m^2/g$ and porous structure of activated carbon favor the dispersion of magnetic nanoparticles in the matrix (Baghdadi et al. 2016). Magnetically activated carbon nanocomposites are mainly prepared by a two-step method in which magnetic nanoparticles are synthesized and combined with activated carbon (Baghdadi et al. 2016; Kang et al. 2016). The one-step method through in situ coprecipitation has also been reported (Zarandi et al. 2016; Danalıoğlu et al. 2017). In some cases, activated carbon is treated with nitric acid to increase the hydrophilicity of activated carbon (Baghdadi et al. 2016). Besides, nitric acid treatment significantly reduces the point of zero charge of the activated carbon. The reported point of zero charge values of the magnetic acid-treated activated carbon nanocomposites and activated carbon is pH 2.0 and 6.5, respectively. Therefore, the addition of acid produces nanocomposites formed by acid carbon. Acid carbons have a higher density of oxygen-containing functional groups, such as carboxyls, carbonyls, phenols, lactones, and quinones, which significantly influence adsorption and reactivity of activated carbon (Kang et al. 2016). Other agents may be used for chemical modification of activated carbon, such as chitosan. In

drug removal, chitosan is added to $Fe_3O_4$–activated carbon to improve adsorbent performance (Danalıoğlu et al. 2017).

Magnetically activated carbon nanocomposites generally have a porous structure with magnetic nanosized particles monodispersed in the pores. Most of the pores consist of mesopores (Kang et al. 2016). The addition of magnetic nanoparticles causes a decrease in nanocomposite surface area, which may be due to pore blockage of the activated carbon structure by oxygen-containing functional groups and magnetite nanoparticles (Baghdadi et al. 2016). Despite the decrease, high surface area magnetic activated carbon nanocomposites were obtained. Kang et al. (2016) prepared $Fe_3O_4$–activated carbon nanocomposites with an area of 1241 $m^2$/g and a total pore volume of 0.549 $cm^3$/g employing a high surface area commercial activated carbon of 1378 $m^2$/g. However, the nanocomposite surface area value will depend on the activated carbon surface. $Fe_3O_4$–activated carbon-chitosan nanocomposite with a smaller area of 204 $m^2$/g was reported by Danalıoğlu et al. (2017) using activated carbon with a area of 560 $m^2$/g.

The findings presented in the studies suggest that the saturation magnetization of magnetically activated carbon nanocomposites seems not to be dependent on the strategy of synthesis adopted, but on the mass ratios of $Fe_3O_4$/activated carbon in the nanocomposite. The nanocomposite prepared by magnetic nanoparticles coprecipitation and mixing of the components with the mass ratio $Fe_3O_4$/activated carbon of 1:8 exhibited saturation magnetization of 5.06 emu/g (Baghdadi et al. 2016). The nanocomposite with the mass ratio $Fe_3O_4$/activated carbon of 1:10 synthesized by in situ coprecipitation presented saturation magnetization of 4.7 emu/g (Do et al. 2011). Although saturation magnetization values are lower than to other magnetic nanocomposites, increasing the amount of activated carbon in the nanocomposite improved the adsorption capacity of the materials, because the incorporation of magnetic nanoparticles in the activated carbon matrix decreases the specific surface area of the nanocomposite. Both the in situ coprecipitation method and the simple mixing of the component method provided superparamagnetic behavior nanocomposites, once both $Fe_3O_4$ nanoparticles were obtained with a size less than 50 nm.

Magnetic carbon nanocomposites can also be prepared by coating the magnetic nanoparticles with carbon to form a core–shell structure. The outer carbon layer, which contains abundant functional groups such as carboxylic and hydroxyl groups, can increase stability and corrosion resistance of magnetic nanoparticles, and improve the adsorptive properties (Mao et al. 2016). Glucose is the main carbon precursor employed in the synthesis of magnetic carbon nanocomposites. In the synthesis of nanocomposites, one- or two-step process can be used, and generally, the hydrothermal method for $Fe_3O_4$@C synthesis is employed. The hydrothermal method was proven to effectively produce core–shell magnetic carbon nanocomposites with some advantages such as easier control of size, morphology, and crystalline phase of magnetic nanoparticles (Huong et al. 2018). However, the amount of carbon used during the coating has a very significant effect on nanocomposite morphology.

Huong et al. (2018) synthesized $Fe_3O_4$@C nanocomposite by using a two-step process of coprecipitation and hydrothermal method. The carbon content in $Fe_3O_4$@C nanocomposite was controlled by adjusting the mass ratio of glucose precursor from 1.25 to 10 wt%. Transmission electron microscopy images showed that most $Fe_3O_4$ nanoparticles had a quasi-spherical shape with an average size of 20 nm and that were coated by carbon. When loading C content was 1.25 wt%, a thin layer covering magnetic nanoparticles was observed, forming a core–shell structure. By increasing the C content for 2.5wt%, the thickness of the carbon layer increased significantly, and in the core–shell structure of $Fe_3O_4$@C nanocomposite was vanished, forming a structure of iron oxide nanoparticles encapsulated in carbon. Besides, at higher loading C content, equal to or greater than 2.5 wt%, large aggregation of $Fe_3O_4$ nanoparticles was also found, which may decrease the stability of the magnetic nanoparticles. The change in the structural morphology of nanocomposite influenced the adsorption process reducing considerably, ca. 25%, the removal efficiency of As(V) by nanocomposite with C content of 10 wt%compared to $Fe_3O_4$@C at the content of 1.25 wt%. The same behavior was reported by Chen et al. (2016b) employing one-step hydrothermal synthesis. The authors evaluated the morphological and structural characteristics of the nanocomposites obtained with 0.3, 0.6, and 1.1 g glucose and selected the nanocomposite prepared with 0.6 g glucose for the Cr(VI) adsorption experiments. The sample with low C content of 0.3 g glucose had almost no surface area, while the sample with high C content of 1.1 g glucose had poor morphology due to encapsulated magnetic nanoparticles.

The coating of magnetic nanoparticles with carbon also plays an important role in the magnetic behavior of the nanocomposite. Depending on the thickness of the C layer, larger particle size nanocomposites can be obtained that can give the material non-superparamagnetic behavior. $Fe_3O_4$@C nanocomposite prepared by Mao et al. (2016) one-step hydrothermal method consisted of particles with an average size of 140 nm. The magnetization curve showed the hysteresis loops, indicating that the material did not exhibit superparamagnetic behavior. The magnetization curve of $Fe_3O_4$@C nanocomposite synthesized by Chen et al. (2016b), using the same synthesis route, also presented hysteresis loops attributed to the large particle size, whichwas greater than 130 nm.

Still, Mao et al. (2016) observed that heat treatment is another parameter that interferes with the chemical and magnetic properties of $Fe_3O_4$@C nanocomposites. Fourier

transform infrared spectroscopy analyses for $Fe_3O_4$@C nanocomposite before and after thermal treatment showed that the process modified the material. A characteristic band of C=O vibrational mode in the nanocomposite was observed before calcination and disappeared in the calcined nanocomposite. Also, a new band appeared at 2000 $cm^{-1}$, indicating the existence of C=C bonds on the adsorbent surface. The changes in the surface of the material caused an increase in the specific surface area, whose values were 18 and 79 $m^2/g$ for the nanocomposites before and after the heat treatment, respectively. On the other hand, the heat treatment may be responsible for the low saturation magnetization value of 9.91 emu/g compared to other core–shell nanocomposites. The authors associated the low saturation magnetization to the transformation of the magnetite into other weaker magnetic phases, such as ɣ-$Fe_2O_3$ and $Fe_3C$.

The reported results show that the synthesis approaches used have a significant influence on the characteristics of carbon-based magnetic nanocomposites. For example, nanocomposite formed by carbon-coated iron oxide nanoparticles showed adsorption capacity for ciprofloxacin of 90.1 mg/g, which was equal to the value found by magnetic active carbon nanocomposite, but with the saturation magnetization about 50% greater (Mao et al. 2016; Danalıoğlu et al. 2017). Enabling to obtain a material with magnetic activated carbon compatible performance with superior magnetic properties. However, to achieve a better performance, $Fe_3O_4$@C must be thermally treated, which could make the synthesis process more laborious and increase the cost. Hence, the cost–benefit assessment should be performed looking for a material that combines efficiency and feasibly in water and wastewater treatment.

Most research evaluates the performance of magnetic nanocomposites for the removal of pollutants belonging to the same chemical class. Studies aiming at the application of materials for the simultaneous removal of inorganic and organic pollutants are scarce. Yang et al. (2015) proposed a synthesis of a three-phasic nanocomposite formed by magnetic particles, carbon, and hydroxyapatite because hydroxyapatite and carbon have an affinity for inorganic and organic contaminants, respectively. Hollow carbon microspheres were decorated with magnetite nanoparticles by the ultrasonic spray pyrolysis technique. In the preparation of the hydroxyapatite@C–$Fe_3O_4$ nanocomposite, the magnetic carbon microspheres were first treated with aspartic acid, allowing subsequent deposition of hydroxyapatite nanocrystals using $Ca(OH)_2$ and $NH_4H_2PO_4$ as precursors. The specific surface area of C–$Fe_3O_4$ was 330 $m^2/g$ and increased with the addition of hydroxyapatite, which was 355 $m^2/g$ for the hydroxyapatite@C–$Fe_3O_4$ composite. Already the saturation magnetization had a value reduction at 50% compared to C–$Fe_3O_4$with a saturation magnetization of 28 emu/g, in good agreement with the weight ratio hydroxyapatite:C–$Fe_3O_4$ of 1:1 used in the synthesis. X-ray diffraction and photoelectron X-ray spectroscopy analyses showed that the nanocomposite was formed by magnetite, hydroxyapatite, and carbon. The work showed the possibility of obtaining a material with greater versatility for the treatment of water and wastewater.

### Carbon nanotubes

Carbon nanotubes are considered one of the most important materials used in nanotechnology research (Zhang et al. 2016). Carbon nanotubes consist of graphene sheets rolled into a cylindrical shape with multiple walls multiwalled carbon nanotubes or a single-walled carbon nanotubes (Gupta et al. 2013). Generally, multiwalled carbon nanotubes have a diameter in the range of 2–100 nm, while the diameter for single-walled carbon nanotubes is between 0.2–2 nm (Azzouz et al. 2018).

The high porosity and the hexagonal arrays of carbon atoms in graphene sheets of carbon nanotubes surface provide the material with adsorption sites (Gupta et al. 2013; Ahmadi et al. 2017). Different articles have shown that multiwalled carbon nanotubes are the most used due to unique properties, such as potential adsorbents, large specific surface area, chemical stability, and mechanical resistance. Due to hydrophobic surfaces, multiwalled carbon nanotubes exhibit strong interactions with organic pollutants (Wang et al. 2015a).

There are several ways of producing carbon nanotubes, and most commercially available carbon nanotubes are synthesized by the chemical vapor deposition technique (Gupta et al. 2013). In most cases, carbon nanotubes have been treated with oxidizing acids like $HNO_3$, $H_2SO_4$, or a mixture of acids to remove amorphous carbon and impurity (Zhou et al. 2014b; Jiang et al. 2016). Also, acid treatment improves the dispersion of carbon nanotubes in aqueous solutions and decreases aggregate formation due to the presence of surface oxygen-containing functional groups (Liu et al. 2015; Yu et al. 2017).

Magnetic carbon nanotubes may have different morphology depending on the route of synthesis employed. The tubular structures forming an entangled network with the magnetic nanoparticles deposited on the surface is the most common, although quasi-spherical shapes have been observed (Gupta et al. 2011; Choucair et al. 2012; Zhou et al. 2014b). The formation of the carbon nanotube magnetic nanocomposite can be evidenced by the presence of a diffraction peak at around 26° (Zhou et al. 2014a). The Fourier transform infrared spectra of carbon nanotube exhibit a band at 1559 $cm^{-1}$ associated with C=C stretching mode (Jiang et al. 2016). However, after the acid treatment, the Fourier transform infrared spectra of the carbon nanotube-based magnetic nanocomposites show characteristic

bands of oxygen-containing groups, such as in the range of 3300–3400 $cm^{-1}$ and 1570–1655 $cm^{-1}$, corresponding to the stretching mode of –OH and C=O, respectively (Gupta et al. 2011; Liu et al. 2015; Jiang et al. 2016).

In $Fe_3O_4$–multiwalled carbon nanotubes nanocomposites, the coprecipitation method was the most used for the synthesis of magnetic nanoparticles. Transmission electron microscopy images of the nanocomposites obtained by coprecipitation revealed that $Fe_3O_4$ particles of average size in the range of 10–20 nm were deposited uniformly on the surface of the carbon nanotubes (Gupta et al. 2011; Liu et al. 2015; Jiang et al. 2016). The $Fe_3O_4$–multiwalled carbon nanotube nanocomposite synthesized by Hu et al. (2011) exhibited a specific surface area of 21 $m^2/g$. The synthesis used multiwalled nanotube with a mean outside diameter of 10–20 nm and $FeSO_4{\cdot}7H_2O$ as the precursor for $Fe_3O_4$ synthesis. A larger specific surface area nanocomposite, 92 $m^2/g$, was prepared by Gupta et al. (2011) also by coprecipitation using a multiwalled nanotube with outer diameter of about 30–50 nm and a mixture of Fe(III) and Fe(II) salts with a molar ratio 1:2. A similar synthesis route was followed by Jiang et al. (2016), and a $Fe_3O_4$-multiwalled carbon nanotube with a saturation magnetization of 50.10 emu/g and superparamagnetic behavior was obtained, which is expected for particles smaller than 30 nm. The synthesis $Fe_3O_4$–multiwalled carbon nanotube using the solvothermal method was also reported (Choucair et al. 2012). Zhang et al. (2012) prepared thiol-functionalized magnetic carbon nanotube using the solvothermal method and obtained materials with morphologies similar to those obtained by the coprecipitation method and specific surface area of 97 $m^2/g$, but with smaller $Fe_3O_4$ particle sizes. The size of magnetite particles was 6 nm. The saturation magnetization was 22.85 emu/g, which is less compared to the other reported magnetic carbon nanotubes. The lowest magnetization saturation can be attributed to the formation of a non-magnetic thiol-functionalized layer.

Magnetic nanoparticles with a core–shell structure were also used to coat carbon nanotubes. Zhou et al. (2014b) synthesized covalently functionalized $Fe_3O_4@SiO_2$–multiwalled carbon nanotube core–shell magnetic microspheres. The magnetic nanoparticles were prepared, covered with silica, and functionalized with amino groups. Finally, the $Fe_3O_4@SiO_2–NH_2$ microspheres were dispersed in multiwalled carbon nanotube particles. For better control of the particle size and shape, the solvothermal method was used for the synthesis of magnetic nanoparticles. Scanning electron microscopy and transmission electron microscopy images confirmed the formation of $Fe_3O_4@SiO_2$ spherical microparticles.

The carbon nanotubes addition caused morphological changes in the microsphere surface and confirmed that multiwalled carbon nanotube attached on the surface of the $Fe_3O_4@SiO_2$. The saturation magnetization for $Fe_3O_4@SiO_2$ was 85.1 emu/g. As expected, the saturation magnetization value was high because core–shell nanoparticles tend to exhibit higher saturation magnetization. The high value contributed to $Fe_3O_4@SiO_2–NH_2$–multiwalled carbon nanotube nanocomposite having a considerably high saturation magnetization value of 47.7 emu/g even after functionalization with amino groups and coating with carbon nanotubes (Zhou et al. 2014b).

Multiwalled carbon nanotube was also combined with cobalt ferrites. Wang et al. (2015a) decorated carbon nanotube with $CoFe_2O_4$ for the removal of sulfamethoxazole and 17β-estradiol in aqueous solution. The multiwalled carbon nanotube–N–$CoFe_2O_4$ nanocomposite was synthesized via a hydrothermal method, mixing solutions of $Co(NO_3)_2.6H_2O$ and $Fe(NO_3)_3.9H_2O$ with amino multiwalled carbon nanotube at 220 °C for 12 h. The results of the elemental analysis indicated that the $CoFe_2O_4$ content was 53.7% in the multiwalled carbon nanotube–N–$CoFe_2O_4$ nanocomposite, which agreed with the theoretical mass ratio of carbon nanotube to $CoFe_2O_4$ of 1:1. The high $CoFe_2O_4$ content in the nanocomposite may have contributed to the considerable saturation magnetization and specific surface area, which were 43.6 emu/g and 134 $m^2/g$, respectively. Zhou et al. (2014a) synthesized a similar nanocomposite by modifying the structure of cobalt ferrite nanoparticles with amino groups and functionalizing with chitosan for Pb(II) removal. Ferrite was prepared by the solvothermal method using ethylene glycol and a reaction temperature of 200 °C for 8 h. Despite the high magnetization value of 67.8 emu/g for $CoFe_2O_4–NH_2$, multiwalled carbon nanotube-$CoFe_2O_4–NH_2$–chitosan showed saturation magnetization value of 4.68 emu/g. As observed for other matrices, the addition of chitosan in the carbon magnetic nanotubes caused the reduction of saturation magnetization values. On the other hand, the specific surface area of the nanocomposite after the addition of chitosan was increased from 137 $m^2/g$ for multiwalled carbon nanotube-$CoFe_2O_4–NH_2$ to 158 $m^2/g$ for multiwalled carbon nanotube-$CoFe_2O_4–NH_2$–chitosan, which provided greater adsorption of the metal ion.

### Graphene-based nanomaterials

In recent years, graphene-based magnetic composites have attracted great interest from researchers in several fields, including environmental remediation (Sabherwal et al. 2016). Graphene is a two-dimensional material composed of carbon atoms hybridized in $sp^2$, with a specific theoretical surface area of 2630 $m^2/g$ (Wanjeri et al. 2018). Graphene oxide is a highly oxidative form of graphene consisting of a variety of oxygen-containing functional groups, such as hydroxyl, carbonyl, carboxyl, and epoxy (Le et al. 2019). Reduced graphene corresponds to the reduced product from graphene oxide and consists basically of carbon hybridized

in $sp^2$. The number of sheets stacked differentiates the graphene from the reduced graphene oxide since the graphene is formed by only one sheet (Dreyer et al. 2011; Soares et al. 2018).

The Hummers method is the most used in the production of graphene oxide; the method consists of the graphite oxidation employing potassium permanganate as an oxidizing agent in the presence of sulfuric acid (Baig et al. 2019). After that, the graphene oxide can be reduced chemically by using agents such as hydrazine, sodium borohydride, and ascorbic acid. Solvothermal and hydrothermal reduction are also used to obtain reduced graphene oxide (Dreyer et al. 2011; Lin et al. 2010; Soares et al. 2018). The X-ray diffraction technique is perhaps the most commonly used to check the formation of graphene oxide and the conversion into reduced graphene oxide. Graphite has a strong diffraction peak at 2θ equal to 26.52°, representing an interlayer distance of 0.34 nm. The characteristic peak of graphite disappears in the graphene oxide X-ray diffraction pattern, and a new peak at 2θ value equal to or lower than 12° appears, leading to a greater spacing between sheets. The 2θ value of the graphene oxide peak depends on the preparation method and the presence of water in the interlamellar space. The graphene oxide peak then disappears following the reduction of the graphene oxide to form reduced graphene oxide (Chella et al. 2015; Zhang et al. 2019b).

In general, graphene is a nonpolar and hydrophobic adsorbent; in contrast, graphene oxide is usually applied as a polar and hydrophilic adsorbent due to the presence of polar groups (Li et al. 2018). The changes in the characteristics of the graphene-based materials allow application as adsorbents for the removal of different classes of water contaminants. Magnetic graphene oxide has a point of zero charges of approximately 4.0, which implies that the material would be negatively charged in most of the natural water environment (Nethaji and Sivasamy 2017). The negatively charged surface could promote the adsorption capacities of cation pollutants (Cui et al. 2015). On the other hand, a material with point of zero charges above 6.0 can be obtained from the modification of magnetic graphene oxide with amino groups. Magnetic graphene oxide functionalized with 2-phenylethylamine exhibited point of zero chargeat pH 6.6 (Wanjeri et al. 2018). The modification of magnetic graphene oxide with chitosan provided a point of zero chargeat pH 6.8 (Sherlala et al. 2019).

Graphene-based magnetic adsorbents commonly exhibit type IV isotherm with an H3-type hysteresis loop, a typical characteristic of mesoporous material. The characteristic isotherm is mainly caused by the dispersion of magnetic particles among the plate-like graphene sheets giving rise to slit-shaped pores (Yang et al. 2018). Although graphene is a material with a high theoretical surface area, graphene oxide usually has a much lower surface area. The reported surface area of graphene oxide generally ranges from approximately 10 to 176 $m^2/g$ (Wanjeri et al. 2018; Yang et al. 2018). The variation may be attributed to the agglomerations of graphene oxide layers during the drying process and also unavoidable van der Waals force between every single sheet of graphene oxide (Wanjeri et al. 2018). The nanocomposite surface area will depend on the surface area of the graphene oxide produced. For example, the $Fe_3O_4$-graphene oxide nanocomposite prepared by Yang et al. (2018) showed a specific surface area of 88 $m^2/g$ employing graphene oxide with an area of 10 $m^2/g$, while the nanocomposite chitosan–$Fe_3O_4$–graphene oxide synthesized by Hosseinzadeh and Ramin (2018) exhibited a specific surface area of 133 $m^2/g$ using graphene oxide with area of 34 $m^2/g$. The specific surface area of magnetic graphene oxide is also the result of the specific surface area of iron oxide, which depends on the degree of ordering of the particles, as discussed later.

In most studies reported in the literature, graphene-based magnetic nanocomposites are prepared by coprecipitation in one step and forming magnetic nanoparticles in the presence of graphene oxide or graphene oxide reduced (Gupta et al. 2017; Su et al. 2017; Yang et al. 2018), or by a thermal reaction in solvents (Guo et al. 2014; Chella et al. 2015; Nethaji and Sivasamy 2017). Another approach involves synthesizing the magnetic nanoparticles separately and coupling to the graphene oxide or graphene oxide reduced sheets (Lin et al. 2013; Wanjeri et al. 2018). The latter strategy allows for precise control of the magnetic nanoparticles quantity in the nanocomposite (Tancredi et al. 2018). Amino groups are commonly used for the covalent coupling of graphene oxide to magnetic nanoparticles. The Fourier transform infrared spectroscopy analysis demonstrates that the magnetic nanoparticles are covalently bonded to the graphene oxide nanosheets through amide bonding due to the presence of bands in 1632 $cm^{-1}$ and 1425 $cm^{-1}$, which correspond to –CONH amide band and C–N stretch of amide, respectively (Wanjeri et al. 2018).

In comparison with other carbonaceous nanomaterials, graphene oxide may be more environmentally friendly and have better biocompatibility (Cui et al. 2015). Therefore, most graphene-based magnetic nanosorbents use graphene oxide as a matrix. In most works, the coprecipitation method is used since the solvothermal and hydrothermal methods can lead to the reduction of graphene oxide to reduced graphene oxide (Baig et al. 2019). Generally, graphene oxide magnetic nanocomposites exhibit a wrinkled sheet structure, a characteristic morphology of the graphene-based materials, with magnetic nanoparticles deposited on the surface (Zhao et al. 2016; Zhang et al. 2019b). In some materials, graphene oxide sheets were not observed due to the formation of amorphous iron oxide that aggregated on the surface of graphene oxide (Yang et al. 2017). Su et al. (2017)

found that the presence of graphene oxide in the synthesis of magnetic nanoparticles by coprecipitation exerts inhibitory effects on crystal formation in nanocomposites. The analysis of transmission electron microscopy and X-ray diffraction showed that $Fe_3O_4$ nanoparticles prepared in the absence of graphene oxide were crystalline, while in the presence of graphene oxide, the nanoparticles were mainly amorphous. The surface area for graphene oxide–$Fe_3O_4$was 341 $m^2$/g. The loading of the amorphous iron oxide nanoparticles on graphene oxide sheets contributed to the high surface area value of the magnetic graphene oxide nanocomposite, which is desirable for the adsorption process. However, the low crystallinity of the magnetic nanoparticles can reduce the magnetization of the material, making magnetic separation difficult. Yang et al. (2017) prepared $Fe_3O_4$–graphene oxide reduced from the synthesis of $Fe_3O_4$-graphene oxide by in situ coprecipitation followed by reduction to graphene oxide reduced using thiourea oxide, and the nanocomposite exhibited morphology similar to the material prepared by Su et al. (2017). The material showed saturation magnetization of 4.38 emu/g, and the low value can be attributed to the aggregation of amorphous iron oxide nanoparticles. Thus, controlling the content of iron oxide nanoparticles and the degree of ordering in graphene-based nanocomposites is a difficult task in the synthesis (He et al. 2010).

Some studies have proposed modifications in the synthesis protocols for the fabrication of graphene-based magnetic nanocomposites, seeking to overcome the demerits associated with the conventional coprecipitation method. A strategy adopted by Yang et al. (2018) was to add the sodium dodecyl sulfate surfactant on the in situ coprecipitation process. The $Fe_3O_4$ nanoparticles exhibited a spherical shape and were well dispersed on the surface of the sheets. The route employing sodium dodecyl sulfate was able to deposit highly crystalline $Fe_3O_4$ nanoparticles onto the sheets, which may have influenced the higher saturation magnetization value, 33.64 emu/g, for materials obtained by the coprecipitation method. Another approach was used by Wanjeri et al. (2018), resulting in a material with similar saturation magnetization value, wich was 33 emu/g. Magnetic nanoparticles were synthesized by coprecipitation in the absence of graphene oxide, coated with silica, forming a core–shell structure. The $Fe_3O_4$@$SiO_2$–graphene oxide nanocomposite was prepared by covalently coupling graphene oxide to $Fe_3O_4$@$SiO_2$–$NH_2$. Finally, magnetic graphene oxide was functionalized with 2-phenylethylamine to increase the hydrophobic interaction between the adsorbent and the pollutants analyzed, organophosphate pesticides. The presence of a characteristic diffraction pattern of $Fe_3O_4$ indicated the stability of the magnetite crystalline phase during the covalent bonding of the graphene oxide with $Fe_3O_4$@$SiO_2$–$NH_2$.

The modification of magnetic graphene oxide with chitosan has been reported for the adsorption of inorganic pollutants. Sherlala et al. (2019) synthesized the chitosan–$Fe_3O_4$–graphene oxide nanocomposite by in situ coprecipitation method with a specific surface area of 152 $m^2$/g. The $Fe_3O_4$–graphene oxide material exhibited a rough, wrinkled-like sheet surface with crystals of the magnetic nanoparticles on the surface of the graphene sheet. For chitosan–$Fe_3O_4$–graphene oxide, the crystals of the magnetic nanoparticles were not observed due to the chitosan coating on the surface. Magnetic graphene oxide had an iron content of 51.1 wt%, which may have contributed to the high saturation magnetization value of 49.30 emu/g. For chitosan–$Fe_3O_4$–graphene oxide, the saturation magnetization was 47.19 emu/g. Although several studies report a decrease in magnetization after modification with chitosan, the saturation magnetization value for chitosan–$Fe_3O_4$–graphene oxide remained high, because the amount of iron in chitosan–$Fe_3O_4$–graphene oxide was little changed, whose value was 50.7 wt%. Hosseinzadeh and Ramin (2018) also modified $Fe_3O_4$–graphene oxide with chitosan but following a different route. The insertion of chitosan in the material was carried out via copolymerization of vinyl monomers in chitosan solution. While the chitosan–$Fe_3O_4$–graphene oxide nanocomposite had a specific surface area of 133 $m^2$/g, similar the value for the nanocomposite by in situ coprecipitation, the value of saturation magnetization was much lower, 3.82 emu/g.

Though graphene oxide has received considerable attention, the large surface area and stability of graphene oxide reduced motivate the synthesis of magnetic graphene oxide reduced for pollutant removal. Yang et al. (2012) synthesized $Fe_3O_4$–graphene oxide and $Fe_3O_4$–graphene oxide reduced nanocomposites with the same saturation magnetization of 31 emu/g, but with different values of surface area. $Fe_3O_4$–graphene oxide reduced exhibited an area of 273 $m^2$/g, while the area for $Fe_3O_4$–graphene oxide was 142 $m^2$/g. For the synthesis of magnetic graphene oxide reduced, the solvothermal and hydrothermal methods can be a good choice, performing the simultaneous formation of superparamagnetic $Fe_3O_4$ nanoparticles and the reduction of graphene oxide (Baig et al. 2019). Guo et al. (2014) synthesized the amino-functionalized magnetic graphene nanocomposite with a specific surface area of 62 $m^2$/g using the hydrothermal method. Ethylenediamine was used as a nitrogen source, ferric chloride as iron ions source, and ethylene glycol as a solvent to achieve a one-step reduction of graphene oxide and the introduction of $Fe_3O_4$ meanwhile. After the reaction, graphene oxide turned from dark brown to black, the color of reduced graphite oxides. Chella et al. (2015) synthesized magnetic graphene nanocomposite using manganese ferrites with saturation magnetization of41.39 emu/g and specific surface area of 79 $m^2$/g. The graphene oxide reduced-$MnFe_2O_4$ nanocomposite was prepared to synthesize ferrites by the solvothermal method in

the presence of graphene oxide using ethylene glycol as a solvent. Although the synthesis of magnetic graphene oxide reduced by solvothermal and hydrothermal methods is advantageous. The surface area values of the nanocomposites obtained by solvothermal and hydrothermal methods were lower than the values when using graphene oxide reduced obtained from graphene oxide reduction with reducing agent, eg., hydrazine (Yang et al. 2012).

## Applications in adsorption processes

The adsorption separation process is one of the most used technologies in water and wastewater treatment due to easy operation, flexibility, and high efficiency (Zhang et al. 2016). Adsorption separation is a surface phenomenon of species accumulation from a fluid phase into a phase which can be a liquid or solid (Mehta et al. 2015). Several kinetic and isothermal models are used to evaluate the performance of an adsorbent (Wang et al. 2018). The most used are the isotherms developed by Langmuir and Freundlich for the equilibrium and kinetic study the Lagergren's equations, also known as pseudo-first order, and pseudo-second order (Reddy and Yun 2016).

In the past decades, different materials have been used as adsorbents of water treatment, such as active carbon (Li et al. 2014), zeolites (Yang et al. 2014b; Wang et al. 2016), chitosan (Tajuddin Sikder et al. 2014) and, recently, magnetic nanomaterials (Zhang et al. 2016; Abdel Maksoud et al. 2020). Iron-based magnetic nanomaterials have attracted interest in adsorption studies of inorganic and organic pollutants in water (Reddy and Yun 2016). However, several conditions influence the pollutants removal from aqueous solution by the adsorption process (Tang and Lo 2013). Tables 2, 3, and 4 enlist the main data published in scientific articles from 2010 to 2019 regarding the adsorption of some pollutants in water by iron-based magnetic nanocomposites. The results concerning pH, maximum adsorption capacity, isotherm, and kinetics are shown. The following discussion attempts to elucidate the linkages between the performance of magnetic nanomaterials in removing pollutants and the adsorption mechanism along with supporting examples in the literature.

### Adsorption of toxic elements

The toxic element ions are released into the environment by the disposal of effluents generated in industrial activities such as smelting, paint production, electroplating, among others (Arancibia-Miranda et al. 2016). There are of great concern due to adverse effects of toxic element ions on the environment and human beings, and the tendency to bioaccumulation (Xu et al. 2012b). Therefore, effective methods of toxic elements removal are extremely urgent and have attracted interest from researchers. Table 2 illustrates the adsorption conditions of some toxic elements in iron-based magnetic nanocomposites. The toxic elements reported include As(III), As(V), Cd(II), Cr(III), Cr(VI), Cu(II), Co(II), Hg(II), Ni(II), Pb(II), and Zn(II).

In summary, the Langmuir model was the one that showed the highest correlation with the experimental data and, therefore, the most used model to explain the process of adsorption of toxic elements in magnetic iron-based nanomaterials. The Langmuir isotherm model assumes monolayer coverage of adsorbates over a homogenous adsorbent surface, and after the equilibrium time, the saturation point is reached, which corresponds to the maximum of adsorption (Chen et al. 2016a). The experimental data of adsorption in the magnetic nanocomposites system usually follow a pseudo-second-order kinetic model, indicating that the adsorption of the toxic elements is dependent on the concentration of the adsorbed element in the nanomaterial, and element concentration in equilibrium (Mehta et al. 2015).

The mechanisms by which inorganic species are adsorbed onto magnetic nanocomposites may involve multiple interactions. Generally, electrostatic interaction, surface complexation, ion exchange, precipitation, and hydrogen bonding might be the primary mechanisms (Wang et al. 2018). The mechanisms will depend on the chemical form of the species in solution; a speciation study is important to propose improvements in the performance of the adsorbent. Besides, the specific role of each mechanism in the toxic elements adsorptions varies depending on the adsorbent properties, such as specific surface area, functional groups, and charges, and the ionic environment of the aqueous solution (Yang et al. 2019). The pH of the solution is one of the most important factors that affect not only the speciation of toxic elements but also the surface charge of the adsorbent material and the complexation behavior of functional groups.

Thermodynamic studies indicate the nature of the toxic elements adsorptions process. The nature of the process varied according to the matrix used in the nanocomposite. For example, the adsorption in materials based on silica (Zhang et al. 2013), chitosan (Ren et al. 2013; Gutha and Munagapati 2016), and graphene oxide (Cui et al. 2015; Zhao et al. 2016; Hosseinzadeh and Ramin 2018) is endothermic, that is, the amount adsorbed increased with increasing temperature. On the other hand, cellulose-based materials, the process is exothermic. The type of magnetic nanoparticle used also appears to be a factor that interferes with the nature of the process. When $Fe_3O_4$ was used, the adsorption of Pb(II) in the magnetic reduced graphene oxide (Guo et al. 2014), while for reduced graphene oxide with $MnFe_2O_4$ (Chella et al. 2015). The enthalpy values for most materials are less than 40 kJ/mol, so the toxic elements adsorption in magnetic nanocomposites could be considered as physical adsorption.

**Table 2** Adsorption parameters of toxic elements from aqueous solution by magnetic iron oxide nanocomposites

| Magnetic nanosorbent | Target pollutant | Contact time | pH | Temperate (°C) | Concentration range (mg/L) | Maximum adsorption capacity(mg/g) | Isotherm model | Kinetic model | References |
|---|---|---|---|---|---|---|---|---|---|
| $Fe_3O_4$@$SiO_2$<br>$Fe_3O_4$@$SiO_2$–$NH_2$ | Cr(III) | 2 h | 5.4 | 25 | 104 | 36.9[a]<br>108.2[a] | Freundlich | – | Egodawatte et al. (2015) |
| $Fe_3O_4$@$SiO_2$ | Zn(II) | 1 h | 6.0 | 25 | – | 119.0 | Langmuir | Pseudo-second order | Emadi et al. (2013) |
| $Fe_3O_4$@$SiO_2$@meso–$SiO_2$–$NH_2$ | Zn(II) | 1 h | 6.0 | 25 | 15–440 | 270.3 | Langmuir | Pseudo-second order | Donia et al. (2012) |
| $Fe_3O_4$@$SiO_2$–$NH_2$ | Pb(II) | 16 h | 5.2 | 25 | 100–400 | 243.9 | Langmuir | Pseudo-second order | Zhang et al. (2013) |
| $Fe_3O_4$@$SiO_2$–$NH_2$ | Cd(II)<br>Cu(II)<br>Pb(II) | 24 h | 6.2 | 25 | 5–50<br>5–50<br>10–100 | 22.5<br>29.9<br>76.7 | Langmuir | Pseudo-second order | Wang et al. (2010) |
| γ-$Fe_2O_3$-SBA-15[c] | As(V) | 3 h | 3.0 | – | 10 | 23.1 | Langmuir | Pseudo-second order | Peng et al. (2018) |
| $Fe_3O_4$@SBA-15-$NH_2$[c] | Pb(II) | 12 h | 6.0 | 25 | 50–300 | 243.9 | Langmuir | Pseudo-second order | Wang et al. (2015b) |
| γ-$Fe_2O_3$–zeolite | As(III) | 2 h | 2.5 | 25 | 10–100 | 19.4[a] | Freundlich | – | Salem Attia et al. (2014) |
| $Fe_3O_4$–zeolite | Pb(II) | 2 h | – | 25 | 71.9 | 196.8[a] | – | – | Yuan et al. (2011) |
| Chitosan–clinoptilolite–$Fe_3O_4$ | Pb(II) | 2 h | 6.0 | 60 | 10–90 | 137.0 | Langmuir | Pseudo-second order | Javanbakht et al. (2016) |
| $Fe_3O_4$–bentonite | Cd(II)<br>Cu(II)<br>Pb(II) | 30 min | – | 25 | 10–300<br>10–200<br>10–800 | 21.7<br>19.6<br>81.5 | Langmuir | Pseudo-second order | Yan et al. (2016) |
| $Fe_3O_4$–bentonite | Co(II) | – | 8.0 | 25 | 800 | 18.8 | Langmuir | Pseudo-second order | Hashemian et al. (2015) |
| $MnFe_2O_4$–bentonite | Cr(VI) | 2 h | 2.0 | 30 | 10–500 | 133.3 | Langmuir | – | Kaur et al. (2015) |
| $Fe_3O_4$–montmorillonite | Cu(II)<br>Ni(II)<br>Pb(II) | 120 s | – | 25 | 97.7–602.3 | 70.9<br>65.8<br>263.2 | Langmuir | Pseudo-second order | Kalantari et al. (2015) |
| Hydroxyapatite–$Fe_3O_4$ | Cd(II)<br>Zn(II) | 24 h | 5.0 | 25 | $10^{-4}$– $10^{-2}$[b] | 220.8<br>140.6 | Langmuir | Pseudo-second order | Feng et al. (2010) |
| Hydroxyapatite–$Fe_3O_4$ | Pb(II) | 1 h | 3.0 | 25 | 0–600 | 434.8 | Langmuir | Pseudo-second order | Zhuang et al. (2015) |
| Hydroxyapatite–$Fe_3O_4$ | Pb(II) | 24 h | 5.0 | 25 | 10–500 | 598.8 | Langmuir | Pseudo-second order | Dong et al. (2010) |
| $Fe_3O_4$@hydroxyapatite | Pb(II) | 24 h | 5.0 | 25 | 0–1000 | 321.2 | – | – | Yang et al. (2014a) |
| $Fe_3O_4$–cellulose–$NH_2$ | Ag(I)<br>Cu(II)<br>Hg(II) | 7 min | 5.4<br>6.3<br>2.0 | 25 | – | 129.4<br>95.3<br>401.2 | Langmuir | Pseudo-second order | Donia et al. (2012) |
| $Fe_3O_4$@$SiO_2$@cellulose@$NH_2$ | Cr(VI) | 5 h | 2.0 | 25 | 50–150 | 171.5 | Langmuir | Pseudo-second order | Sun et al. (2014) |

**Table 2** (continued)

| Magnetic nanosorbent | Target pollutant | Contact time | pH | Temperate (°C) | Concentration range (mg/L) | Maximum adsorption capacity(mg/g) | Isotherm model | Kinetic model | References |
|---|---|---|---|---|---|---|---|---|---|
| Chitosan–$Fe_3O_4$ | Ni(II)<br>Pb(II) | 2 h | 6.0 | 25 | 50–80 | 52.6<br>63.3 | Langmuir | – | Tran et al. (2010) |
| $Fe_3O_4$–chitosan–cyanoguanidine | Hg(II) | – | 7.0 | 30 | 150 | 285 | Langmuir–Freundlich | Pseudo-second order | Wang et al. (2013) |
| $Fe_3O_4$–chitosan–4-((pyridin-2-ylimino) methyl) benzaldehyde | Pb(II) | 105 min | 5.0 | 50 | 30–90 | 104.2 | Langmuir | Pseudo-second order | Gutha and Munagapati (2016) |
| $Fe_3O_4$–$SiO_2$–chitosan–ethylenediaminetetraacetic acid | Cd(II)<br>Cu(II)<br>Pb(II) | 12 h | 5.0 | 25 | 0.2–5.0[b] | 63.3<br>44.4<br>123.5 | Langmuir | Pseudo-second order | Ren et al. (2013) |
| $Fe_3O_4$–chitosan–polyethyleneimine | Pb(II) | 105 min | 5.0 | 50 | 30–90 | 124.0 | Langmuir | Pseudo-second order | Wang et al. (2017) |
| γ-$Fe_2O_3$–alginate | Pb(II) | 4 h | 4.7 | 25 | 0.25–24.0[b] | 99.5 | Langmuir | Pseudo-second order | Bée et al. (2011) |
| γ-$Fe_2O_3$–alginate | Pb(II) | 12 h | 7.0 | 30 | 100–400 | 50.0 | Langmuir | Pseudo-second order | Idris et al. (2012) |
| $Fe_3O_4$@polyaniline | Hg(II) | 5.17 h | 5.4 | 20 | 20–100 | 307.0 | Langmuir | Pseudo-second order | Davodi et al. (2017) |
| $Fe_3O_4$@$NH_2$–polydopamine | Cr(VI) | 4 h | 2.0 | 25 | 50–1000 | 284.1 | Langmuir | Pseudo-second order | Li et al. (2017b) |
| $Fe_3O_4$@polyaniline | Cr(VI) | 3 h | 2.0 | 25 | 100 | 200.0 | Langmuir | Pseudo-second order | Han et al. (2013) |
| Polyaniline–γ-$Fe_2O_3$ | Cr(VI) | 30 min | 2.0 | 25 | 2.5–100 | 196.0 | Langmuir | Pseudo-second order | Chávez-Guajardo et al. (2015) |
| $Fe_3O_4$–activated carbon | Cd(II)<br>Pb(II) | 1 h | 6.0<br>5.0 | 25 | 10–200 | 49.8<br>86.2 | Langmuir | Pseudo-second order | Kang et al. (2016) |
| $Fe_3O_4$@C | As(V) | 2 h | 1.0–2.0 | 25 | 10–50 | 20.1 | Langmuir | Pseudo-second order | Huong et al. (2018) |
| $Fe_3O_4$@C | Cr(VI) | 2.5 h | 4.0 | 25 | 20–100 | 61.7 | Langmuir | Pseudo-second order | Chen et al. (2016b) |
| Hydroxyapatite@C-$Fe_3O_4$ | Hg(II)<br>Pb(II) | 24 h | 8.0 | 25 | 0–5[b] | 64.2<br>292.5 | Langmuir | – | Yang et al. (2015) |
| $Fe_3O_4$–multiwalled carbon nanotubes | Pb(II)<br>Zn(II) | 6 h | 5.0 | 25 | 200<br>30 | 67.3<br>3.8 | Langmuir | Pseudo-second order | Jiang et al. (2016) |
| $Fe_3O_4$–multiwalled carbon nanotubes | Cu(II) | 10 h | 6.0 | 25 | 5–50 | 8.1 | Langmuir | Pseudo-second order | Liu et al. (2015) |
| Multiwalled carbon nanotubes–$CoFe_2O_4$–$NH_2$–chitosan | Pb(II) | – | 6.0 | 30 | 10–60 | 140.1 | Langmuir | Pseudo-second order | Zhou et al. (2014a) |

**Table 2** (continued)

| Magnetic nanosorbent | Target pollutant | Contact time | pH | Temperate (°C) | Concentration range (mg/L) | Maximum adsorption capacity(mg/g) | Isotherm model | Kinetic model | References |
|---|---|---|---|---|---|---|---|---|---|
| Graphene oxide–$Fe_3O_4$ | As(III)<br>As(V) | 24 h | 7.0<br>3.0 | 25 | 0.1–1200 | 147.0<br>113.0 | Langmuir | Pseudo-second order | Su et al. (2017) |
| Graphene oxide–$Fe_3O_4$ | Pb(II) | 2 days | 6.5 | 30 | 10–15 | 588.0 | Langmuir | – | Yang et al. (2012) |
| $Fe_3O_4$–graphene oxide–$NH_2$ | Cr(VI) | 12 h | 2.0 | 25 | – | 123.4 | Langmuir | Pseudo-second order | Zhao et al. (2016) |
| Ethylenediaminetetraacetic acid–$Fe_3O_4$–graphene oxide | Pb(II)<br>Hg(II)<br>Cu(II) | 3 h | 4.2<br>4.1<br>5.1 | 25 | 100 | 508.4[a]<br>268.4[a]<br>301.2[a] | Freundlich Temkin | Pseudo-second order | Cui et al. (2015) |
| Chitosan–$Fe_3O_4$–graphene oxide | Cu(II) | 12 h | 7.0 | 25 | 20–300 | 217.4 | Langmuir | Pseudo-second order | Hosseinzadeh and Ramin (2018) |
| $MnFe_2O_4$–reduced graphene oxide | Cd(II)<br>Pb(II) | 3 h<br>2 h | 7.0<br>5.0 | 37 | 10–70 | 76.9<br>100.0 | Langmuir | Pseudo-second order | Chella et al. (2015) |
| $Fe_3O_4$–reduced graphene oxide–$NH_2$ | Cr(IV)<br>Pb(II)<br>Hg(II)<br>Cd(II)<br>Ni(II) | 4 h<br>2 h | 1.0 –3.5<br>6.0–7.0 | 20 | – | 17.3[a]<br>28.0[a]<br>23.0[a]<br>27.8[a]<br>22.1[a] | Freundlich | Pseudo-second order | Guo et al. (2014) |

[a]Experimental value

[b]mmol/L

[c]SBA-15: mesoporous silica santa barbara amorphous-15

However, due to the complexity of the adsorption mechanisms involved, further studies are necessary.

The application of silica-based materials in the metal ions adsorption has been extensively studied. Since $SiO_2$ is stable under acidic conditions, iron oxide-$SiO_2$ nanocomposite can be used as an adsorbent in acidic solutions. Also, the surface of silica is dominated by hydroxyl or silanol groups that can participate in adsorption as well as chemical modification of the silica surface with magnetic nanoparticles and amino groups, for example (Emadi et al. 2013; Mallakpour and Naghdi 2018). Studies show that the incorporation of magnetic iron oxide nanoparticles increases the adsorption capacity of silica materials, and also imparting magnetic properties of the material (Diagboya and Dikio 2018). Egodawatte et al. (2015) found that the $Fe_3O_4$–$SiO_2$ nanocomposite exhibited a superior adsorption capacity of 36.9 mg/g for Cr(III), relative to 8.8 mg/g for unmodified silica. When functionalized with amino groups, the adsorption capacity was even higher, which was 108.2 mg/g. The increase in the adsorption capacity of the silica magnetic nanocomposite with the addition of amino groups was also observed in the Zn(II) removal. The maximum adsorption capacity of $Fe_3O_4$@$SiO_2$@meso-$SiO_2$–$NH_2$ was 270.3 mg/g, and for $Fe_3O_4$@$SiO_2$ was 119.0 mg/g under the same conditions of time, temperature and pH (Emadi et al. 2013; Kheshti and Hassanajili 2017). In the silica magnetic nanocomposites, the adsorption process occurs mainly by electrostatic interactions between the metal ions and the silanol and hydroxyl groups (Diagboya and Dikio 2018). With the addition of amino groups, besides electrostatic interactions, complexation interactions can occur between metal ions and amino groups in $Fe_3O_4$@$SiO_2$–$NH_2$, which can contribute to the increase in adsorption capacity (Kheshti and Hassanajili 2017).

It is known that the specific surface area is a property of the material that favors the improvement of adsorption performance. However, not always, the adsorbent that has a greater surface area will have a greater adsorption capacity. An example is the magnetic mesoporous silica santa barbara amorphous-15; ɣ-$Fe_2O_3$–santa barbara amorphous-15, which despite having a specific surface area of 1049 $m^2$/g, presented a low maximum adsorption capacity for As(V) of 23.1 mg/g (Peng et al. 2018). On the other hand, the material $Fe_3O_4$@santa barbara amorphous-15-$NH_2$ with specific surface area of 173 $m^2$/g exhibited adsorption capacity for Pb(II) of 243.9 $m^2$/g (Wang et al. 2015b). The nature and the number of functional groups largely determine the surface chemistry of nanomaterials and, consequently, the

**Table 3** Adsorption parameters of pesticides from aqueous solution by magnetic iron oxide nanocomposites

| Magnetic nanosorbent | Target pollutant | Contact time | pH | Temperate (°C) | Concentration range (mg/L) | Maximum adsorption capacity (mg/g) | Isotherm model | Kinetic model | References |
|---|---|---|---|---|---|---|---|---|---|
| $Fe_3O_4$–zeolite–H (5.4 wt% $Fe_3O_4$)<br>$Fe_3O_4$–zeolite–H (7.1 wt% $Fe_3O_4$) | Simazine | 24 h | 6.5<br>3.0 | 25 | 20 | 6.1<br>6.3 | Freundlich | Pseudo-second order | Pansini et al. (2018) |
| Sepiolite–$Fe_3O_4$ | Atrazine | 2 h | 6.5 | 25 | 2–28 | 1.8 | Langmuir | Pseudo-second order | Liu et al. (2014a) |
| $Fe_3O_4$–$NH_2$–molecularly imprinted polymer | Chlorpyrifos<br>Diazinon<br>Phosalone | 1 h | – | 25 | 0.2–1.2 | 172.4<br>192.3<br>196.1 | Langmuir | Pseudo-second order | Masoumi et al. (2016) |
| $Fe_3O_4$@$SiO_2$–multiwalled carbon nanotubes | Pentachlorophenol | 30 min | 2.5 | 25 | 1–100 | 96.4[a] | Freundlich | Pseudo-second order | Zhou et al. (2014b) |
| Graphene oxide–$Fe_3O_4$ | 2.4-dichlorophenoxyacetic | – | 3.0 | – | 50–750 | 67.3[a] | Freundlich | Pseudo-second order | Nethaji and Sivasamy (2017) |
| $Fe_3O_4$@$SiO_2$@graphene oxide–polyethyleneimine | Chlorpyrifos<br>Parathion<br>Malathion | 15 min | 7.0 | 25 | 0.3–5 | 11.1[a]<br>10.6[a]<br>10.9[a] | Sips | Pseudo-second order | Wanjeri et al. (2018) |
| $Fe_3O_4$–reduced graphene oxide | Ametryn | 70 min | 5.0 | 25 | 2–54 | 54.8 | Langmuir | Pseudo-second order | Boruah et al. (2017) |

[a]Experimental value

possibility of adsorption (Yang et al. 2019). The $Fe_3O_4$@$SiO_2$–$NH_2$ material showed different values of adsorption capacity for Pb(II), and the difference may be related to the content of amino groups in the nanocomposite. The adsorption capacity of $Fe_3O_4$@$SiO_2$–$NH_2$with $NH_2$ 3.92 wt% was 76.7 mg/g, while the value was 243.9 mg/g for $Fe_3O_4$@$SiO_2$–$NH_2$with $NH_2$ 5.45 wt% (Wang et al. 2010; Zhang et al. 2013).

In clay and zeolite materials, the adsorption of toxic elements occurs mainly by ion exchange due to the predominance of negative charges formed by isomorphic substitution (Chen et al. 2016a). As with silica nanocomposites, the materials may have improved adsorption capacity due to the presence of active sites on the layers of zeolite, clay minerals, and the surfaces of magnetic nanoparticles. For example, the maximum adsorption capacity of As(V) was 19.30 mg/g for nanocomposite ɣ-$Fe_2O_3$–zeolite, which is greater than the 5.46 mg/g obtained using non-magnetic zeolite (Salem Attia et al. 2014). The increase in the adsorption capacity caused by the modification of magnetic zeolite with chitosan has also been reported. The adsorption capacity of clinoptilolite–$Fe_3O_4$ to Pb(II) was 37.5 mg/g, and the value increased to 137.0 mg/g for chitosan-clinoptilolite-$Fe_3O_4$ (Javanbakht et al. 2016). However, even with amino groups, the adsorption capacity value was lower than reported for unmodified magnetic synthetic zeolite described by Yuan et al. (2011). The adsorption capacity of Pb(II) by $Fe_3O_4$–zeolite nanocomposite was 196.8 mg/g. Studies indicate that natural zeolites such as clinoptilolite have low adsorption capacity for metals as compared to the synthetic zeolite, mainly due to the smaller specific surface area (Abdullah et al. 2019). The area of chitosan-clinoptilolite–$Fe_3O_4$ was 28 $m^2$/g, which is lower than the 571 $m^2$/g of $Fe_3O_4$–zeolite (Yuan et al. 2011; Javanbakht et al. 2016).

Several factors, such as the hydrated ions size and free energy of hydration, may be responsible for the selectivity of the ion exchange adsorption mechanism. Metal cations with smaller hydrated radius and less hydration energy have easier access to the exchange sites (Cheng et al. 2012). In the work of Yan et al. (2016), maximum adsorption capacity of the $Fe_3O_4$-bentonite adsorbent was found to follow the decreasing order Pb(II), Cd(II),

**Table 4** Adsorption parameters of pharmaceutical-derived compounds from aqueous solution by magnetic iron oxide nanocomposites

| Magnetic nanosorbent | Target pollutant | Contact time | pH | Temperate (°C) | Concentration range (mg/L) | Maximum adsorption capacity (mg/g) | Isotherm model | Kinetic model | References |
|---|---|---|---|---|---|---|---|---|---|
| $Fe_3O_4$–zeolite | Cefalexin | 2 h | 7.0 | 25 | 0–100 | 27.2 | Langmuir | Pseudo-second order | Mohseni-Bandpi et al. (2016) |
| $Fe_3O_4$–chitosan | Diclofenac | 2 h | 7.0–8.0 | 25 | 50 | 57.5 | Langmuir | – | Zhang et al. (2014) |
| $Fe_3O_4$@$SiO_2$–Si–quaternary chitosan | Diclofenac | 30 min | 6,0 | 25 | 40–670 | 240.4 | Langmuir | – | Soares et al. (2019) |
| $Fe_3O_4$–activated carbon | Carbamazepine | 30 min | – | 25 | 2–20 | 182.9 | Langmuir | Pseudo-second order | Baghdadi et al. (2016) |
| $Fe_3O_4$@C | Ciprofloxacin | 3 h | 7,0 | 30 | 10–60 | 90.1 | Langmuir | Pseudo-second order | Mao et al. (2016) |
| $Fe_3O_4$–activated carbon–chitosan | Ciprofloxacin<br>Erythromycin<br>Amoxicillin | 2 h | 7,0 | 25 | 5–60 | 90.1<br>178.6<br>526.3 | Langmuir | Pseudo-second order | Danalıoğlu et al. (2017) |
| Hydroxyapatite@C–$Fe_3O_4$ | Ampicillin | 24 h | 6 | 25 | 0–5[b] | 3.5 | Langmuir | – | Yang et al. (2015) |
| Multiwalled carbon nanotubes–N–$CoFe_2O_4$ | Sulfamethoxazole 17 β-estradiol | 100 min | 5,5 | 25 | 0.4–2.4 | 7.4[a]<br>20.0[a] | Freundlich | Pseudo-second order | Wang et al. (2015a) |
| $Fe_3O_4$–multiwalled carbon nanotubes | Furazolidone | 5 h | 6.0 | 25 | 1.0–15.0 | 19.2 | Langmuir | Pseudo-second order | Liu et al. (2015) |
| $Fe_3O_4$–multiwalled carbon nanotubes | 17α-methyltestosterone | 3 min | 7,0 | 20 | 0.08–2 | 0.12 | Langmuir | – | Hu et al. (2011) |
| Graphene oxide–$Fe_3O_4$ | Methadone | 30 min | 6.2 | 22.5 | 30 | 87.2[a] | Langmuir | Pseudo-second order | Gupta et al. (2017) |
| $Fe_3O_4$–graphene oxide | Tetracycline | 10 min | – | 25 | 0–100 | 39.1 | Langmuir | Pseudo-second order | Lin et al. (2013) |
| $Fe_3O_4$–reduced graphene oxide–nitrilotriacetic acid | Tetracycline | 24 h | 4.0 | 25 | 50 | 212[a] | – | Pseudo-second order | Li et al. (2017a, b) |
| $Fe_3O_4$–reduced graphene oxide–thiourea dioxide | Tetracycline | 24 h | 4.0 | 40 | 5–100 | 1233 | Langmuir | Pseudo-second order | Yang et al. (2017) |

[a]Experimental value

[b]mmol/L

and Cu(II), different from the expected order if considering only the hydrated radius Pb(II), Cu(II), and Cd(II). Although Cu(II) has a lower hydrated radius compared to Cd(II), the hydration energy of − 496.9 kcal/mol is higher compared to Cd(II), which value is − 429.8 kcal/mol(Cheng et al. 2012). Similar behavior was observed in the work of Kalantari et al. (2015) for the Pb(II), Ni(II), and Cu(II) removal by $Fe_3O_4$–montmorillonite. The adsorption decreasing order was Pb(II), Cu(II), and Ni(II). Though Ni(II) has a hydrated radius of 4.04 Å that favors the exchange process, the hydration energy of -503.3 kcal/mol is greater than hydration energy of Cu(II).

The pH is another factor that influences the adsorption of toxic elements in the magnetic materials of zeolite and clays. Although the negative charges formed by the isomorphic substitution are not dependent on pH, the amount of the adsorbate is changed with the pH variation. Javanbakht et al. (2016) found that the adsorption of Pb(II) in the magnetic nanocomposite based on zeolite was lower in an acid solution due to the hydronium ions competing with the lead

ions for the exchange sites. The pH influence in the adsorption capacity can also be related to change in the surface charges of the adsorbent. The highest adsorption of Cr(VI) $MnFe_2O_4$–bentonite occurred at pH 2.0, and electrostatic interaction was the predominant adsorption mechanism. In aqueous solution, the ions Cr(VI) are found in the forms $Cr_2O_7^{2-}$, $CrO_4^{2-}$, $HCrO_4^-$, $H_2CrO_4$. At pH 2.0, $HCrO_4^-$, and $Cr_2O_7^{2-}$ species predominate, and the nanocomposite surface will be positively charged. Resulting in greater attraction for the negatively charged complex Cr(VI) ions in solution (Kaur et al. 2015).

The hydroxyapatite mineral is another natural material that is used to remove toxic elements. The application of magnetic hydroxyapatite to remove Pb(II) was the most reported. In general, the Pb(II) adsorption by hydroxyapatite–$Fe_3O_4$ occurs mainly through the ion exchange mechanism, with the replacement of the $Ca^{2+}$ ions present in the hydroxyapatite by the $Pb^{2+}$ ions. The hydroxyapatite–$Fe_3O_4$ nanocomposites were evaluated by Zhuang et al. (2015), and Dong et al. (2010) in the Pb(II) removal and the maximum adsorption capacity were 434.8 mg/g and 598.8 mg/g, respectively. The highest value of the second work can be attributed to the material synthesized by Dong et al. (2010) that presented a larger surface area,109 $m^2$/g, than the material prepared by Zhuang et al. (2015), 59 $m^2$/g. Core–shell structures were also evaluated in the Pb(II) removal. The maximum adsorption capacity was 321.2 m/g for $Fe_3O_4$@ hydroxyapatite, which was lower of than materials with a porous structure (Yang et al. 2014a). On the other hand, $Fe_3O_4$@hydroxyapatite showed better magnetic properties, which is an important aspect for the material separation from the aqueous solution and reuse adsorbent. Hydroxyapatite materials also performed well for removing other metals, such as Cd(II) and Zn(II) with adsorption capacity of 220.8 mg/g and 140.6 mg/g, respectively (Feng et al. 2010).

Nanocomposites formed by a polymeric matrix represent a promising class of adsorbent materials for metals removal from water and wastewater, due to the functional groups of the polymeric matrices that provide specific bindings to target pollutants (Lofrano et al. 2016). Many research aims to use natural polymers as a low-cost adsorbent. Donia et al. (2012) studied the adsorption of Ag(I), Cu(II), and Hg(II) in $Fe_3O_4$–cellulose–$NH_2$. The maximum capacity found was 129.4, 95.3, and 401.2 mg/g for Ag(I), Cu(II), and Hg(II), respectively. The maximum uptake was observed at pH 5.4 and 6.3 for Cu(II) and Ag(I), respectively. According to the authors, the mechanism of adsorption was due to complex formation between the nitrogen lone pair of electrons and metal ion. For Hg(II), the optimum pH was 2.0, and electrostatic interactions were responsible for the adsorption of Hg(II). The pH adjustment of the solution to 2.0 was carried out by adding HCl, leading to the formation of $HgCl_3^-$. At pH 2.0, there is protonation of amino groups, favoring the interaction of the material with $HgCl_3^-$. In the same work, the performance of $Fe_3O_4$–cellulose–$NH_2$ in the Al(III), Cu(II), Ni(II), Zn(II), and Cr(III) removal from a battery industry effluent was evaluated. The removal percentage found was between 65 and 100% with a contact time of 7 min. Behavior similar to the Hg(II) adsorption in the cellulose nanocomposite was observed by Sun et al. (2014), removing Cr(VI). The maximum amount of Cr(VI) adsorbed of 171.5 mg/g by $Fe_3O_4$ @$SiO_2$@cellulose@$NH_2$ was reached at pH 2.0, where Cr(VI) is found in the chemical forms $HCrO_4^-$ and $Cr_2O_7^{2-}$.

Among the materials considered biosorbent, chitosan is one of the most studied for removing pollutants in water, mainly due to the presence of hydroxyl and amine groups, which can serve as chelating sites (Wang et al. 2017; Brião et al. 2020). Chitosan-magnetite nanocomposites were able to remove toxic metal ions, such as Ni(II) and Pb(II), whose maximum adsorption capacity was 52.6 mg/g and 63.3 mg/g, respectively (Tran et al. 2010). One of the advantages of using chitosan as a matrix for magnetic nanoparticles is the ease of chemical surface modification, which can lead to the improvement of the adsorbent. The results presented in different studies indicated that the maximum adsorption capacity of amino-functionalized magnetic chitosan for Pb(II) removal was greater compared to non-functionalized magnetic chitosan with values of 104.2, 123.5, and 124.0 mg/g using amino groups 4-((pyridin-2-illimino) methyl) benzaldehyde as a source, ethylenediaminetetraacetic acid, and polyethyleneimine, respectively (Ren et al. 2013; Gutha and Munagapati 2016; Wang et al. 2017). The Hg(II) removal was also evaluated in magnetic chitosan functionalized with cyanoguanidine. The maximum capacity of the $Fe_3O_4$@ chitosan-cyanoguanidine nanosorbent was 285 mg/g obtained at pH 7.0(Wang et al. 2013). Considering that the water after the treatment should have a pH between 6.5 to 9.0, the need not adjust the pH can be advantageous.

Alginate is also a biopolymer that has been used in studies of metals removal, and the carboxylate groups are the main responsible for the adsorption of metallic cations (Bakr et al. 2015). Bée et al. (2011) studied the Pb(II) adsorption mechanism in the calcium alginate-maghemite nanocomposite monitoring the calcium ions released into the solution. The authors concluded that the adsorption occurred through the ion exchange mechanism between Ca(II) and Pb(II) ions, which explains the results presented in the study by Idris et al. (2012), where Pb(II) adsorption was lower at low pH due to the competition of $H^+$ ions for the exchange sites. At pH values above 10, there was also a striking decrease in the uptake capacity due to the formation of insoluble Pb(II) hydroxide formation, which made the adsorption of Pb(II) ions difficult via the ion-exchange mechanism. The ɣ-$Fe_2O_3$–alginate nanocomposite showed an adsorption capacity for Pb(II) of 100 mg/g, similar to the

values reported for magnetic chitosan functionalized with amino groups.

Magnetic nanocomposites based on synthetic polymers also exhibited good performance in removing toxic elements, especially Cr(VI). Davodi et al. (2017) prepared the polydopamine@$Fe_3O_4$nanocomposite and obtained an adsorbent with a maximum adsorption capacity of 307 mg/g for Hg(II) at pH 5.4. The point of zero charge for nanocomposite was 3.0 and at pH 5.4 the nanocomposite will have a predominance of negative charges, favoring the adsorption of Hg(II). Li et al. (2017b) employed the polydopamine nanocomposite functionalized with amino groups to remove Cr(VI). The maximum capacity found was 284.1 mg/g at pH 2.0. The authors believe that in addition to the electrostatic interactions between the –OH and $–NH_2$ groups and Cr(VI) ions, Cr(VI) removal occurred by a reduction reaction, possibly because, in an acidic system, some Cr(VI) was partially reduced to Cr(III) by the C–H and C–OH groups of the adsorbent were oxidized to other forms. The highest values of Cr(VI) removal capacity were also obtained at pH 2.0 for polyaniline nanocomposites. Polyaniline–$Fe_3O_4$ was the adsorbent chosen by Han et al. (2013). The maximum adsorption capacity of Cr(VI) was 200 mg/g reached in 3 h. Chávez-Guajardo et al. (2015) used a similar adsorbent containing maghemite as magnetic nanoparticle. Polyaniline–ɣ-$Fe_2O_3$ exhibited a maximum adsorption capacity of 196 mg/g achieved in just 35 min, suggesting that the change in the type of magnetic nanoparticle did not influence the maximum adsorption capacity since the values were close to the nanosorbents of polyaniline. However, the adsorption equilibrium was reached in a shorter time when maghemite was used, probably due to the larger size of particle in the polyaniline–$Fe_3O_4$ nanocomposite (Han et al. 2013; Chávez-Guajardo et al. 2015).

Carbonaceous materials, including activated carbon, carbon nanotubes, and graphene oxide, have been widely studied for adsorption of various environmental contaminants (Yang et al. 2019). Activated carbon has been broadly used as a commercial adsorbent for the treatment of pollutants. Although activated carbon generally has a high specific surface area, chemical treatments are necessary to increase the adsorption capacity of activated carbon (Abdullah et al. 2019). Kang et al. (2016) evaluated the performance of magnetic activated carbon for Cd(II) e Pb(II) removal and the influence of acid treatment in the adsorption capacity. The results showed that the maximum adsorption capacities of activated carbon and activated carbon treated with nitric acid for Cd(II) removal were 6.50 and 60.4 mg/g, respectively, and 11.8 and 99.6 mg/g for Pb(II), respectively. The adsorbent capacities increased significantly with nitric acid treatment; however, there was a reduction in the adsorption capacity when activated carbon treated with nitric acid was combined with magnetic nanoparticles, 49.8 and 86.2 mg/g for Cd(II) and Pb(II), respectively, attributed to the decrease in the active sites of activated carbon treated with nitric acid that was occupied by magnetic nanoparticles, suggesting that for activated carbon material, the magnetic nanoparticles did not contribute to the increase in the adsorption capacity of the nanocomposite, unlike other matrices.

Magnetic carbon nanocomposites with a core–shell structure were also studied. Huong et al. (2018) evaluated the adsorption capacity of $Fe_3O_4$@C for As(V). The maximum adsorption capacity obtained by the Langmuir model was 20.1 mg/g at pH 1–2. The adsorption mechanism occurred through electrostatic interactions between the functional groups of the nanocomposite, eg., –COOH and –OH, and As(V) ions, which was influenced by the structure morphology of $Fe_3O_4$@C. However, there was a reduction of the As(V) quantity adsorbed with the carbon content increase. The increase in the carbon content caused the encapsulating of the magnetic nanoparticles, impairing the interaction of –OH groups with arsenic ions. At low pH conditions, the number of $H^+$ ions in the solution increased, and –OH and –COOH became positively charged $–OH_2^+$ and $–COOH_2^+$, increasing the adsorption capacity of $H_2AsO_4^-$. The same mechanism has been reported for the adsorption of Cr(VI) in $Fe_3O_4$@C, whose maximum capacity of 61.7 mg/g was obtained at pH 4.0 (Chen et al. 2016b).

An advantage of carbon-based materials is the easy modification of the chemical surface, which allows the combination of different materials in a single structure. For example, Yang et al. (2015) proposed the Hg(II) and Pb(II) removal in the three-phasic nanocomposite formed by magnetic particles, carbon, and hydroxyapatite. The results showed that the maximum adsorption capacity increased when hydroxyapatite was added to the C–$Fe_3O_4$ material, mainly for Pb(II). The adsorption capacities for Hg(II) and Pb(II) in C–$Fe_3O_4$ were 54.2 and 10.2 mg/g, respectively, while in hydroxyapatite@C–$Fe_3O_4$, the adsorption capacities were 64.2 and 292.5 mg/g, respectively, which corroborates with other studies that used magnetic hydroxyapatite to remove Pb(II) and confirm the good performance of the material in the lead adsorption.

Another carbon-based material that has been used in the remediation of toxic elements from water is carbon nanotubes. Although the hydrophobic character of multiwalled carbon nanotubes is more appropriate to remove organic pollutants more efficiently. $Fe_3O_4$-multiwalled carbon nanotubes exhibited low maximum adsorption capacity for metals, eg., 8.1 mg/g for Cu(II) and 3.8 mg/g for Zn(II) (Liu et al. 2015; Jiang et al. 2016). Nonetheless, the surfaces of carbon nanotubes are subject to modification. Zhou et al. (2014a) prepared multiwalled carbon nanotube coated with $CoFe_2O_4$ modified with amino groups. To improve the performance of multiwalled carbon nanotube magnetic, a modification

was made adding the chitosan. The efficiency of the material for Pb(II) removal was tested, and the maximum adsorption capacity was 140 mg/g. The material without chitosan was also evaluated, and the maximum adsorption capacity obtained was 66 mg/g, proving the improvement in the performance of the adsorbent modified with the biopolymer.

Graphene and derivatives of graphene were also used for the adsorption of toxic elements. The $Fe_3O_4$-graphene oxide nanocomposite reached the maximum adsorption capacity in 24 h for As(III) and As(V) of 147 and 113 mg/g, respectively (Su et al. 2017), which is the highest reported for arsenic removal in magnetic nanocomposites. Higher values of adsorption capacity were also found for metals. The maximum adsorption capacity in an equilibrium time of 3 h for Cu(II), Hg(II), and Pb(II) was 301.2, 268.5, and 508.4 mg/g, respectively (Cui et al. 2015).

Studies with reduced graphene oxide nanocomposites for toxic elements removal have been reported, but in a smaller number than graphene oxide materials. Chella et al. (2015) used $MnFe_2O_4$-reduced graphene oxide to remove Pb(II) and Cd(II). The maximum adsorption capacity for Pb(II) and Cd(II) were 100.0 and 76.9 mg/g at 37°C, respectively. The adsorption capacity was also measured for $MnFe_2O_4$ and reduced graphene oxide, and the results for Pb(II) and Cd(II) were 45, 30, 25, and 15 mg/g, respectively. The synthesized magnetic nanoparticles have an adsorption capacity higher than that of bare graphene, which may have increased the adsorption capacity of the nanocomposite because magnetic nanoparticles have surface charges that can act as active sites for removing metals. Guo et al. (2014) used the reduced graphene oxide nanocomposite functionalized with amino groups for adsorption of Cr(VI), Pb(II), Hg(II), Cd(II), and Ni(II) from contaminated water. The equilibrium adsorption capacity obtained was 17, 28, 23, and 29 mg/g for Cr(VI), Pb(II), Hg(II), Cd(II), and Ni(II), respectively. Despite the presence of amino groups, the reduced graphene oxide nanocomposites showed adsorption capacity lower than the values found for graphene oxide, probably due to the reduced number of functional groups responsible for the active sites involved in the toxic element removal.

## Adsorption of pesticides

Pesticides represent one of the most important classes of organic pollutants, mainly due to the widespread use and increasing toxicity. Environmental Protection Agency describes pesticide as any substance which is used to prevent, destroy, repel, or mitigate any pest (Sabarwal et al. 2018). Studies have revealed that surface waters in river basins contain a large number of pesticides and the transformation products, which can pose risks to aquatic organisms, even at low concentrations (Moschet et al. 2014; Vieira et al. 2016; Glinski et al. 2018). Exposure to pesticides is thought to be linked to numerous health disorders such as Parkinson's disease, cancer, endocrine disruption, respiratory and reproductive disorders, and, therefore, the removal of pollutants from water is necessary (Sabarwal et al. 2018).

The use of magnetic nanocomposites has been investigated in the removal of pesticides by the adsorption process. According to Table 3, the most studied pesticides were herbicides and insecticides. Both the Langmuir and Freundlich models were used to explain the adsorption mechanism of pesticides in magnetic nanocomposites. The Freundlich model is ideal for adsorption on heterogeneous and multilayer surfaces. Thus, the Freundlich model assumes that the pesticide molecules interact with nanocomposites' active sites with different energies (Uddin 2017; Wang et al. 2018). Like the toxic elements, the pseudo-second-order equation was the one that best fitted the adsorption kinetics data.

The mechanisms in which magnetic nanocomposites absorb pesticides were also associated with diverse types of interactions. Generally, electrostatic interaction and π–π interaction, π-stacking interaction, π–π electron-donor–acceptor interaction, hydrophobic interaction, and physisorption might be the primary mechanisms (Wang et al. 2018). The structural, physical, chemical, and magnetic properties of the nanosorbent contribute to various reaction mechanisms with different pesticides. For example, acidic zeolite with different $Fe_3O_4$ contents removed the herbicide simazine by different mechanisms. The maximum capacity of the $Fe_3O_4$–zeolite–H material with 5.4 wt% $Fe_3O_4$ was reached at pH 6.5, and the simazine uptake by magnetic adsorbent involved a typical acid–base reaction, because the nanocomposite presented a high amount of acid hydrogen sites, and simazine behaves as a base because of the electron lone pairs located in the lateral chains of the molecule. For the material with 7.1 wt% $Fe_3O_4$, the maximum capacity was obtained at pH 3.0, and the intermolecular hydrogen bond in the simazine-magnetite played a crucial role. The pH of point of zero charge was 5.6 and at pH 3.0 the material surface was positively charged due to the hydronium cations adsorbed, which formed hydrogen bonds between the surface of the adsorbent and the molecules of simazine. Although the mechanisms have been different, both materials exhibited similar adsorption capacity of ca. 6.0 mg/g (Pansini et al. 2018). From a water treatment perspective, the use of an adsorbent that exhibits maximum adsorption in pH as close as possible to the natural water is advantageous.

The interactions between magnetic nanocomposites and pesticides are also dependent on temperature. The adsorption capacity of magnetic sepiolite clay for atrazine decreases with increasing temperature, indicating that the adsorption was exothermic. A possible explanation relies on the mobility of atrazine molecules increased with increasing temperature, which led to the weak forces more weakened with further increasing temperature, resulting in a decrease

in the adsorption capacity of magnetic sepiolite (Liu et al. 2014a). Thermodynamic studies revealed that the adsorption process of the insecticide pentachlorophenol in magnetic carbon nanotubes was also exothermic. The enthalpy variation was −6.14 kJ/mol and the low enthalpy variation value indicated that pentachlorophenol adsorption could be considered as physical adsorption. In addition, the negative value of Gibbs free energy variation indicated a spontaneous process (Zhou et al. 2014b).

In general, carbon-based magnetic materials perform better at removing pesticides compared to inorganic materials and therefore have been further studied. Zhou et al. (2014b) evaluated the potential of magnetic carbon nanotube coated with $SiO_2$ in the pentachlorophenol removal from aqueous solution. The highest pentachlorophenol uptake of 96.4 mg/g was obtained at 30 min and pH 2.5. The maximum capacity dramatically decreased from 96.4 to 52.1 mg/g when pH varied from 2.5 to 9. Pentachlorophenol is a weak acid compound with $pK_a$ 4.75, and at a pH above 4.75, the ionized form of pentachlorophenol is predominant. At pH 2.5, the adsorbent surface was negatively charged, since the point of zero charge at pH 4.1, forming an electrostatic repulsion force between pentachlorophenol and the adsorbent surface, which resulted in a decrease in adsorption capacity. Similar behavior was observed by Nethaji and Sivasamy (2017) for the herbicide 2,4-dichlorophenoxy-acetic acid removal by graphene oxide-$Fe_3O_4$ with point of zero charge at pH 4.0. The material exhibited maximum adsorption capacity of 67.3 mg/g at pH 3.0, and the value decreased considerably at high pH.

Despite the high values of adsorption capacity for pesticides, the need for a very low pH can be an inconvenience in water treatment. Therefore, studies aimed at improving materials are essential. Modification with amino groups, for example, can increase the point of zero charges of the nanocomposite and widen the range of pH values. The $Fe_3O_4$@$SiO_2$@graphene oxide-2-phenylethylamine adsorbent showed an isoelectric point of 6.6 due to the amino groups, which required no adjustments to the pH during adsorption (Wanjeri et al. 2018).

Another parameter that must be considered is the concentration of pollutants in the aqueous solution. When working with lower concentrations of the pollutant, low values of adsorption capacity are obtained. Wanjeri et al. (2018) applied the $Fe_3O_4$@$SiO_2$@graphene oxide-2-phenylethylamine nanocomposite as an adsorbent for organophosphate insecticides, namely chlorpyrifos, malathion, and parathion. Due to the high toxicity of insecticides, European Union Directive has established a maximum permitted concentration of 0.5 ng/mL for total organophosphate insecticides in drinking water. Therefore, the authors used pesticide concentrations in the order of µg/mLin the adsorption tests. The maximum adsorption capacity was achieved in 15 min and the values were 11.1, 10.6, and 10.9 mg/g for chlorpyrifos, malathion, and parathion, respectively. The $Fe_3O_4$@$SiO_2$@graphene oxide-2-phenylethylamine adsorbent was tested for water samples from Vaal River and Dam in South Africa, and showed greater than 86.9% recovery for the analyzed pesticides, reducing the concentration of organophosphate insecticides to acceptable levels. However, there are still a few works that evaluate the application of magnetic nanocomposites in the remediation of real samples. Such a study is essential, as the efficiency of the material for a given pollutant can be altered in the presence of other substances. Boruah et al. (2017) found that the adsorption efficiency of the $Fe_3O_4$–reduced graphene oxide nanocomposite was enhanced in the presence of different ions, such as $Mg^{2+}$, $Ca^{2+}$, $Na^+$, and $SO_4^{2-}$, and a maximum for ametrine adsorption of 63.7 mg/g was found in seawater medium. The adsorption occurred due to electrostatic interactions between conjugated double bonds of pesticide molecules and the oxygen of the functional groups of the reduced graphene oxide–$Fe_3O_4$ nanocomposite. The presence of cations led to the formation of an electrical double layer at the nanocomposite-water interface due to the presence of negative surface charge of reduced graphene oxide sheets, increasing the electrostatic interactions between nanocomposite and pesticides molecules.

The magnetic molecularly imprinted polymer was the material that showed the highest values of adsorption capacity toward pesticides because molecular imprinting is a technique with predetermined ligand selectivity. Masoumi et al. (2016) used $Fe_3O_4$–$NH_2$-molecularly imprinted polymer to remove the insecticides chlorpyrifos, diazinon, and phosalone. The nanocomposite showed an excellent affinity with the tested pesticides, being the material that provided the highest values of adsorption capacity, even at low concentrations in the range 0.2–1.2 mg/L. The maximum adsorption capacity of chlorpyrifos, diazinon, and phosalone was 172, 192, and 196 mg/g, respectively. When the molecularly imprinted polymer test was performed without the magnetic nanoparticles, the maximum adsorption was lower for the three studied pesticides, with values of 95, 102, and 85 mg/g for chlorpyrifos, diazinon, and phosalone, respectively. The results indicated that besides the magnetic nanoparticles being advantageous for facilitating separation of the adsorbent from aqueous solution by an external magnetic field, the material exhibited improvement in the adsorption capacity.

## Adsorption of pharmaceutical-derived compounds

Pharmaceuticals represent a class of health care products that are intensively used worldwide mainly to promote human health and are classified based on therapeutic applications (Kyzas et al. 2014). Anti-inflammatories and analgesics, antibiotics, psychiatric drugs, antihypertensives, and

hormonal contraceptives are the main classes of highest consumption worldwide (Tijani et al. 2016), which the products have been the cause the contamination of aquatic matrices through the discharge of residual effluents, with antibiotics being the most commonly found in wastewater treatment plants (Jiang et al. 2013; Polesel et al. 2016). Studies on the adsorptions of pharmaceutical-derived compounds on magnetic nanocomposite are objects of great interests. Table 4 summarizes the adsorption parameters of magnetic nanocomposites for diverse classes of pharmaceuticals.

For most pharmaceuticals, the Langmuir isotherm was used to elucidate the adsorption mechanism in magnetic nanocomposites. The pseudo-second-order model was better suiting the adsorption kinetics, indicating that the adsorption process depends on the initial adsorbate concentration. According to thermodynamic parameters, the adsorption process is spontaneous and preferably exothermic for most materials. The adsorption of the cephalexin antibiotic by $Fe_3O_4$–zeolite showed enthalpy variation of − 25.5 kJ/mol (Mohseni-Bandpi et al. 2016). Negative values of enthalpy variation were also obtained for carbon-based materials $Fe_3O_4$–activated carbon and $Fe_3O_4$–multiwalled carbon nanotubes in the removal of the antiepileptic carbamazepine and antimicrobial furazolidone, respectively (Liu et al. 2015; Baghdadi et al. 2016). For magnetic graphene-based materials, positive enthalpy variation values were reported for the adsorption of the antibiotic tetracycline; values of 31.2 and 6.6 kJ/mol were observed for $Fe_3O_4$–graphene oxide-nitroacetic acid and $Fe_3O_4$–reduced graphene oxide-thiourea oxide, respectively (Li et al. 2017a; Yang et al. 2017). The enthalpy variation values suggest that tetracycline adsorption in magnetic nanocomposites based on graphene can be considered as physical adsorption.

Several mechanisms can govern the adsorption of pharmaceutical compounds on the magnetic nanoparticles. The increase in surface functional groups of nanocomposites is the main contributor to the process of drug elimination (Wang et al. 2018). The maximum adsorption capacity of diclofenac in magnetic chitosan was 57.5 mg/g, and a much higher value of 240.4 mg/g was obtained using magnetic quaternary chitosan. The higher efficiency of diclofenac uptake can be attributed to the presence of quaternary ammonium groups in the modified chitosan, which are responsible for the electrostatic interaction with the diclofenac, which under the optimal pH of 7.0, is found in the anionic form (Zhang et al. 2014; Soares et al. 2019). The increase in the adsorption capacity of graphene-based materials when modified was also reported in the tetracycline adsorption. The maximum adsorption capacity of tetracycline by $Fe_3O_4$–graphene oxide was 39.1 mg/g, whereas, for $Fe_3O_4$–graphene oxide–nitroacetic acid and $Fe_3O_4$–reduced graphene oxide-thiourea oxide, the maximum adsorption capacity was 212 and 1233 mg/g, respectively. However, the contact time of the $Fe_3O_4$-graphene oxide was considerably shorter, 30 min, while the contact time of the modified graphene oxides was 24 h (Lin et al. 2013; Li et al. 2017a; Yang et al. 2017). The maximum adsorption capacity of 87.2 mg/g for opioid methadone by unmodified magnetic graphene oxide was also reached in a short time of 30 min (Gupta et al. 2017).

Antibiotic removal was also evaluated using carbon-based magnetic nanocomposites, such as carbon nanotubes and activated carbons. Mao et al. (2016) studied the process of removing ciprofloxacin with the nanosorbent $Fe_3O_4$@C and found 98% removal for ciprofloxacin at pH 7.0 and 30 °C. The maximum adsorption capacity was 90.1 mg/g. Danalıoğlu et al. (2017) investigated antibiotic removal using magnetic-activated carbon modified with chitosan. The adsorption experiments were carried out under similar conditions to those used by Mao et al. (2016) and resulted in maximum adsorption capacity values of 90.1, 178.6, and 526.3 mg/g for ciprofloxacin, erythromycin, and amoxicillin, respectively. The values of the maximum adsorption capacity of ciprofloxacin were equal in both studies, even though $Fe_3O_4$–activated carbon–chitosan exhibiting a specific surface area higher than the area of $Fe_3O_4$@C. The comparable adsorption capacity of $Fe_3O_4$@C to the magnetic activated carbon functionalized with chitosan was attributed to the thermal treatment applied to the $Fe_3O_4$@C. The heating at 600 °C removed some surface groups such as C=O, which do not contribute to ciprofloxacin adsorption, thereby providing more active sites for adsorption. The main mechanism that leads to ciprofloxacin adsorption is the π–π electron donor–acceptor interaction between the benzene ring of ciprofloxacin and the adsorbent carboxyl groups (Mao et al. 2016).

Magnetic multiwalled carbon nanotubes were the object of study by Hu et al. (2011) for the synthetic hormone 17α-methyltestosterone removal. $Fe_3O_4$-multiwalled carbon nanotube was able to remove 90% of the 17α-methyltestosterone in just 3 min of contact, and no significant changes were observed after 0.5 and 8 h. A comparative study was carried out using only $Fe_3O_4$, and the value of the 17α-methyltestosterone removal percentage reduced considerably to 10%. The variation of removel percentage is related to the types of interactions between 17α-methyltestosterone and the material surface. As 17α-methyltestosterone is a hydrophobic compound and the surface of $Fe_3O_4$-multiwalled carbon nanotube has hydrophobic groups, the interaction with $Fe_3O_4$-multiwalled carbon nanotube will be more favorable in comparison with $Fe_3O_4$ that has a polar surface. Notwithstanding, the maximum adsorption capacity of $Fe_3O_4$–multiwalled carbon nanotube was minimal, whose value was 0.12 mg/g. The steroid hormone 17β-estradiol removal by multiwalled carbon nanotube–N–$CoFe_2O_4$nanocomposite was also investigated. The experimental results indicated that the maximum

adsorption capacity was 20.0 mg/g for 17β-estradiol (Wang et al. 2015a). The low values of adsorption capacity show the difficulty of removing endocrine-disrupting chemicals in aqueous systems. Low values of adsorption in magnetic nanotubes have also been found for other pharmaceuticals. The maximum adsorption capacity for the antibiotic sulfamethoxazole in multiwalled carbon nanotube–N–$CoFe_2O_4$ was 7.4 mg/g (Wang et al. 2015a), and for the antimicrobial furazolidone in $Fe_3O_4$-multiwalled carbon nanotubewas 19.2 mg/g (Liu et al. 2015).

Magnetic nanocomposites with inorganic matrices also showed lower values of adsorption capacity when compared to materials based on graphene and carbon. The magnetite–zeolite material had an adsorption capacity for cephalexin of 27.9 mg/g at pH 6.0 and a contact time of 2 h (Mohseni-Bandpi et al. 2016). The maximum capacity of the hydroxyapatite-coated magnetic carbon for the antibiotic ampicillin was 3.5 mg/g at pH 6.0 and contact time 24 h. In addition to the nanocomposite hydroxyapatite @C–$Fe_3O_4$, the ampicillin removal by C–$Fe_3O_4$ and hydroxyapatite was studied. Hydroxyapatite showed no ampicillin removal capacity, whereas C–$Fe_3O_4$ exhibited a maximum removal capacity of ca. 14.0 mg/g. In the same work, the hydroxyapatite@C–$Fe_3O_4$ performance toward Pb(II) removal was evaluated, as a result, hydroxyapatite showed the ability to adsorb Pb (Yang et al. 2015). From the results presented and discussed in "Adsorption of toxic elements" section , hydroxyapatite nanomaterials have a higher affinity for metals, whose adsorption occurs through the ion exchange mechanism.

The efficiency of the magnetic nanocomposite was evaluated in the antibiotic's removal in real samples. $Fe_3O_4$–graphene oxide nanocomposite was utilized as an adsorbent for removing the tetracycline group from samples of mineral water and river water in the study by Lin et al. (2013). Oxytetracycline, tetracycline, chlortetracycline, and doxycycline were chosen as the target analytes. Tetracyclines were not detected in the blank samples. Thus, a 500 mL spiked water sample containing four tetracyclines was used as the test sample solution. The samples were subjected to treatment using 50 mg $Fe_3O_4$–graphene oxide for mineral water and 60 mg for river water. The tetracyclines removal was monitored through the chromatographic peaks, and the absence of peaks after the adsorption test indicated the efficiency of the material for antibiotics elimination in low concentrations in the range of 0.1–0.2 mg/L.

## Regeneration and reusability of magnetic nanosorbents

The regeneration ability of the adsorbent is essential to evaluate the cost-effectiveness of the material in water treatment (Bhaumik et al. 2011). The reuse of nanocomposites may reduce the total cost (Zhang et al. 2016), besides increasing the sustainability of the process (Tang and Lo 2013). Usually, the regeneration of the magnetic iron oxide nanocomposites is performed by chemical treatment through the desorption process after recovering the material from aqueous solution via magnetic separation (Nethaji and Sivasamy 2017; Abdullah et al. 2019), as illustrated in Fig. 3. The desorption process not only can regenerate the magnetic nanosorbents and restore the adsorption capacity but also recover valuable components, like metals, from the adsorbed phase (Tang and Lo 2013). The regenerated nanosorbent is subjected to adsorption and desorption experiments to evaluate the reusability. Typically, desorption tests are performed subjecting the adsorbent to a suitable eluent. The eluent choice will depend on the structure of the nanocomposite, the nature of the pollutant, and the adsorption mechanism (Zhang et al. 2016). Table 5 summarizes some data from desorption and regeneration studies of magnetic nanocomposites.

Acid has been suggested for regeneration in numerous studies, and the concentration of the eluent is a determining factor found that the higher Pb(II), Hg(II) and Cu(II) desorption efficiency from ethylenediaminetetraacetic acid-$Fe_3O_4$-graphene oxide was obtained at higher HCl concentration (Tang and Lo 2013; Cui et al. 2015). At the concentration of 0.01 mol/L, the desorption percentage for the target pollutants was very low, ranging from 9 to 16%. However, when the concentration was increased to 0.5 mol/L, the desorption efficiency was above 90%. Nevertheless, the stability of the magnetic nanoparticles in acidic or basic media has to be taken into consideration. The desorption of the pollutants with strong acid or alkaline may lead to magnetic nanoparticle dissolution (Tang and Lo 2013). Wang

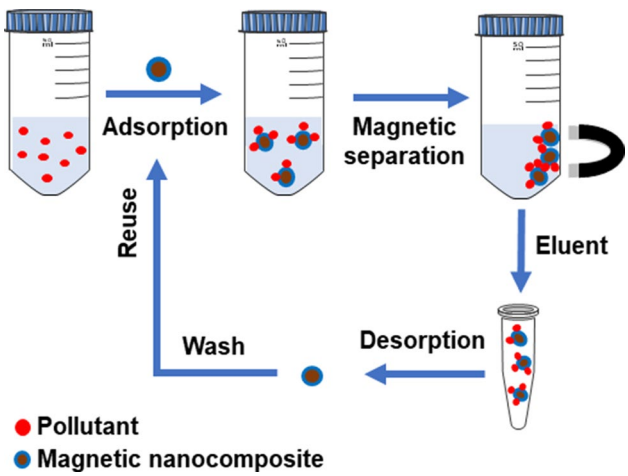


**Fig. 3** Procedure used for magnetic nanosorbent regeneration. Steps: target pollutant adsorption, magnetic separation of the nanosorbent from the solution, pollutant desorption by eluent, and reuse of the magnetic nanosorbent

**Table 5** Desorption and regeneration of magnetic iron oxide nanocomposites

| Magnetic nanosorbent | Target pollutant | Eluent | Experimental conditions | Desorption (%) | Cycles | References |
|---|---|---|---|---|---|---|
| γ-$Fe_2O_3$–zeolite | As(III) | NaOH (0.1 M) | Dose adsorbent: 0.05 g<br>Eluent volume: 50 mL<br>Contact time: 2 h | 80 | Five | Salem Attia et al. (2014) |
| Hydroxyapatite–$Fe_3O_4$ | Cd(II)<br>Zn(II) | EDTA (0.003 M) | Dose adsorbent: 0.1 g<br>Eluent volume: 20 mL<br>pH: 2.54<br>Contact time: 24 h | 62.2 (Cd)<br>67.0 (Zn) | – | Feng et al. (2010) |
| Hydroxyapatite–$Fe_3O_4$ | Pb(II) | EDTA (0.001 M) | Dose adsorbent: 0.05 g<br>Eluent volume: 50 mL<br>Contact time: 24 h | 55.5 | – | Dong et al. (2010) |
| $Fe_3O_4$@$SiO_2$@cellulose@$NH_2$ | Cr(VI) | NaOH (0.1 M) | Dose adsorbent: 0.02 g<br>Eluent volume: 50 mL<br>Contact time: 30 min | 98 | Five | Sun et al. (2014) |
| $Fe_3O_4$–$SiO_2$–chitosan–EDTA | Cd(II)<br>Cu(II)<br>Pb(II) | $Na_2$EDTA (0.01 M) | Dose adsorbent: 0.01 g<br>Eluent volume: 10 mL<br>pH: 5.0<br>Contact time: 8 h | 90 | Five | Ren et al. (2013) |
| γ-$Fe_2O_3$–alginate | Pb(II) | HCl (0.1 M) | Dose adsorbent: 10 g<br>Eluent volume: 50 mL<br>pH: 7<br>Contact time: 1 h | 87.8 | Five | Idris et al. (2012) |
| $Fe_3O_4$@C | Sulfonamides | Methanol (%60 v/v) | Dose adsorbent: 50 mg<br>pH: 6.7<br>Contact time: 24 h | 95 | Nine | Bao et al. (2014) |
| $Fe_3O_4$@C | Ciprofloxacin | NaOH 3% and methanol ($v_{NaOH}$:$v_{met.}$: 1:5) | Dose adsorbent: 0.1 g<br>Eluent volume: 50 mL<br>pH: 7<br>Contact time: 3 h | – | Five | Mao et al. (2016) |
| $Fe_3O_4$–activated carbon–chitosan | Ciprofloxacin<br>Erythromycin | Phosphate buffer ($KH_2PO_4 + K_2HPO_4$) | Dose adsorbent: 1 mg<br>Eluent volume: 25 mL<br>Contact time:7 h | 14.7 (Ciprofloxacin)<br>15.4 (Erythromycin) | – | Danalıoğlu et al. (2017) |
| Graphene oxide–$Fe_3O_4$ | 2.4-dichlorophenoxyacetic | Acetone | Dose adsorbent: 0.5 g | – | Three | Nethaji and Sivasamy (2017) |
| $Fe_3O_4$@$SiO_2$@graphene oxide–polyethyleneimine | Chlorpyrifos<br>Parathion<br>Malathion | Acetone | Dose adsorbent: 15 mg<br>Eluent volume: 2 mL<br>Contact time: 2 min | 89–100 | Ten | Wanjeri et al. (2018) |

**Table 5** (continued)

| Magnetic nanosorbent | Target pollutant | Eluent | Experimental conditions | Desorption (%) | Cycles | References |
|---|---|---|---|---|---|---|
| EDTA–$Fe_3O_4$–graphene oxide | Pb(II)<br>Hg(II)<br>Cu(II) | HCl (0.5 M) | Dose adsorbent: 10 mg<br>Eluent volume: 25 mL<br>pH: natural<br>Contact time: 1.5 h | 94.0 (Pb)<br>92.9 (Hg)<br>95.3 (Cu) | Five | Cui et al. (2015) |
| $Fe_3O_4$–reduced graphene oxide | Ametryn | Acetone | Dose adsorbent: 10 mg<br>pH: 5.0<br>Contact time: 2 min | – | Seven | Boruah et al. (2017) |

*EDTA* ethylenediaminetetraacetic acid

et al. (2010) evaluated the stability of $Fe_3O_4$@$SiO_2$–$NH_2$ nanocomposite under acidic conditions by monitoring the Fe leached content. For $Fe_3O_4$, 42.7% Fe was leached out after the material been in HCl 1 mol/L for 12 h, but less than 1 wt% for the amino-functionalized adsorbent with the same treatment, reflecting a substantially enhanced stability of $Fe_3O_4$@$SiO_2$–$NH_2$ nanoparticles under acidic conditions. Emadi et al. (2013) tested the same conditions for the $Fe_3O_4$@$SiO_2$ nanocomposite, and the Fe leaching was less than 3 wt%, showing the important role of silica coating in stabilizing magnetic nanoparticles.

As discussed earlier, the adsorption of most pollutants onto magnetic nanocomposites is highly dependent on the solution pH, allowing the material to regenerate by changing the pH. For example, the adsorption of As(III) ions on ɣ-$Fe_2O_3$–zeolite and Cr(VI) on $Fe_3O_4$@$SiO_2$@cellulose@$NH_2$ was favored at low pH (2.0–2.2), so the desorption can be achieved by increasing the solution pH. Therefore, NaOH solution as eluent was used for desorption. (Salem Attia et al. 2014; Sun et al. 2014). Desorption of Pb(II) from the nanomaterial ɣ-$Fe_2O_3$–alginate by HCl resulted in 87.8% metal recovery and did not decrease dramatically during the five sorption–desorption cycles. The desorption efficiency can be attributed to the formation of anionic complexes between Pb(II) and $Cl^-$. As the adsorption of Pb(II) on alginate materials involves the ion exchange mechanism preferentially, the formation of complexes decreased the sorption affinity for adsorbent (Idris et al. 2012).

Besides acids and bases solution, ethylenediaminetetraacetic acid has been reported as a desorbing agent for metals. Ethylenediaminetetraacetic acid has some advantages over acidic and alkaline eluents, ethylenediaminetetraacetic acid forms stable complexes with metal ions and does not dissolve the magnetic nanoparticles. Ren et al. (2013) investigated the increase concentration of disodium ethylenediaminetetraacetate and $HNO_3$from 0.01 to 0.1 mol/L in desorption of Cd(II), Cu(II), and Pb(II) by $Fe_3O_4$–$SiO_2$–chitosan–ethylenediaminetetraacetic acid. For all disodium ethylenediaminetetraacetate concentrations evaluated, the desorption percentage was above 90%, while for $HNO_3$, the desorption percentage was above 92% using 1 mol/L, but was very low by using 0.1 mol/L. However, about 0.77–1.02% of the $Fe_3O_4$ magnetic cores would be leached out after suspending the nanocomposite in 1 mol/L $HNO_3$ for 12 h. Thus, disodium ethylenediaminetetraacetate proved to be better eluent for metals regeneration on magnetic chitosan. For hydroxyapatite nanocomposites, ethylenediaminetetraacetic acid solution was the most effective in the desorption of Cd(II), Pb(II), and Zn(II) compared to the eluents HCl, acetic acid, NaOH and $Ca(NO_3)_2$. The metals adsorption on hydroxyapatite-$Fe_3O_4$ occurs preferentially through the ion exchange mechanism, and the formation of metal-ethylenediaminetetraacetic acid complex decreases the sorption affinity for the adsorbent. The desorption efficiency of magnetic hydroxyapatite was still low related to other magnetic materials, with values in the range of 55.5–67.0% (Feng et al. 2010; Dong et al. 2010). On the other hand, the low desorption efficiency for hydroxyapatite–$Fe_3O_4$ reduces the transportation of toxic metals ions in natural water (Dong et al. 2010).

Another option to regenerate the nanosorbent is extraction by organic solvent, typically used in the organic pollutants recovery such as pharmaceutical compounds and pesticides (Zhang et al. 2016). Acetone was one of the most reported solvents for pesticide recovery. Wanjeri et al. (2018) used acetone for the recovery of chlorpyrifos, parathion, and malathion pesticides adsorbed on magnetic graphene oxide. The recovery percentage of the pesticides after ten cycles of the adsorption and desorption process was in the range of 89–100%, indicating that the nanocomposite could be reused up to 10 times without a significant loss of adsorption. Other works of pesticide removal by graphene-based magnetic nanocomposites also report acetone as an efficient extractor solvent. The graphene-based nanocomposites regenerated with acetone were able to adsorb 89% of the herbicide ametrine for the seventh cycle (Boruah et al. 2017) and 91% of

the herbicide 2,4-dichlorophenoxyacetic for the third cycles (Nethaji and Sivasamy 2017). Methanol was used as a desorbing agent for the antibiotics recovery. For sulfonamide class antibiotics, more than 95% of the adsorbed antibiotics were released after extraction with methanol, and the regenerated $Fe_3O_4$@C showed a slight loss in the adsorption capacity even after nine test cycles (Bao et al. 2014). For ciprofloxacin, the removal rate on $Fe_3O_4$@C decreased from 98 to 61% after five rounds of recycling (Mao et al. 2016). Despite the efficiency of the solvents as an eluent, there is the drawback of toxicity. Environmentally friendly eluents, for example, phosphate buffer solution, were tested. However, the desorption percentages for ciprofloxacin and erythromycin were low, 15.4 and 14.7%, respectively (Danalıoğlu et al. 2017).

Chemical treatments are frequently employed for regeneration purposes due to cost-effectiveness and rapid process. However, one of the disadvantages is the tendency to destroy the surface properties of adsorbents (Abdullah et al. 2019). Mao et al. (2016) found that the textural properties of the $Fe_3O_4$@C material were modified after the recycling cycles. The specific surface areas decreased from 79 to 51 $m^2/g$, and the mesopores disappeared gradually with the increase in recycling times. Therefore, other methods of regeneration have been studied. In cases where the adsorbate exhibits low thermal stability and the adsorbent a good thermal and chemical stability, thermal regeneration of the adsorbents presents as a simple, inexpensive and fast process when compared to the use of eluents (Wong et al. 2016; Pansini et al. 2018). The thermal treatment was the process adopted by Wang et al. (2015a) in the regeneration of multiwalled carbon nanotube–N–$CoFe_2O_4$ containing sulfamethoxazole and 17β-estradiol since the carbon nanotubes are stable at temperatures below 400 °C. The results showed that the regenerated multiwalled carbon nanotube–N–$CoFe_2O_4$ had the ability to pharmaceutical compounds removing from the aqueous solution after consecutive cycles. The increase in the number of reuse cycles presents just a slight mass loss of the adsorbent, remaining practically constant from the second cycle, another stable material at high temperatures in the zeolites. Pansini et al. (2018) performed a study and verified that the thermal treatment of 5 min at 300 °C caused an efficient regeneration of $Fe_3O_4$–zeolite adsorbents. Also, the thermal treatment caused the decomposition of the analyzed pollutant, simazine herbicide, without causing damage to the adsorbent.

## Magnetic nanomaterials toxicity

The high number of recent research available in the literature shows that there is an increasing attraction in the use of iron-based nanomaterials for treating water and wastewater. However, the assessment of risks to the environment and human health is necessary to regulate the use of the materials (Reddy and Yun 2016). Although the studies indicate that magnetic nanocomposites are susceptible to separation from the aqueous solution and regeneration, the release into the environment is inevitable. The small size and high reactivity of magnetic nanoparticles, while providing advantages to the material, can induce toxic and harmful effects to ecosystems and humans (Tang and Lo 2013). The research on health risks and ecological impacts of iron oxide nanomaterials is minimal because iron oxide nanomaterials are generally regarded as non-toxic or low-toxic materials (Zhang et al. 2015). Nevertheless, recent studies with iron-based magnetic nanoparticles report cytotoxic, genotoxic, and neurotoxic effects (Villacis et al. 2017). Thus, the data on the toxicity of magnetic iron-based nanomaterials with a focus on ecotoxicological studies, with emphasis on toxicity in the aquatic environment will be presented.

Most toxicity tests for iron nanoparticles in an aquatic environment use zebrafish as a model organism employing both adult fish and embryos (Haque and Ward 2018). Zebrafish model is known to be sensitive to various environmental pollutants and has close homology with the human genome (Zheng et al. 2018). Also, zebrafish model presents fast embryonic development, a cost-effective, and short-term reproduction period (Madhubala et al. 2019). The toxic effects of different magnetic iron nanoparticles in zebrafish have been reported. Kaloyianni et al. (2020) showed that concentrations of magnetite nanoparticles ranging between 0.1 and 2000 mg/L could induce apoptotic effects on the gills and liver of adult zebrafish. Furthermore, the exposure of zebrafish to $Fe_3O_4$ nanoparticles for 8 days caused a significant reduction in swimming velocity compared to the non-treated fish. The change in locomotor behavior may be due to induced neurotoxicity by magnetic nanoparticles. Toxic effects of maghemite nanoparticles on zebrafish have also been observed. Villacis et al. (2017) reported damage to zebrafish deoxyribonucleic acid at all concentrations of ɣ-$Fe_2O_3$ nanoparticles assessed, 4.7 to 74.4 mg/L, for 96 h. In addition to general negative effects on cell growth and the decreased ability of the cell to produce new proteins, acute toxic of cobalt ferrites in zebrafish embryos has been presented in the studies of Ahmad et al. (2015). $CoFe_2O_4$ nanoparticles with concentrations of 10 to 500 µmol/L caused malformation, hatching delay, membrane damage, and oxidative stress. The $CoFe_2O_4$ nanoparticles induced cell death by the process of apoptosis, even at the lowest concentration of magnetic nanoparticles.

A few studies have also shown that iron-based magnetic nanoparticles have produced toxicological effects on plants. In general, the effects of iron nanoparticles on plants have been related to the aggregation of the particles at the root surface, inhibiting the water and nutrients

absorption (Miralles et al. 2012; Martínez-Fernández and Komárek 2016) or changes in the redox conditions of the site, affecting the rate of oxygen release (Ma et al. 2013). The work by Wang et al. showed that $Fe_3O_4$ nanoparticles often induce more oxidative stress than $Fe_3O_4$ bulk particles in the ryegrass and pumpkin roots and shoots as indicated by significantly increased and catalase enzyme activities and lipid peroxidation. However, $Fe_3O_4$ magnetic nanoparticles appear unable to be translocated in the ryegrass and pumpkin plants (Wang et al. 2011). In the study by Martínez-Fernández and Komárek (2016), the nanoparticles of maghemite caused a nutritional reduction in tomatoes. The treatment with 100 mg/L of γ-$Fe_2O_3$ nanoparticles inhibited 40% of the root hydraulic conductivity, causing the reduction in the Mo and Zn concentrations in shoots.

A study using *chlorella pyrenoidosa* revealed that the different iron nanoparticles have different toxicity according to the oxidation state and crystal phase. The algal growth inhibition decreased with the oxidation of the magnetic nanoparticles with an order of nanoscale zero-valent iron > $Fe_3O_4$ **n**anoparticles > $Fe_2O_3$nanoparticles, and α-$Fe_2O_3$ presented significantly higher toxicity than γ-$Fe_2O_3$(Lei et al. 2016). The $Fe^{2+}$ ions trigger reactions that generate reactive oxygen species such as hydroxyl radicals. The oxidative stress can cause inflammatory reactions, deoxyribonucleic acid damage, lipid peroxidation, and death cell finally (Sengul and Asmatulu 2020). In aqueous solution, $Fe^0$ is quickly oxidized to $Fe^{2+}$, and, therefore, nanoscale zero-valent iron nanoparticles would be susceptible to oxidative reactions (Tang and Lo 2013; Lei et al. 2016). Such results are essential for choosing the magnetic nanoparticle that will compose the adsorbent thinking about the fate of the material in the environment.

Despite the studies point out the toxicity of magnetic nanoparticles, a few research deals with the effects of magnetic nanocomposites in the ecosystem. Most of the coated magnetic nanoparticles toxicity studies are performed in biomedical fields and are very limited to toxicity information is available related to coatings used in environmental remediation settings (Zheng et al. 2018). Nanoparticles toxicity studies are important since the physical–chemical, optical, electrical, and magnetic properties of magnetic nanoparticles are modified when incorporated into the matrix. Therefore, surface protection may eliminate or induce toxicity according to the nature of the matrix used (Turan et al. 2019). Zheng et al. (2018) used adult zebrafish to evaluate the in vivo toxicity of bare $Fe_3O_4$ nanoparticles and starch-coated $Fe_3O_4$ nanoparticles. The results indicated that the starch coating mitigated the toxic effects of $Fe_3O_4$ magnetic nanoparticles on gill, but intensified the toxicity over the liver tissue. Therefore, the effects are dependent on the tissues examined. Silica-coated nanoparticles noted that the silica caused an induction of toxicity associated with the generation of reactive oxygen species on the surface that induced cytotoxic effects (Turan et al. 2019).

The reactivity of magnetic nanoparticles can be used beneficially, for example, the bactericidal ability of magnetic nanoparticles makes the materials even more attractive for the viewing of water treatment (Tang and Lo 2013). Singh et al. (2011) applied $Fe_3O_4$ nanoparticles for the removal of bacterial pathogensfrom water using *escherichia coli*as a model microorganism. The authors observed that magnetic nanoparticles were absorbed through the bacterial cell membrane, leading to cell death. Antibacterial activity has also been reported for magnesium ferrite. *Escherichia coli* bacteria loaded with $MnFe_2O_4$–graphene nanocomposite exhibited 82% cell inactivation, while graphene without magnetic nanoparticles caused 37% cell loss (Chella et al. 2015).

The reported studies are useful for understanding the fate and toxicity of iron-based nanomaterials in the environment; however, studies are performed under laboratory conditions. Phytotoxicity tests, for example, were carried out under hydroponic conditions. Once magnetic nanoparticles are released into the natural environment, environmental factors such as light irradiation, organic matter, coexisting contaminants, temperature, and chemical surface modifications, will affect the physical–chemical properties and toxicity of magnetic nanoparticles (Ren et al. 2016). Furthermore, pollutants can be associate with nanoparticles due to small size, potentiating the adverse effects (Liu et al. 2014b). Thus, more attention should be paid to assessing the toxicity of magnetic nanomaterials in the natural environment.

## Conclusion

The concern with the water scarcity resources and the quality of water offered to the population has led to the search for wastewater treatment technologies that are more efficient and inexpensive. Nanomaterials have attracted interest in water remediation, and in recent years, much research has been conducted on the synthesis and application of new materials. Recently, magnetic nanomaterials have received particular attention, mainly nanostructured iron oxides. Several iron-based magnetic nanocomposites are proposed as adsorbents for inorganic and organic pollutants. Among the nanocomposites, those that contain magnetite as a magnetic material were the most reported. The most significant number of studies evaluated the performance of nanosorbents in removing toxic metals.

The coprecipitation method was the most used for the synthesis of magnetic iron nanoparticles, being a low-cost and straightforward method. However, coprecipitation method presents a disadvantage of the difficulty in controlling the particle size, which can interfere in the material

physical–chemical and magnetic properties. Other methods, such as hydrothermal and solvothermal, were chosen to obtain the nanoparticles. Hydrothermal and solvothermal enable to control the particle size and morphology better, favoring mainly the formation of core–shell structures. However, thermal methods require the use of high temperature and pressure.

The studies presented showed that the magnetic particles could be combined with different materials, forming nanocomposites, which for water treatment, is more interesting. Inorganic and organic matrices can act by immobilizing magnetic nanoparticles, preventing the release into the water during treatment. Therefore, nanocomposites can enable the application of nanotechnology with existing treatment methods such as fixed-bed filtration. Also, the matrices can allow the functionalization of magnetic nanoparticles, improving the performance and making the use more flexible for different pollutant classes. On the other hand, functionalization can compromise the magnetic properties of the material, compromising to quickly and easily separate from water.

The performance of nanocomposites as adsorbents for inorganic species, pharmaceutical-derived compounds, and pesticides removal will depend on several factors, such as characteristics of the synthesized material, the affinity between the nanosorbent and the pollutant, experimental conditions, among others. Factors as adsorption time, adjust the pH, adsorbent dosage, pollutant concentration must be evaluated, aiming at the material viability. Another critical issue is the nanomaterial regeneration and reuse. For the use of nanomaterials in the treatment of large volumes of water, the adsorbent should be reused, not only for economic but also for environmental reasons. Not reusing the material implies generating a new waste, which will need to be treated, and, with that, more steps will be inserted into the treatment process.

Despite several studies about syntheses and the application of magnetic nanomaterials for adsorption processes, there are still gaps regarding the use for contaminated water remediation. Much of the research was carried out on a bench-scale and for samples produced in the laboratory. Few studies were found for real water samples analysis. The material application for natural water samples is important since studies have shown that the presence of other substances may interfere with the adsorption process of the target pollutant. Furthermore, the synthesis of materials on a large scale is challenging, requiring the optimization of the number of steps adopted, ideal conditions, reagents quantity used, reaction yield, and at the same time obtain a material with the desirable properties for an adsorbent. For commercialization and industrial-scale application, more detailed studies are needed so that the impacts of the new materials on the environment and human health are known. In general, toxicological studies involving magnetic nanoparticles are limited, and the results are still unclear.

In summary, studies with several magnetic nanocomposites are being carried out, aiming at the application as an adsorbent in water treatment for the removal of the diversified compound.

**Acknowledgements** The authors are thankful to Conselho Nacional de Desenvolvimento Científico e Tecnológico (CNPq), Coordenação de Aperfeiçoamento de Pessoal de Nível Superior—Brazil (CAPES), Fundação de Amparo a Pesquisa no Rio de Janeiro (FAPERJ) (E-26/202.755/2019), and Universidade do Estado do Rio de Janeiro (Programa Pro-Ciencia) for their financial support. JSG has a research scholarship from CNPq (304869/2019-8). JSG and DVC have a research grant from UERJ (ProgramaPró-Ciência). This study was financed in part by the Coordenação de Aperfeiçoamento de Pessoal de Nível Superior—Brasil (CAPES)—FinanceCode 001.

**Author contributions** LRM was involved in conceptualization and writing—original draft preparation. JSG helped in idea for the article, conceptualization, writing—review and editing, and supervision. AA S contributed to writing—review and editing. DVC was involved in conceptualization and writing—review and editing.

## References

Abdel Maksoud MIA, Elgarahy AM, Farrell C et al (2020) Insight on water remediation application using magnetic nanomaterials and biosorbents. Coord Chem Rev 403:213096. https://doi.org/10.1016/j.ccr.2019.213096

Abdullah NH, Shameli K, Abdullah EC, Abdullah LC (2019) Solid matrices for fabrication of magnetic iron oxide nanocomposites: synthesis, properties, and application for the adsorption of heavy metal ions and dyes. Compos B Eng 162:538–568. https://doi.org/10.1016/j.compositesb.2018.12.075

Ahmad F, Liu X, Zhou Y, Yao H (2015) An in vivo evaluation of acute toxicity of cobalt ferrite ($CoFe_2O_4$) nanoparticles in larval-embryo Zebrafish (*Danio rerio*). Aquat Toxicol 166:21–28. https://doi.org/10.1016/j.aquatox.2015.07.003

Ahmadi M, Elmongy H, Madrakian T, Abdel-Rehim M (2017) Nanomaterials as sorbents for sample preparation in bioanalysis: a review. Anal Chim Acta 958:1–21. https://doi.org/10.1016/j.aca.2016.11.062

Ai L, Zhou Y, Jiang J (2011) Removal of methylene blue from aqueous solution by montmorillonite/$CoFe_2O_4$ composite with magnetic separation performance. Desalination 266:72–77. https://doi.org/10.1016/j.desal.2010.08.004

Anirudhan TS, Jalajamony S, Suchithra PS (2009) Improved performance of a cellulose-based anion exchanger with tertiary amine functionality for the adsorption of chromium(VI) from aqueous solutions. Colloids Surf, A 335:107–113. https://doi.org/10.1016/j.colsurfa.2008.10.035

Anirudhan TS, Deepa JR, Christa J (2016) Nanocellulose/nanobentonite composite anchored with multi-carboxyl functional groups as an adsorbent for the effective removal of Cobalt(II) from nuclear industry wastewater samples. J Colloid Interface Sci 467:307–320. https://doi.org/10.1016/j.jcis.2016.01.023

Arancibia-Miranda N, Baltazar SE, García A et al (2016) Nanoscale zero valent supported by Zeolite and Montmorillonite: template effect of the removal of lead ion from an aqueous solution. J

Hazard Mater 301:371–380. https://doi.org/10.1016/j.jhazmat.2015.09.007
Azzouz A, Kailasa SK, Lee SS et al (2018) Review of nanomaterials as sorbents in solid-phase extraction for environmental samples. TrAC Trends Anal Chem 108:347–369. https://doi.org/10.1016/j.trac.2018.08.009
Baghdadi M, Ghaffari E, Aminzadeh B (2016) Removal of carbamazepine from municipal wastewater effluent using optimally synthesized magnetic activated carbon: adsorption and sedimentation kinetic studies. J Environ Chem Eng 4:3309–3321. https://doi.org/10.1016/j.jece.2016.06.034
Baig N, Ihsanullah SM, Saleh TA (2019) Graphene-based adsorbents for the removal of toxic organic pollutants: a review. J Environ Manag 244:370–382. https://doi.org/10.1016/j.jenvman.2019.05.047
Bakhshayesh S, Dehghani H (2014) Nickel and cobalt ferrites nanoparticles: synthesis, study of magnetic properties and their use as magnetic adsorbent for removing lead(II) ion. J Iran Chem Soc 11:769–780. https://doi.org/10.1007/s13738-013-0351-0
Bakr ASA, Moustafa YM, Motawea EA et al (2015) Removal of ferrous ions from their aqueous solutions onto $NiFe_2O_4$-alginate composite beads. J Environ Chem Eng 3:1486–1496. https://doi.org/10.1016/j.jece.2015.05.020
Bao X, Qiang Z, Chang JH et al (2014) Synthesis of carbon-coated magnetic nanocomposite ($Fe_3O_4$@C) and its application for sulfonamide antibiotics removal from water. J Environ Sci (China) 26:962–969. https://doi.org/10.1016/S1001-0742(13)60485-4
Bée A, Talbot D, Abramson S, Dupuis V (2011) Magnetic alginate beads for Pb(II) ions removal from wastewater. J Colloid Interface Sci 362:486–492. https://doi.org/10.1016/j.jcis.2011.06.036
Behrens S, Appel I (2016) Magnetic nanocomposites. Curr Opin Biotechnol 39:89–96. https://doi.org/10.1016/J.COPBIO.2016.02.005
Bhaumik M, Maity A, Srinivasu VV, Onyango MS (2011) Enhanced removal of Cr(VI) from aqueous solution using polypyrrole/$Fe_3O_4$ magnetic nanocomposite. J Hazard Mater 190:381–390. https://doi.org/10.1016/j.jhazmat.2011.03.062
Boparai HK, Joseph M, O'Carroll DM (2011) Kinetics and thermodynamics of cadmium ion removal by adsorption onto nano zerovalent iron particles. J Hazard Mater 186:458–465. https://doi.org/10.1016/j.jhazmat.2010.11.029
Boruah PK, Sharma B, Hussain N, Das MR (2017) Magnetically recoverable $Fe_3O_4$/graphene nanocomposite towards efficient removal of triazine pesticides from aqueous solution: Investigation of the adsorption phenomenon and specific ion effect. Chemosphere 168:1058–1067. https://doi.org/10.1016/j.chemosphere.2016.10.103
Chávez-Guajardo AE, Medina-Llamas JC, Maqueira L et al (2015) Efficient removal of Cr(VI) and Cu(II) ions from aqueous media by use of polypyrrole/maghemite and polyaniline/maghemite magnetic nanocomposites. Chem Eng J 281:826–836. https://doi.org/10.1016/j.cej.2015.07.008
Chella S, Kollu P, Komarala EVPR et al (2015) Solvothermal synthesis of $MnFe_2O_4$-graphene composite-investigation of its adsorption and antimicrobial properties. Appl Surf Sci 327:27–36. https://doi.org/10.1016/j.apsusc.2014.11.096
Chen J, Hong X, Xie Q et al (2015) Exfoliated polypyrrole/montmorillonite nanocomposite with flake-like structure for Cr(VI) removal from aqueous solution. Res Chem Intermed 41:9655–9671. https://doi.org/10.1007/s11164-015-1955-z
Chen L, Zhou CH, Fiore S et al (2016a) Functional magnetic nanoparticle/clay mineral nanocomposites: preparation, magnetism and versatile applications. Appl Clay Sci 127–128:143–163. https://doi.org/10.1016/j.clay.2016.04.009
Chen M, Shao LL, Li JJ et al (2016b) One-step hydrothermal synthesis of hydrophilic $Fe_3O_4$/carbon composites and their application in removing toxic chemicals. RSC Adv 6:35228–35238. https://doi.org/10.1039/c6ra01408a
Cheng TW, Lee ML, Ko MS et al (2012) The heavy metal adsorption characteristics on metakaolin-based geopolymer. Appl Clay Sci 56:90–96. https://doi.org/10.1016/j.clay.2011.11.027
Choucair M, Gong B, Stride JA (2012) Engineering solvothermal reactions to produce multi-walled carbon nanotubes. J Nanopart Res. https://doi.org/10.1007/s11051-012-0901-x
Crane RA, Scott TB (2012) Nanoscale zero-valent iron: future prospects for an emerging water treatment technology. J Hazard Mater 211–212:112–125. https://doi.org/10.1016/j.jhazmat.2011.11.073
Cui L, Wang Y, Gao L et al (2015) EDTA functionalized magnetic graphene oxide for removal of Pb(II), Hg(II) and Cu(II) in water treatment: adsorption mechanism and separation property. Chem Eng J 281:1–10. https://doi.org/10.1016/j.cej.2015.06.043
Dai P, Wang Y, Wu M, Xu Z (2012) Optical and magnetic properties of ɣ-$Fe_2O_3$ nanoparticles encapsulated in SBA-15 fabricated by double solvent technique. Micro Nano Lett 7:219–222. https://doi.org/10.1049/mnl.2011.0715
Danalıoğlu ST, Bayazit ŞS, Kerkez Kuyumcu Ö, Salam MA (2017) Efficient removal of antibiotics by a novel magnetic adsorbent: magnetic activated carbon/chitosan (MACC) nanocomposite. J Mol Liq 240:589–596. https://doi.org/10.1016/j.molliq.2017.05.131
Davodi B, Ghorbani M, Jahangiri M (2017) Adsorption of mercury from aqueous solution on synthetic polydopamine nanocomposite based on magnetic nanoparticles using Box–Behnken design. J Taiwan Inst Chem Eng 80:363–378. https://doi.org/10.1016/j.jtice.2017.07.024
de Brião GV, de Andrade JR, da Silva MGC, Vieira MGA (2020) Removal of toxic metals from water using chitosan-based magnetic adsorbents. A review. Environ Chem Lett 18:1145–1168. https://doi.org/10.1007/s10311-020-01003-y
Dendisová M, Jeništová A, Parchaňská-Kokaislová A et al (2018) The use of infrared spectroscopic techniques to characterize nanomaterials and nanostructures: a review. Anal Chim Acta 1031:1–14. https://doi.org/10.1016/j.aca.2018.05.046
Diagboya PNE, Dikio ED (2018) Silica-based mesoporous materials; emerging designer adsorbents for aqueous pollutants removal and water treatment. Microporous Mesoporous Mater 266:252–267. https://doi.org/10.1016/j.micromeso.2018.03.008
Do MH, Phan NH, Nguyen TD et al (2011) Activated carbon/$Fe_3O_4$ nanoparticle composite: fabrication, methyl orange removal and regeneration by hydrogen peroxide. Chemosphere 85:1269–1276. https://doi.org/10.1016/j.chemosphere.2011.07.023
Dong L, Zhu Z, Qiu Y, Zhao J (2010) Removal of lead from aqueous solution by hydroxyapatite/magnetite composite adsorbent. Chem Eng J 165:827–834. https://doi.org/10.1016/j.cej.2010.10.027
Dong L, Zhu Z, Qiu Y, Zhao J (2016) Removal of lead from aqueous solution by hydroxyapatite/manganese dioxide composite. Front Environ Sci Eng 10:28–36. https://doi.org/10.1007/s11783-014-0722-5
Donia AM, Atia AA, Abouzayed FI (2012) Preparation and characterization of nano-magnetic cellulose with fast kinetic properties towards the adsorption of some metal ions. Chem Eng J 191:22–30. https://doi.org/10.1016/j.cej.2011.08.034
Dreyer DR, Murali S, Zhu Y et al (2011) Reduction of graphite oxide using alcohols. J Mater Chem 21:3443–3447. https://doi.org/10.1039/c0jm02704a
Dutra FVA, Pires BC, Nascimento TA, Borges KB (2018) Functional polyaniline/multiwalled carbon nanotube composite as an efficient adsorbent material for removing pharmaceuticals

from aqueous media. J Environ Manag 221:28–37. https://doi.org/10.1016/j.jenvman.2018.05.051
Egodawatte S, Datt A, Burns EA, Larsen SC (2015) Chemical insight into the adsorption of Chromium(III) on iron oxide/mesoporous silica nanocomposites. Langmuir 31:7553–7562. https://doi.org/10.1021/acs.langmuir.5b01483
Ekberg B, Mosbach K (1989) Molecular imprinting: a technique for producing specific separation materials. Trends Biotechnol 7:92–96. https://doi.org/10.1016/0167-7799(89)90006-1
Emadi M, Shams E, Amini MK (2013) Removal of zinc from aqueous solutions by magnetite silica core-shell nanoparticles. J Chem. https://doi.org/10.1155/2013/787682
Esmat M, Farghali AA, Khedr MH, El-Sherbiny IM (2017) Alginate-based nanocomposites for efficient removal of heavy metal ions. Int J Biol Macromol 102:272–283. https://doi.org/10.1016/j.ijbiomac.2017.04.021
Feng Y, Gong JL, Zeng GM et al (2010) Adsorption of Cd (II) and Zn (II) from aqueous solutions using magnetic hydroxyapatite nanoparticles as adsorbents. Chem Eng J 162:487–494. https://doi.org/10.1016/j.cej.2010.05.049
Gallo A, Bianco C, Tosco T et al (2019) Synthesis of eco-compatible bimetallic silver/iron nanoparticles for water remediation and reactivity assessment on bromophenol blue. J Clean Prod 211:1367–1374. https://doi.org/10.1016/j.jclepro.2018.10.298
Gao Y, Li Y, Zhang L et al (2012) Adsorption and removal of tetracycline antibiotics from aqueous solution by graphene oxide. J Colloid Interface Sci 368:540–546. https://doi.org/10.1016/j.jcis.2011.11.015
Glinski DA, Purucker ST, Van Meter RJ et al (2018) Analysis of pesticides in surface water, stemflow, and throughfall in an agricultural area in South Georgia, USA. Chemosphere 209:496–507. https://doi.org/10.1016/j.chemosphere.2018.06.116
Grieger KD, Fjordbøge A, Hartmann NB et al (2010) Environmental benefits and risks of zero-valent iron nanoparticles (nZVI) for in situ remediation: risk mitigation or trade-off? J Contam Hydrol 118:165–183. https://doi.org/10.1016/j.jconhyd.2010.07.011
Guo X, Du B, Wei Q et al (2014) Synthesis of amino functionalized magnetic graphenes composite material and its application to remove Cr(VI), Pb(II), Hg(II), Cd(II) and Ni(II) from contaminated water. J Hazard Mater 278:211–220. https://doi.org/10.1016/j.jhazmat.2014.05.075
Gupta VK, Agarwal S, Saleh TA (2011) Chromium removal by combining the magnetic properties of iron oxide with adsorption properties of carbon nanotubes. Water Res 45:2207–2212. https://doi.org/10.1016/j.watres.2011.01.012
Gupta VK, Kumar R, Nayak A et al (2013) Adsorptive removal of dyes from aqueous solution onto carbon nanotubes: a review. Adv Coll Interface Sci 193–194:24–34. https://doi.org/10.1016/j.cis.2013.03.003
Gupta VK, Agarwal S, Asif M et al (2017) Application of response surface methodology to optimize the adsorption performance of a magnetic graphene oxide nanocomposite adsorbent for removal of methadone from the environment. J Colloid Interface Sci 497:193–200. https://doi.org/10.1016/j.jcis.2017.03.006
Gutha Y, Munagapati VS (2016) Removal of Pb(II) ions by using magnetic chitosan-4-((pyridin-2-ylimino)methyl)benzaldehyde Schiff's base. Int J Biol Macromol 93:408–417. https://doi.org/10.1016/j.ijbiomac.2016.08.084
Han X, Gai L, Jiang H et al (2013) Core-shell structured $Fe_3O_4$/PANI microspheres and their Cr(VI) ion removal properties. Synth Met 171:1–6. https://doi.org/10.1016/j.synthmet.2013.02.025
Haque E, Ward AC (2018) Zebrafish as a model to evaluate nanoparticle toxicity. Nanomaterials 8:1–18. https://doi.org/10.3390/nano8070561
Hashemian S, Saffari H, Ragabion S (2015) Adsorption of cobalt(II) from aqueous solutions by $Fe_3O_4$/bentonite nanocomposite. Water Air Soil Pollut. https://doi.org/10.1007/s11270-014-2212-6
He F, Fan J, Ma D, Zhang L, Leung C, Chan HL (2010) The attachment of $Fe_3O_4$ nanoparticles to graphene oxide by covalent bonding. Carbon 48(11):3139–3144
He J, Bardelli F, Gehin A et al (2016) Novel chitosan goethite bionanocomposite beads for arsenic remediation. Water Res 101:1–9. https://doi.org/10.1016/j.watres.2016.05.032
Hokkanen S, Repo E, Sillanpää M (2013) Removal of heavy metals from aqueous solutions by succinic anhydride modified mercerized nanocellulose. Chem Eng J 223:40–47. https://doi.org/10.1016/j.cej.2013.02.054
Hosseinzadeh H, Ramin S (2018) Effective removal of copper from aqueous solutions by modified magnetic chitosan/graphene oxide nanocomposites. Int J Biol Macromol 113:859–868. https://doi.org/10.1016/j.ijbiomac.2018.03.028
Hu CY, Lo SL, Liou YH et al (2010) Hexavalent chromium removal from near natural water by copper-iron bimetallic particles. Water Res 44:3101–3108. https://doi.org/10.1016/j.watres.2010.02.037
Hu X, Liu B, Deng Y et al (2011) Adsorption and heterogeneous Fenton degradation of 17α-methyltestosterone on nano $Fe_3O_4$/MWCNTs in aqueous solution. Appl Catal B 107:274–283. https://doi.org/10.1016/j.apcatb.2011.07.025
Huong PTL, Huy LT, Lan H et al (2018) Magnetic iron oxide-carbon nanocomposites: impacts of carbon coating on the As(V) adsorption and inductive heating responses. J Alloy Compd 739:139–148. https://doi.org/10.1016/j.jallcom.2017.12.178
Idris A, Ismail NSM, Hassan N et al (2012) Synthesis of magnetic alginate beads based on maghemite nanoparticles for Pb(II) removal in aqueous solution. J Ind Eng Chem 18:1582–1589. https://doi.org/10.1016/j.jiec.2012.02.018
Javanbakht V, Ghoreishi SM, Habibi N, Javanbakht M (2016) A novel magnetic chitosan/clinoptilolite/magnetite nanocomposite for highly efficient removal of Pb(II) ions from aqueous solution. Powder Technol 302:372–383. https://doi.org/10.1016/j.powtec.2016.08.069
Ji F, Li C, Tang B et al (2012) Preparation of cellulose acetate/zeolite composite fiber and its adsorption behavior for heavy metal ions in aqueous solution. Chem Eng J 209:325–333. https://doi.org/10.1016/j.cej.2012.08.014
Jiang JQ, Zhou Z, Sharma VK (2013) Occurrence, transportation, monitoring and treatment of emerging micro-pollutants in waste water—a review from global views. Microchem J 110:292–300. https://doi.org/10.1016/j.microc.2013.04.014
Jiang L, Yu H, Zhou X et al (2016) Preparation, characterization, and adsorption properties of magnetic multi-walled carbon nanotubes for simultaneous removal of lead(II) and zinc(II) from aqueous solutions. Desalin Water Treat 57:18446–18462. https://doi.org/10.1080/19443994.2015.1090924
Jin J, Yang Z, Xiong W et al (2019) Cu and Co nanoparticles co-doped MIL-101 as a novel adsorbent for efficient removal of tetracycline from aqueous solutions. Sci Total Environ 650:408–418. https://doi.org/10.1016/j.scitotenv.2018.08.434
Kalantari K, Ahmad MB, Fard Masoumi HR et al (2015) Rapid and high capacity adsorption of heavy metals by $Fe_3O_4$/montmorillonite nanocomposite using response surface methodology: preparation, characterization, optimization, equilibrium isotherms, and adsorption kinetics study. J Taiwan Inst Chem Eng 49:192–198. https://doi.org/10.1016/j.jtice.2014.10.025
Kaloyianni M, Dimitriadi A, Ovezik M et al (2020) Magnetite nanoparticles effects on adverse responses of aquatic and terrestrial animal models. J Hazard Mater. https://doi.org/10.1016/j.jhazmat.2019.121204

Kang AJ, Baghdadi M, Pardakhti A (2016) Removal of cadmium and lead from aqueous solutions by magnetic acid-treated activated carbon nanocomposite. Desalin Water Treat 57:18782–18798. https://doi.org/10.1080/19443994.2015.1095123

Kaur M, Singh M, Mukhopadhyay SS et al (2015) Structural, magnetic andadsorptive properties of clay ferrite nanocomposite and its use for effective removal of Cr(VI) from water. J Alloy Compd 653:202–211. https://doi.org/10.1016/j.jallcom.2015.08.265

Khajeh M, Laurent S, Dastafkan K (2013) Nanoadsorbents: classification, preparation, and applications (with emphasis on aqueous media). Chem Rev 113:7728–7768. https://doi.org/10.1021/cr400086v

Khan ST, Malik A (2019) Engineered nanomaterials for water decontamination and purification: from lab to products. J Hazard Mater 363:295–308. https://doi.org/10.1016/j.jhazmat.2018.09.091

Kheshti Z, Hassanajili S (2017) Novel multifunctional mesoporous microsphere with high surface area for removal of zinc ion from aqueous solution: preparation and characterization. J Inorg Organomet Polym Mater 27:1613–1626. https://doi.org/10.1007/s10904-017-0621-x

Kumar S, Jain S (2014) One-step synthesis of superparamagnetic $Fe_3O_4$@PANI nanocomposites. J Chem 2014:1–6. https://doi.org/10.1155/2014/837682

Kumar R, Khan MA, Haq N (2014) Application of carbon nanotubes in heavy metals remediation. Crit Rev Environ Sci Technol 44:1000–1035. https://doi.org/10.1080/10643389.2012.741314

Kyzas GZ, Bikiaris DN, Seredych M et al (2014) Removal of dorzolamide from biomedical wastewaters with adsorption onto graphite oxide/poly(acrylic acid) grafted chitosan nanocomposite. Biores Technol 152:399–406. https://doi.org/10.1016/j.biortech.2013.11.046

Lakouraj MM, Mojerlou F, Zare EN (2014) Nanogel and superparamagnetic nanocomposite based on sodium alginate for sorption of heavy metal ions. Carbohyd Polym 106:34–41. https://doi.org/10.1016/j.carbpol.2014.01.092

Langeroudi MP, Binaeian E (2018) Tannin-APTES modified $Fe_3O_4$nanoparticles as a carrier of Methotrexate drug: kinetic, isotherm and thermodynamic studies. Mater Chem Phys 218:210–217. https://doi.org/10.1016/j.matchemphys.2018.07.044

Larraza I, López-Gónzalez M, Corrales T, Marcelo G (2012) Hybrid materials: Magnetite–Polyethylenimine–Montmorillonite, as magnetic adsorbents for Cr(VI) water treatment. J Colloid Interface Sci 385:24–33. https://doi.org/10.1016/j.jcis.2012.06.050

Le GTT, Chanlek N, Manyam J et al (2019) Insight into the ultrasonication of graphene oxide with strong changes in its properties and performance for adsorption applications. Chem Eng J 373:1212–1222. https://doi.org/10.1016/j.cej.2019.05.108

Lei C, Zhang L, Yang K et al (2016) Toxicity of iron-based nanoparticles to green algae: effects of particle size, crystal phase, oxidation state and environmental aging. Environ Pollut 218:505–512. https://doi.org/10.1016/j.envpol.2016.07.030

Li Q, Wu Z, Tu B et al (2010) Highly hydrothermal stability of ordered mesoporous aluminosilicates Al-SBA-15 with high Si/Al ratio. Microporous Mesoporous Mater 135:95–104. https://doi.org/10.1016/j.micromeso.2010.06.016

Li W-G, Gong X-J, Wang K et al (2014) Adsorption characteristics of arsenic from micro-polluted water by an innovative coal-based mesoporous activated carbon. Biores Technol 165:166–173. https://doi.org/10.1016/j.biortech.2014.02.069

Li M-F, Liu Y-G, Zeng G-M et al (2017a) Tetracycline absorbed onto nitrilotriacetic acid-functionalized magnetic graphene oxide: influencing factors and uptake mechanism. J Colloid Interface Sci 485:269–279. https://doi.org/10.1016/j.jcis.2016.09.037

Li R, An Q-D, Mao B-Q et al (2017b) PDA-meditated green synthesis of amino-modified, multifunctional magnetic hollow composites for Cr(VI) efficient removal. J Taiwan Inst Chem Eng 80:596–606. https://doi.org/10.1016/j.jtice.2017.08.036

Li N, Jiang HL, Wang X et al (2018) Recent advances in graphene-based magnetic composites for magnetic solid-phase extraction. TrAC Trends Anal Chem 102:60–74. https://doi.org/10.1016/j.trac.2018.01.009

Liang C, Wei M-C, Tseng H-H, Shu E-C (2013) Synthesis and characterization of the acidic properties and pore texture of Al-SBA-15 supports for the canola oil transesterification. Chem Eng J 223:785–794. https://doi.org/10.1016/j.cej.2013.03.065

Lin Z, Yao Y, Li Z et al (2010) Solvent-assisted thermal reduction of graphite oxide. J Phys Chem C 114:14819–14825. https://doi.org/10.1021/jp1049843

Lin Y, Xu S, Li J (2013) Fast and highly efficient tetracyclines removal from environmental waters by graphene oxide functionalized magnetic particles. Chem Eng J 225:679–685. https://doi.org/10.1016/j.cej.2013.03.104

Liu J, Bin Y, Matsuo M (2012) Magnetic behavior of Zn-Doped $Fe_3O_4$ nanoparticles estimated in terms of crystal domain size. J Phys Chem C 116:134–143. https://doi.org/10.1021/jp207354s

Liu Z, Wang H, Liu C et al (2012) Magnetic cellulose-chitosan hydrogels prepared from ionic liquids as reusable adsorbent for removal of heavy metal ions. Chem Commun 48:7350–7352. https://doi.org/10.1039/c2cc17795a

Liu H, Chen W, Liu C et al (2014) Magnetic mesoporous clay adsorbent: preparation, characterization and adsorption capacity for atrazine. Microporous Mesoporous Mater 194:72–78. https://doi.org/10.1016/j.micromeso.2014.03.038

Liu Y, Tourbin M, Lachaize S, Guiraud P (2014) Nanoparticles in wastewaters: hazards, fate and remediation. Powder Technol 255:149–156. https://doi.org/10.1016/j.powtec.2013.08.025

Liu J, Wang C, Xiong Z (2015) Adsorption behavior of magnetic multiwalled carbon nanotubes for the simultaneous adsorption of furazolidone and Cu(II) from aqueous solutions. Environ Eng Sci 32:960–969. https://doi.org/10.1089/ees.2015.0093

Lofrano G, Carotenuto M, Libralato G et al (2016) Polymer functionalized nanocomposites for metals removal from water and wastewater: an overview. Water Res 92:22–37. https://doi.org/10.1016/j.watres.2016.01.033

Lu F, Astruc D (2018) Nanomaterials for removal of toxic elements from water. Coord Chem Rev 356:147–164. https://doi.org/10.1016/j.ccr.2017.11.003

Luo X, Lei X, Xie X et al (2016) Adsorptive removal of Lead from water by the effective and reusable magnetic cellulose nanocomposite beads entrapping activated bentonite. Carbohyd Polym 151:640–648. https://doi.org/10.1016/j.carbpol.2016.06.003

Ma X, Gurung A, Deng Y (2013) Phytotoxicity and uptake of nanoscale zero-valent iron (nZVI) by two plant species. Sci Total Environ 443:844–849. https://doi.org/10.1016/j.scitotenv.2012.11.073

Madhubala V, Kalaivani T, Kirubha A et al (2019) Study of structural and magnetic properties of hydro/solvothermally synthesized α-$Fe_2O_3$nanoparticles and its toxicity assessment in zebrafish embryos. Appl Surf Sci 494:391–400. https://doi.org/10.1016/j.apsusc.2019.07.090

Madhura L, Singh S, Kanchi S et al (2019) Nanotechnology-based water quality management for wastewater treatment. Environ Chem Lett 17:65–121. https://doi.org/10.1007/s10311-018-0778-8

Mallakpour S, Naghdi M (2018) Polymer/$SiO_2$ nanocomposites: Production and applications. Prog Mater Sci 97:409–447. https://doi.org/10.1016/j.pmatsci.2018.04.002

Mansouriieh N, Sohrabi MR, Khosravi M (2016) Adsorption kinetics and thermodynamics of organophosphorus profenofos pesticide onto Fe/Ni bimetallic nanoparticles. Int J Environ Sci Technol 13:1393–1404. https://doi.org/10.1007/s13762-016-0960-0

Mao H, Wang S, Lin J-Y et al (2016) Modification of a magnetic carbon composite for ciprofloxacin adsorption. J Environ Sci (China) 49:179–188. https://doi.org/10.1016/j.jes.2016.05.048

Martínez-Fernández D, Komárek M (2016) Comparative effects of nanoscale zero-valent iron (nZVI) and $Fe_2O_3$ nanoparticles on root hydraulic conductivity of *Solanum lycopersicum* L. Environ Exp Bot 131:128–136. https://doi.org/10.1016/j.envexpbot.2016.07.010

Masoumi A, Hemmati K, Ghaemy M (2016) Recognition and selective adsorption of pesticides by superparamagnetic molecularly imprinted polymer nanospheres. RSC Advances 6:49401–49410. https://doi.org/10.1039/c6ra05873f

Mehta D, Mazumdar S, Singh SK (2015) Magnetic adsorbents for the treatment of water/wastewater—a review. J Water Process Eng 7:244–265. https://doi.org/10.1016/j.jwpe.2015.07.001

Miralles P, Church TL, Harris AT (2012) Toxicity, uptake, and translocation of engineered nanomaterials in vascular plants. Environ Sci Technol 46:9224–9239. https://doi.org/10.1021/es202995d

Mohammed L, Gomaa HG, Ragab D, Zhu J (2017) Magnetic nanoparticles for environmental and biomedical applications: a review. Particuology 30:1–14. https://doi.org/10.1016/j.partic.2016.06.001

Mohseni-Bandpi A, Al-Musawi TJ, Ghahramani E et al (2016) Improvement of zeolite adsorption capacity for cephalexin by coating with magnetic $Fe_3O_4$ nanoparticles. J Mol Liq 218:615–624. https://doi.org/10.1016/j.molliq.2016.02.092

Morin-Crini N, Fourmentin M, Fourmentin S et al (2019) Synthesis of silica materials containing cyclodextrin and their applications in wastewater treatment. Environ Chem Lett 17:683–696. https://doi.org/10.1007/s10311-018-00818-0

Moschet C, Wittmer I, Simovic J et al (2014) How a complete pesticide screening changes the assessment of surface water quality. Environ Sci Technol 48:5423–5432. https://doi.org/10.1021/es500371t

Mueller NC, Braun J, Bruns J et al (2012) Application of nanoscale zero valent iron (NZVI) for groundwater remediation in Europe. Environ Sci Pollut Res 19:550–558. https://doi.org/10.1007/s11356-011-0576-3

Nadar SS, Orupattur NV, Suresh S et al (2018) Recent progress in nanostructured magnetic framework composites (MFCs): synthesis and applications. J Taiwan Inst Chem Eng 91:653–677. https://doi.org/10.1016/j.jtice.2018.06.029

Nam SW, Jung C, Li H et al (2015) Adsorption characteristics of diclofenac and sulfamethoxazole to graphene oxide in aqueous solution. Chemosphere 136:20–26. https://doi.org/10.1016/j.chemosphere.2015.03.061

Nethaji S, Sivasamy A (2017) Graphene oxide coated with porous iron oxide ribbons for 2,4-Dichlorophenoxyacetic acid (2,4-D) removal. Ecotoxicol Environ Saf 138:292–297. https://doi.org/10.1016/j.ecoenv.2017.01.001

Oliveira LMF, Nascimento MA, Guimarães YM et al (2018) Removal of beta-lactams antibiotics through zero-valent copper nanoparticles. J Braz Chem Soc 29:1630–1637. https://doi.org/10.21577/0103-5053.20180034

Pan S, Zhang Y, Shen H, Hu M (2012) An intensive study on the magnetic effect of mercapto-functionalized nano-magnetic $Fe_3O_4$ polymers and their adsorption mechanism for the removal of Hg(II) from aqueous solution. Chem Eng J 210:564–574. https://doi.org/10.1016/j.cej.2012.09.016

Pansini M, Sannino F, Marocco A et al (2018) Novel process to prepare magnetic metal-ceramic nanocomposites from zeolite precursor and their use as adsorbent of agrochemicals from water. J Environ Chem Eng 6:527–538. https://doi.org/10.1016/j.jece.2017.12.030

Peng X, Zhao Y, Yang T et al (2018) One-step and acid free synthesis of ϒ-$Fe_2O_3$/SBA-15 for enhanced arsenic removal. Microporous Mesoporous Mater 258:26–32. https://doi.org/10.1016/j.micromeso.2017.08.050

Petrie B, Barden R, Kasprzyk-Hordern B (2014) A review on emerging contaminants in wastewaters and the environment: current knowledge, understudied areas and recommendations for future monitoring. Water Res 72:3–27. https://doi.org/10.1016/j.watres.2014.08.053

Polesel F, Andersen HR, Trapp S, Plósz BG (2016) Removal of antibiotics in biological wastewater treatment systems—a critical assessment using the activated sludge modeling framework for Xenobiotics (ASM-X). Environ Sci Technol 50:10316–10334. https://doi.org/10.1021/acs.est.6b01899

Qu H, Caruntu D, Liu H, O'Connor CJ (2011) Water-dispersible iron oxide magnetic nanoparticles with versatile surface functionalities. Langmuir 27:2271–2278. https://doi.org/10.1021/la104471r

Ramimoghadam D, Bagheri S, Hamid SBA (2014) Progress in electrochemical synthesis of magnetic iron oxide nanoparticles. J Magn Magn Mater 368:207–229. https://doi.org/10.1016/j.jmmm.2014.05.015

Reddy DHK, Yun YS (2016) Spinel ferrite magnetic adsorbents: alternative future materials for water purification? Coord Chem Rev 315:90–111. https://doi.org/10.1016/j.ccr.2016.01.012

Ren Y, Abbood HA, He F et al (2013) Magnetic EDTA-modified chitosan/$SiO_2$/$Fe_3O_4$ adsorbent: preparation, characterization, and application in heavy metal adsorption. Chem Eng J 226:300–311. https://doi.org/10.1016/j.cej.2013.04.059

Ren C, Hu X, Zhou Q (2016) Influence of environmental factors on nanotoxicity and knowledge gaps thereof. NanoImpact 2:82–92. https://doi.org/10.1016/j.impact.2016.07.002

Sabarwal A, Kumar K, Singh RP (2018) Hazardous effects of chemical pesticides on human health-cancer and other associated disorders. Environ Toxicol Pharmacol 63:103–114. https://doi.org/10.1016/j.etap.2018.08.018

Sabherwal P, Mutreja R, Suri CR (2016) Biofunctionalized carbon nanocomposites: new-generation diagnostic tools. TrAC Trends Anal Chem 82:12–21. https://doi.org/10.1016/j.trac.2015.10.006

Salem Attia TM, Hu XL, Yin DQ (2014) Synthesised magnetic nanoparticles coated zeolite (MNCZ) for the removal of arsenic (As) from aqueous solution. J Exp Nanosci 9:551–560. https://doi.org/10.1080/17458080.2012.677549

Sánchez-García I, Núñez A, Bonales LJ et al (2019) Study of the adsorption capacity of graphene oxide under gamma radiation in different media. Radiat Phys Chem 165:108395. https://doi.org/10.1016/j.radphyschem.2019.108395

Sengul AB, Asmatulu E (2020) Toxicity of metal and metal oxide nanoparticles: a review. Environ Chem Lett 18:1659–1683. https://doi.org/10.1007/s10311-020-01033-6

Sherlala AIA, Raman AAA, Bello MM, Buthiyappan A (2019) Adsorption of arsenic using chitosan magnetic graphene oxide nanocomposite. J Environ Manag 246:547–556. https://doi.org/10.1016/j.jenvman.2019.05.117

Shokrollahi H (2017) A review of the magnetic properties, synthesis methods and applications of maghemite. J Magn Magn Mater 426:74–81. https://doi.org/10.1016/j.jmmm.2016.11.033

Shukla S, Arora V, Jadaun A et al (2015) Magnetic removal of entamoeba cysts from water using chitosan oligosaccharide-coated iron oxide nanoparticles. Int J Nanomed 10:4901–4917. https://doi.org/10.2147/IJN.S77675

Siddiqui MTH, Nizamuddin S, Baloch HA et al (2018) Synthesis of magnetic carbon nanocomposites by hydrothermal carbonization and pyrolysis. Environ Chem Lett 16:821–844. https://doi.org/10.1007/s10311-018-0724-9

Silva MF, Pineda EAG, Bergamasco R (2014) Application of nanostructured iron oxides as adsorbents and photocatalysts for

wastewater pollutant removal. Quím Nova 38:393–398. https://doi.org/10.5935/0100-4042.20140311
Singh S, Barick KC, Bahadur D (2011) Surface engineered magnetic nanoparticles for removal of toxic metal ions and bacterial pathogens. J Hazard Mater 192:1539–1547. https://doi.org/10.1016/j.jhazmat.2011.06.074
Singh NB, Nagpal G, Agrawal S, Rachna (2018) Water purification by using adsorbents: a review. Environ Technol Innov 11:187–240. https://doi.org/10.1016/j.eti.2018.05.006
Soares CPP, de Baptista RL, Cesar DV (2018) Solvothermal reduction of graphite oxide using alcohols. Mater Res. https://doi.org/10.1590/1980-5373-MR-2017-0726
Soares SF, Fernandes T, Sacramento M et al (2019) Magnetic quaternary chitosan hybrid nanoparticles for the efficient uptake of diclofenac from water. Carbohyd Polym 203:35–44. https://doi.org/10.1016/j.carbpol.2018.09.030
Spiridonov VV, Panova IG, Makarova LA et al (2017) The one-step synthesis of polymer-based magnetic ɣ-$Fe_2O_3$/carboxymethyl cellulose nanocomposites. Carbohyd Polym 177:269–274. https://doi.org/10.1016/j.carbpol.2017.08.126
Stanicki D, Elst LV, Muller RN, Laurent S (2015) Synthesis and processing of magnetic nanoparticles. Curr Opin Chem Eng 8:7–14. https://doi.org/10.1016/j.coche.2015.01.003
Stöber W, Fink A, Bohn E (1968) Controlled growth of monodisperse silica spheres in the micron size range. J Colloid Interface Sci 26:62–69. https://doi.org/10.1016/0021-9797(68)90272-5
Su H, Ye Z, Hmidi N (2017) High-performance iron oxide–graphene oxide nanocomposite adsorbents for arsenic removal. Colloids Surf, A 522:161–172. https://doi.org/10.1016/j.colsurfa.2017.02.065
Sun X, Yang L, Li Q et al (2014) Amino-functionalized magnetic cellulose nanocomposite as adsorbent for removal of Cr(VI): synthesis and adsorption studies. Chem Eng J 241:175–183. https://doi.org/10.1016/j.cej.2013.12.051
Tajuddin Sikder M, Tanaka S, Saito T, Kurasaki M (2014) Application of zerovalent iron impregnated chitosan-caboxymethyl-β-cyclodextrin composite beads as arsenic sorbent. J Environ Chem Eng 2:370–376. https://doi.org/10.1016/j.jece.2014.01.009
Tancredi P, Moscoso Londoño O, Rivas Rojas PC, Socolovsky LM (2018) Step-by-step synthesis of iron-oxide nanoparticles attached to graphene oxide: a study on the composite properties and architecture. Mater Res Bull 107:255–263. https://doi.org/10.1016/j.materresbull.2018.08.003
Tang SCN, Lo IMC (2013) Magnetic nanoparticles: essential factors for sustainable environmental applications. Water Res 47:2613–2632. https://doi.org/10.1016/j.watres.2013.02.039
Teja AS, Koh P (2009) Synthesis, properties, and applications of magnetic iron oxide nanoparticles. Prog Cryst Growth Charact Mater 55:22–45. https://doi.org/10.1016/j.pcrysgrow.2008.08.003
Tijani JO, Fatoba OO, Babajide OO, Petrik LF (2016) Pharmaceuticals, endocrine disruptors, personal care products, nanomaterials and perfluorinated pollutants: a review. Environ Chem Lett 14:27–49. https://doi.org/10.1007/s10311-015-0537-z
Tombácz E, Turcu R, Socoliuc V, Vékás L (2015) Magnetic iron oxide nanoparticles: recent trends in design and synthesis of magnetoresponsive nanosystems. Biochem Biophys Res Commun 468:442–453. https://doi.org/10.1016/j.bbrc.2015.08.030
Tran HV, Tran LD, Nguyen TN (2010) Preparation of chitosan/magnetite composite beads and their application for removal of Pb(II) and Ni(II) from aqueous solution. Mater Sci Eng, C 30:304–310. https://doi.org/10.1016/j.msec.2009.11.008
Tu Y-J, You C-F, Chang C-K (2012a) Kinetics and thermodynamics of adsorption for Cd on green manufactured. J Hazard Mater 235–236:116–122. https://doi.org/10.1016/j.jhazmat.2012.07.030
Tu Y-J, You C-F, Chang C-K et al (2012b) Arsenate adsorption from water using a novel fabricated copper ferrite. Chem Eng J 198–199:440–448. https://doi.org/10.1016/j.cej.2012.06.006
Turan NB, Erkan HS, Engin GO, Bilgili MS (2019) Nanoparticles in the aquatic environment: usage, properties, transformation and toxicity—a review. Process Saf Environ Prot 130:238–249. https://doi.org/10.1016/j.psep.2019.08.014
Uddin MK (2017) A review on the adsorption of heavy metals by clay minerals, with special focus on the past decade. Chem Eng J 308:438–462. https://doi.org/10.1016/j.cej.2016.09.029
Vieira DC, Noldin JA, Deschamps FC, Resgalla C (2016) Ecological risk analysis of pesticides used on irrigated rice crops in southern Brazil. Chemosphere 162:48–54. https://doi.org/10.1016/j.chemosphere.2016.07.046
Villacis RAR, Filho JS, Piña B et al (2017) Integrated assessment of toxic effects of maghemite (ɣ-$Fe_2O_3$) nanoparticles in zebrafish. Aquat Toxicol 191:219–225. https://doi.org/10.1016/j.aquatox.2017.08.004
Wang J, Zheng S, Shao Y et al (2010) Amino-functionalized $Fe_3O_4$@$SiO_2$ core-shell magnetic nanomaterial as a novel adsorbent for aqueous heavy metals removal. J Colloid Interface Sci 349:293–299. https://doi.org/10.1016/j.jcis.2010.05.010
Wang H, Kou X, Pei Z et al (2011) Physiological effects of magnetite ($Fe_3O_4$) nanoparticles on perennial ryegrass (*Lolium perenne* L.) and pumpkin (*Cucurbita mixta*) plants. Nanotoxicology 5:30–42. https://doi.org/10.3109/17435390.2010.489206
Wang Y, Qi Y, Li Y et al (2013) Preparation and characterization of a novel nano-absorbent based on multi-cyanoguanidine modified magnetic chitosan and its highly effective recovery for Hg(II) in aqueous phase. J Hazard Mater 260:9–15. https://doi.org/10.1016/j.jhazmat.2013.05.001
Wang F, Sun W, Pan W, Xu N (2015a) Adsorption of sulfamethoxazole and 17β-estradiol by carbon nanotubes/$CoFe_2O_4$ composites. Chem Eng J 274:17–29. https://doi.org/10.1016/j.cej.2015.03.113
Wang S, Wang K, Dai C et al (2015b) Adsorption of $Pb^{2+}$ on amino-functionalized core-shell magnetic mesoporous SBA-15 silica composite. Chem Eng J 262:897–903. https://doi.org/10.1016/j.cej.2014.10.035
Wang H, Zhang H, Jiang JQ, Ma X (2016) Adsorption of bisphenol a onto cationic-modified zeolite. Desalin Water Treat 57:26299–26306. https://doi.org/10.1080/19443994.2016.1172265
Wang Y, Wu D, Wei Q et al (2017) Rapid removal of Pb(II) from aqueous solution using branched polyethylenimine enhanced magnetic carboxymethyl chitosan optimized with response surface methodology. Sci Rep 7:1–11. https://doi.org/10.1038/s41598-017-09700-5
Wang T, Ai S, Zhou Y et al (2018) Adsorption of agricultural wastewater contaminated with antibiotics, pesticides and toxic metals by functionalized magnetic nanoparticles. J Environ Chem Eng 6:6468–6478. https://doi.org/10.1016/j.jece.2018.10.014
Wanjeri VWO, Sheppard CJ, Prinsloo ARE et al (2018) Isotherm and kinetic investigations on the adsorption of organophosphorus pesticides on graphene oxide based silica coated magnetic nanoparticles functionalized with 2-phenylethylamine. J Environ Chem Eng 6:1333–1346. https://doi.org/10.1016/j.jece.2018.01.064
Wong KT, Eu NC, Ibrahim S et al (2016) Recyclable magnetite-loaded palm shell-waste based activated carbon for the effective removal of methylene blue from aqueous solution. J Clean Prod 115:337–342. https://doi.org/10.1016/j.jclepro.2015.12.063
Xiu Z-M, Jin Z-H, Li T-L et al (2010) Effects of nano-scale zero-valent iron particles on a mixed culture dechlorinating trichloroethylene. Biores Technol 101:1141–1146. https://doi.org/10.1016/j.biortech.2009.09.057

Xu L, Pan J, Dai J et al (2012a) Preparation of thermal-responsive magnetic molecularly imprinted polymers for selective removal of antibiotics from aqueous solution. J Hazard Mater 233–234:48–56. https://doi.org/10.1016/j.jhazmat.2012.06.056

Xu P, Zeng GM, Huang DL et al (2012b) Use of iron oxide nanomaterials in wastewater treatment: a review. Sci Total Environ 424:1–10. https://doi.org/10.1016/j.scitotenv.2012.02.023

Xu W-H, Wang L, Wang J et al (2013) Superparamagnetic mesoporous ferrite nanocrystal clusters for efficient removal of arsenite from water. CrystEngComm 15:7895–7903. https://doi.org/10.1039/c3ce40944a

Yamaura M, Fungaro DA (2013) Synthesis and characterization of magnetic adsorbent prepared by magnetite nanoparticles and zeolite from coal fly ash. J Mater Sci 48:5093–5101. https://doi.org/10.1007/s10853-013-7297-6

Yan L, Li S, Yu H et al (2016) Facile solvothermal synthesis of $Fe_3O_4$/bentonite for efficient removal of heavy metals from aqueous solution. Powder Technol 301:632–640. https://doi.org/10.1016/j.powtec.2016.06.051

Yang X, Chen C, Li J et al (2012) Graphene oxide-iron oxide and reduced graphene oxide-iron oxide hybrid materials for the removal of organic and inorganic pollutants. RSC Adv 2:8821–8826. https://doi.org/10.1039/c2ra20885g

Yang H, Masse S, Zhang H et al (2014) Surface reactivity of hydroxyapatite nanocoatings deposited on iron oxide magnetic spheres toward toxic metals. J Colloid Interface Sci 417:1–8. https://doi.org/10.1016/j.jcis.2013.11.031

Yang M, Lin J, Zhan Y, Zhang H (2014) Adsorption of phosphate from water on lake sediments amended with zirconium-modified zeolites in batch mode. Ecol Eng 71:223–233. https://doi.org/10.1016/j.ecoleng.2014.07.035

Yang H, Liu Q, Masse S et al (2015) Hierarchically-organized, well-dispersed hydroxyapatite-coated magnetic carbon with combined organics and inorganics removal properties. Chem Eng J 275:152–159. https://doi.org/10.1016/j.cej.2015.04.026

Yang Y, Hu X, Zhao Y et al (2017) Decontamination of tetracycline by thiourea-dioxide—reduced magnetic graphene oxide: effects of pH, ionic strength, and humic acid concentration. J Colloid Interface Sci 495:68–77. https://doi.org/10.1016/j.jcis.2017.01.075

Yang Z-F, Li L-Y, Hsieh C-T et al (2018) Fabrication of magnetic iron oxide@graphene composites for adsorption of copper ions from aqueous solutions. Mater Chem Phys 219:30–39. https://doi.org/10.1016/j.matchemphys.2018.07.053

Yang X, Wan Y, Zheng Y et al (2019) Surface functional groups of carbon-based adsorbents and their roles in the removal of heavy metals from aqueous solutions: a critical review. Chem Eng J 366:608–621. https://doi.org/10.1016/j.cej.2019.02.119

Yu R, Jiang C-F, Chu W et al (2017) Decoration of CNTs' surface by $Fe_3O_4$ nanoparticles: influence of ultrasonication time on the magnetic and structural properties. Chin Chem Lett 28:302–306. https://doi.org/10.1016/j.cclet.2016.07.014

Yuan ML, Song C, Yan GJ (2011) Some research on the magnetic X zeolite composites. Adv Mater Res 311–313:2040–2047. https://doi.org/10.4028/www.scientific.net/AMR.311-313.2040

Zarandi MJE, Sohrabi MR, Khosravi M et al (2016) Optimizing Cu(II) removal from aqueous solution by magnetic nanoparticles immobilized on activated carbon using Taguchi method. Water Sci Technol 74:38–47. https://doi.org/10.2166/wst.2016.152

Zhang C, Sui J, Li J et al (2012) Efficient removal of heavy metal ions by thiol-functionalized superparamagnetic carbon nanotubes. Chem Eng J 210:45–52. https://doi.org/10.1016/j.cej.2012.08.062

Zhang J, Zhai S, Li S et al (2013) Pb(II) removal of $Fe_3O_4$@$SiO_2$-$NH_2$ core-shell nanomaterials prepared via a controllable sol-gel process. Chem Eng J 215–216:461–471. https://doi.org/10.1016/j.cej.2012.11.043

Zhang Y, Shen Z, Dai C, Zhou X (2014) Removal of selected pharmaceuticals from aqueous solution using magnetic chitosan: sorption behavior and mechanism. Environ Sci Pollut Res 21:12780–12789. https://doi.org/10.1007/s11356-014-3212-1

Zhang Y, Zhu L, Zhou Y, Chen J (2015) Accumulation and elimination of iron oxide nanomaterials in zebrafish (*Danio rerio*) upon chronic aqueous exposure. J Environ Sci (China) 30:223–230. https://doi.org/10.1016/j.jes.2014.08.024

Zhang Y, Wu B, Xu H et al (2016) Nanomaterials-enabled water and wastewater treatment. NanoImpact 3–4:22–39. https://doi.org/10.1016/j.impact.2016.09.004

Zhang Z, Chen H, Wu W et al (2019) Efficient removal of Alizarin Red S from aqueous solution by polyethyleneimine functionalized magnetic carbon nanotubes. Biores Technol 293:122100. https://doi.org/10.1016/j.biortech.2019.122100

Zhang Z, Schniepp HC, Adamson DH (2019) Characterization of graphene oxide: variations in reported approaches. Carbon 154:510–521. https://doi.org/10.1016/j.carbon.2019.07.103

Zhao F, Tang WZ, Zhao D et al (2014) Adsorption kinetics, isotherms and mechanisms of Cd(II), Pb(II), Co(II) and Ni(II) by a modified magnetic polyacrylamide microcomposite adsorbent. J Water Process Eng 4:47–57. https://doi.org/10.1016/j.jwpe.2014.09.003

Zhao D, Gao X, Wu C et al (2016) Facile preparation of amino functionalized graphene oxide decorated with $Fe_3O_4$ nanoparticles for the adsorption of Cr(VI). Appl Surf Sci 384:1–9. https://doi.org/10.1016/j.apsusc.2016.05.022

Zheng H-B, Mo J-Z, Zhang Y et al (2014) Facile synthesis of magnetic molecularly imprinted polymers and its application in magnetic solid phase extraction for fluoroquinolones in milk samples. J Chromatogr A 1329:17–23. https://doi.org/10.1016/j.chroma.2013.12.083

Zheng M, Lu J, Zhao D (2018) Effects of starch-coating of magnetite nanoparticles on cellular uptake, toxicity and gene expression profiles in adult zebrafish. Sci Total Environ 622–623:930–941. https://doi.org/10.1016/j.scitotenv.2017.12.018

Zhou L, Ji L, Ma P, Shao Y (2014a) Development of carbonnanotubes/$CoFe_2O_4$ magnetic hybrid material for removal of tetrabromobisphenol A and Pb (II). J Hazard Mater 265:104–114. https://doi.org/10.1016/j.jhazmat.2013.11.058

Zhou L, Pan S, Chen X et al (2014b) Kinetics and thermodynamics studies of pentachlorophenol adsorption on covalently functionalized $Fe_3O_4$@$SiO_2$-MWCNTs core–shell magnetic microspheres. Chem Eng J 257:10–19. https://doi.org/10.1016/j.cej.2014.07.060

Zhou S, Li Y, Chen J et al (2014c) Enhanced Cr(VI) removal from aqueous solutions using Ni/Fe bimetallic nanoparticles: characterization, kinetics and mechanism. RSC Adv 4:50699–50707. https://doi.org/10.1039/c4ra08754b

Zhu H, Jia S, Wan T et al (2011) Biosynthesis of spherical $Fe_3O_4$/bacterial cellulose nanocomposites as adsorbents for heavy metal ions. Carbohyd Polym 86:1558–1564. https://doi.org/10.1016/j.carbpol.2011.06.061

Zhuang F, Tan R, Shen W et al (2015) Monodisperse magnetic hydroxyapatite/$Fe_3O_4$ microspheres for removal of lead(II) from aqueous solution. J Alloy Compd 637:531–537. https://doi.org/10.1016/j.jallcom.2015.02.216